Future use of Aquifer Thermal Energy Storage below the historic centre of Amsterdam
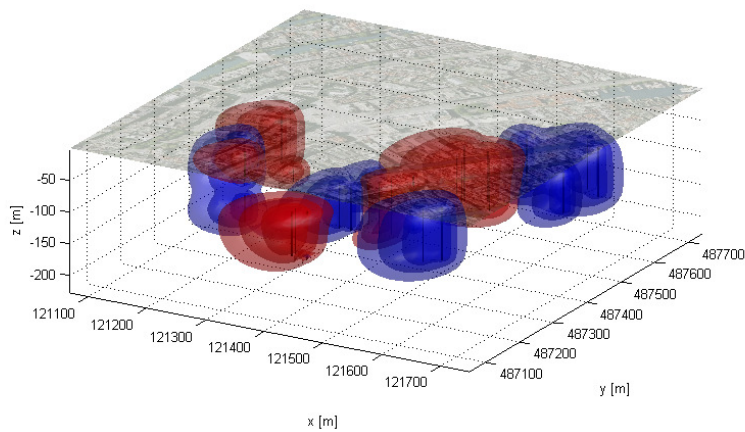
Ruben Johannes Caljé

January 2010

Future use of Aquifer Thermal Energy Storage below the historic centre of Amsterdam

Korte Ouderkerkerdijk 7
Amsterdam
The Netherlands

PO BOX 94370
1090 GJ Amsterdam
The Netherlands

P +31 889 39 40 00
F +31 20 608 39 00

KvK 41216593

www.waternet.nl

Waternet is the merged organisation of the Waterboard Amstel, Gooi & Vecht, the Service for Surface Water and Sewerage Management of the City of Amsterdam, and the Amsterdam Water Supply.

It is the first and only organisation in the Netherlands that manages the complete cycle of surface water, groundwater, drinking water, the sewerage system and wastewater.

Waternet, started in 2006, is a relative young organisation, but its roots date back to 1307 when the oldest predecessor of the Waterboard officially was founded, and to 1851 when the Amsterdam Water Supply started.

Preface

This thesis report is the result of a study of Aquifer Thermal Energy Storage (ATES) systems. This is done at the end of the Master Study Hydrology at the Faculty Civil Engineering & Geosciences of the TU Delft. The thesis was carried out at Waternet, the merged organization of the Waterboard Amstel, Gooi & Vecht, the Service for Surface Water and Sewerage Management of the City of Amsterdam, and the Amsterdam Water Supply. With the increasing number of energy storage systems, Waternet is exploring its role concerning ATES systems, so that the subsurface of Amsterdam and its surroundings is used as efficient and sustainable as possible. Therefore, more knowledge had to be obtained about energy storage in the subsurface, which resulted in this thesis report.

During this thesis many persons supported me. First of all I wish to thank prof.dr.ir. T. N. Olsthoorn for his enthusiasm and drive. From Waternet drs. F. J.C. Smits was always available for questions and advise, which was much appreciated. Together with drs. F.M. Taselaar from Hompe & Taselaar and drs. B. Drijver from IF Technology they contributed many helpful ideas while discussing the goals and results of this research. Benno Drijver could share his experience in ATES systems, while Frans Taselaar would shed a new and interesting light on the different research questions. From the graduation committee of the TU Delft I wish to thank dr.ir. T. J. Heimovaara and dr.ir. M. Bakker for their help in finalizing the report.

For data provision I wish to thank Lex de Vogel from the province of North-Holland, Sjaak Sallé from NYSE Euronext, Marlies Lambrechts from the municipality of Amsterdam and Jos Waagmeester from IF Technology.

The report starts with an introduction of ATES systems, and their use in the Netherlands and Amsterdam in particular. The research questions are first introduced and an approach to answer them is proposed. From there, the used model is described, followed by the cases to answer the different questions concerning ATES-systems. A number of short chapters concerning soil characteristics and the calibration of the model precede the modeling results. In the final discussion the meaning and limitations of the results are explored. In the end the main conclusions and some recommendations for more optimal future use of energy storage are enumerated.

I hope you enjoy reading this report,

Ruben Caljé

Summary

Aquifer Thermal Energy Storage (ATES) uses the subsurface to store cold and warm water in order to use this thermal energy for cooling and heating of buildings. In Amsterdam this technique is being used more frequently in the last couple of years, caused by the increased demand for sustainable technologies and the available optimal aquifer conditions below the city.

This reports answers questions relating to heterogeneity, salt mixing, thermal pollution, cooperation, and arranging of ATES systems. This is done using a flow and transport groundwater model, which takes into account density and viscosity variations, as a result of temperature and salinity changes. Questions relating to heterogeneity and salinity are answered by means of a case study of the Stopera building, which had an ATES system installed in 2002. The buildings around the Dam Square are used as a case to simulate a hypothetical collective system, which is compared to a hypothetical case with individual systems.

Heterogeneity is modeled in two ways: by simulation of a gravel layer, which was found in drillings, and by geostatistically generating heterogeneities in the horizontal plane. When a gravel layer is present, the retrieved energy will be up to 10% lower, compared to the homogeneous situation. This loss in efficiency can be reduced by installing a blind piece of casing opposite this layer This decreases the maximum efficiency loss to 5%. When heterogeneities are generated in the horizontal plane, the retrieved temperatures and energy amounts seem to be independent of these heterogeneities. Some ranges of heterogeneities were tested, which showed that only for large ranges, in the order of the distance between the warm and cold well, there is a decline of 3 % in efficiency.

ATES systems not only pump water; along with the water they also pump salt, back and forth between the screens. This will inevitably mix the salt and change the original vertical salt gradient into a horizontal one. It is shown that this effect remains within 100 m from the wells.

The overall energy efficiency of a collective system is higher than that of individual systems. Also, less water needs to be pumped to regenerate the aquifer. Fewer wells need to be installed, as each well is used to its maximum capacity. Another benefit of collective ATES systems is that when different connected buildings need cooling and heating at the same time, thermal energy will be exchanged between the buildings without intervention of the subsurface.

Monowells are an interesting alternative for collective systems in a thick aquifer, in cases with little space to install the wells, as in historic city centers. Monowells can be placed wherever they are needed, as the horizontal influence of the wells is minimal, while the wells can still have a large capacity because of the thick aquifer in Amsterdam. The efficiency is a little lower than doublets however, and large hydrological effects can take place when many wells pump simultaneously in the top and bottom of an aquifer.

The NYSE Euronext building used the subsurface for its cooling from 1989 to 1999, heating the aquifer. In 2000 the system was abandoned, because the extracted cooling water started raising in temperature. The warm bubble, however, is still present in the subsurface, where it will affect future ATES below the Dam Square.

Finally, a MATLAB model is developed to assess different arrangements of ATES wells. A situation in which the warm and cold wells are placed in lanes is compared to a situation with no placement restrictions. If the most densely built area of Amsterdam, the Zuidas, was to use ATES for its entire thermal energy need, lane enforcement has its benefits: more buildings can use ATES and the wells will have a higher efficiency, while the distance between buildings and their wells is equal for both simulations. For all less densely built areas, the 'laissez-faire' situation and lane enforcement both have their specific advantages. In both situations all buildings can install an ATES system. The 'laissez-faire' situation will reduce installed pipe length, while the performance of the situation with lanes is slightly higher.

List of Figures

List of tables

List of symbols

Name	Symbol	Unit
Density	ρ	kg/m^3
Bulk density of the aquifer medium	ρ_s	Kg/m^3
Fresh water density	ρ_0	kg/m^3
Concentration	C	kg/m^3
Reference salinity concentration	C_0	kg/m^3
Temperature	T	$^{\circ}$C
Original aquifer temperature	T_0	$^{\circ}$C
Hydraulic conductivity	K	m/d
Dynamic viscosity	μ	kg/(ms)
Reference viscosity	μ_0	kg/(ms)
Specific heat capacity	c_p	J/(kg$^{\circ}$C)
Thermal conductivity	k_T	W/(m$^{\circ}$C)
Energy	E	J
Exergy	ε	J
Hydraulic gradient	i	-
Time	t	d
Hydraulic head	H	m
Fresh water head	h_0	m
Pumping rate of a well	Q	m^3/d
Porosity	θ	-
Specific storage	S_s	m^{-1}
Specific yield	S_y	m^{-1}
Effective molecular diffusion coefficient	$D_{m\_salinity}$	m^2/d
Longitudinal dispersivity	α_L	m
Horizontal Transverse dispersivity	α_{TH}	m
Vertical Transverse dispersivity	α_{TV}	m

1. Introduction

Aquifer Thermal Energy Storage (ATES) is a relatively new technology, used in the Netherlands for about 20 years. It makes use of the subsurface to store thermal energy. This is a difference between ATES and Geothermal energy, which uses the thermal energy already present in the earth. ATES can be seen as a large battery, where thermal energy is to be charged and delivered to and from the subsurface, before it can be supplied to the building when it needs the energy.

1.1 Different types of groundwater energy storage systems

There are several types of energy storage systems that utilize the soil and groundwater to store thermal energy. The first distinction is between open systems, Aquifer Thermal Energy Storage (ATES) and closed systems, called Borehole Thermal Energy Storage (BTES). The operation of these systems is explained in sections 1.1.1 and 1.1.4 and in Figure 1.

1.1.1 Open systems (ATES):

Open systems pump groundwater from 25 to 250 m below the surface. An ATES system uses two wells: a 'cold' well with water of 6-9 ^{o}C and a 'warm' well with

Figure 1: Principle of open (above) and closed (below) energy storage systems (IF Technology).

water of 14-17 ^{o}C. Cold and warm is relative to the natural temperature of the subsurface of 10-13 ^{o}C. In summer, cold water is extracted from the cold well and used for cooling of the building. The heated water is then injected into the warm well. In winter the flow is reversed and water is extracted from the warm well to heat the building, where it cools down and is subsequently injected into the cold well.

In the Netherlands, open energy storage systems are mostly used in office buildings, where the demand for cooling is usually larger than the demand for heating. ATES acts like a large battery: when it is not charged, it cannot deliver thermal energy. Therefore, the cold bubble must be charged in winter, even when there is no demand for heating.

There are several different kinds of open energy storage systems, see Figure 2. The most used concept is a doublet, where the cold and warm wells are located in the same aquifer about 100 m apart.

Another concept is a mono-well. Only one well is drilled, having two usually separated screens in the same aquifer. The upper of the two screens of these wells is used to store warm water, and the lower one is used to store cold water. Because of the buoyancy heated water will move upward and cold water

downward. Therefore, the cold water must not be stored in the upper part of the well, as the cold water would move down and then mix with the rising warm water below it. An aquitard is preferred to separate the warm and cold screen, but there are also monowells where the vertical distance between the warm and cold screen is made large enough to avoid interference.

ATES systems are used in countries like Sweden, Germany, the Netherlands, Belgium and some other European countries. In the past couple of years more countries discover the possibilities of ATES to save energy and reduce CO_2 output. The Netherlands are probably the technological leaders with this technology (Nielsen, 2003).
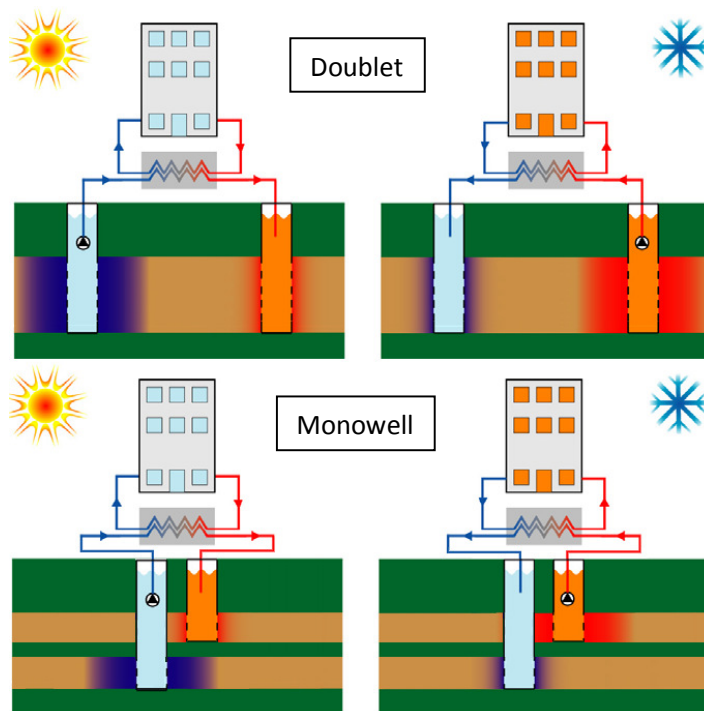
Figure 2: **Principle of doublets and monowells.**

1.1.2 Heat pumps

The temperature of the water from the warm well is not high enough to heat a building. Therefore, most systems use a heat pump to raise the temperature of the water from the warm well to about 35-45 $^{\circ}$C. With water of this temperature it is possible to heat the building using low-temperature heating systems, like floor heating. A heat pump extracts thermal energy from the pumped water of the warm well to increase the temperature of the water in the separate heating circuit inside the building. The original water is cooled down in this process, and stored in the cold well, to be used in the next summer. The water from the cold well can be used directly for cooling of the building, without the intervention of the heat pump.

A term often used in combination with heat pumps is the coefficient of performance (COP). This term describes the ratio of useful heat production to work input, in formula:

$$COP = \frac{Q}{W}$$

[1]

Where: *COP* is the coefficient of performance [-]; *Q* is the amount of useful heat [J]; and *W* the amount of energy required to produce this heat [J].

Modern heat pumps have a COP of 4 to 5 in heating mode, and 3 to 4 in cooling mode, during optimal circumstances. Because of mechanical, electrical and thermal losses the COP will never reach this

optimal value. The true value it will reach is called the Seasonal Performance Factor (SPF), and will be 0.5 to 0.7 of the COP value.

1.1.3   Energy analysis

The energy to drive the heat pumps is electric energy. This needs to be produced, with an average efficiency of 0.4. In this way heat pumps are not much more efficient than conventional heating, with an COP of 0.95. However, if the electric energy is produced with sustainable technologies like wind, sun and hydropower, heat pumps can save a lot of CO_2. Also, what is not taken into account here, is that during the productions of heat by the heat pump, cold water is produced, which is stored and can be used for cooling of the building later on without the use of the heat pump. So to use this cold energy only water pumps are needed to transport it to the surface, and the COP of cooling will be very high. This is the reason ATES is more interesting for buildings that have a high cooling demand.

The benefits of thermal heat storage can be explained by an analysis of energy quality as well. For conventional heating the energy is generated by fossil fuels. This form of energy has a high quality, as it can be recovered as work to almost 100% and can be used for many activities. When this form is used to heat a building in a conventional way, water with a temperature of about 80 to 90 ^{o}C is produced to eventually heat a building to 20 ^{o}C. So the energy is transferred to very low quality in two steps, first from fossil fuel to water of 80-90 ^{o}C, and then to a room temperature of 20 ^{o}C. A similar process takes place for cooling a building.

With ATES and heat pumps it is possible to use low quality energy to heat or cool a building. Water with a temperature of 13-16 ^{o}C is upgraded to 35-45 ^{o}C, which is used to heat the building.

1.1.4   Closed systems (BTES)

Closed systems use a coolant to transport the energy from the surface to the subsurface and back. This coolant is transported in pipes through which it exchanges heat with the soil particles and local groundwater. In this way, no water is pumped out of the subsurface or injected into it. BTES systems can also reach a depth of 200 m, but usually are less deep than ATES systems. They need much more boreholes to produce the same amount of energy as ATES systems, as only the direct vicinity of the borehole is influenced by the BTES. Because there is no direct contact between the water in the borehole and the subsurface, BTES does not need a layer with a high hydraulic conductivity. This kind of system is used in smaller projects and is popular in countries like Switzerland, Sweden, Germany and Austria (Omer, 2007). This thesis is about ATES systems, as these have a larger capacity then BTES systems. Also, the geo-hydrological conditions in Amsterdam are ideal for ATES. Therefore, BTES will not be evaluated any further, except for a short discussion about the administrative context in section 1.6.

1.2   Research on ATES systems

There has been much research on ATES systems, starting from 1970 with theoretical studies. In the past couple of years, there has been some research by Dutch universities and companies on the applied use of ATES.

The variables influencing the performance of ATES systems have been identified (Sommer, 2007):

- Density differences of warm and cold water do not seem to have any relevant influence on the performance of an ATES system in the temperature range between 6 to 18 $^{\circ}$C.
- Viscosity differences only have an influence of 0.3% on the performance in this temperature range. However, the model on which the results are based, did not take heterogeneities of the subsoil into account.
- The capacity of the well depends on the hydraulic conductivity, but if the capacity is not a constraint, the hydraulic conductivity does not influence the performance of an ATES, as long as the subsurface is homogeneous.
- The dispersivity has a negative linear influence on the energy efficiency of ATES.
- If the distance between the wells of a doublet or its screen length increases, so does the performance, until an asymptotic value has been reached, which, according to the model, was about 90 %.
- The higher the temperature difference is, the greater the energy performance. This might seem a strange result, but is explained by the fact that a smaller amount of water has to be pumped in the wells, and so the water will flow less fast and far. Therefore, dispersion is smaller and less energy is lost. However, the model does not incorporate any ambient groundwater flow, so a very small cold or warm bubble will not flow away from the well. This might not be a realistic case.

Vermaas (2008) did a comprehensive study of some problems encountered with ATES systems in the Netherlands. He also evaluated an imbalance of thermal energy storage with regard to the energy performance. An imbalance reduces the performance and enlarges the imbalance itself, because the temperature difference, ΔT, will become lower.

Research done to estimate the effect of heterogeneities on the performance of energy storage systems showed that heterogeneity of the subsoil has a substantial effect on the temperature profile in the subsurface, but there are different views on the effect on the performance of the system. The performance is said to decrease by 5 to 10%, depending on the number of heterogeneities of the subsoil (Ferguson, 2007), but in another case study where a calculation was made with and without a heterogeneous subsurface the heterogeneity did not have any effect on the performance (Bridger, 2006).

Van de Weerdhof (2005), student from the TU Delft, took a closer look at the energy storage systems in The Hague. This research on several systems and their interference shows that the systems do not have much influence on each other, provided they pump water constantly and do this synchronized with neighboring systems. Desynchronized pumping has a negative influence on the performance.

1.3   Use in the Netherlands

The number of open Energy Storage systems has been increasing over the last two decades, see Figure 3. The majority of the larger systems in the Netherlands are open systems. This is because of the favorable conditions in the subsurface: generally consisting of sand from 70 to around 200 m depth, where the

aquifer is quite permeable and the flow of groundwater is slow. Therefore, on most locations it is possible to inject and extract the water and keep the warm and cold bubble in place over a season. Currently there are about 900 permits for ATES-systems (Vermaas, 2008).
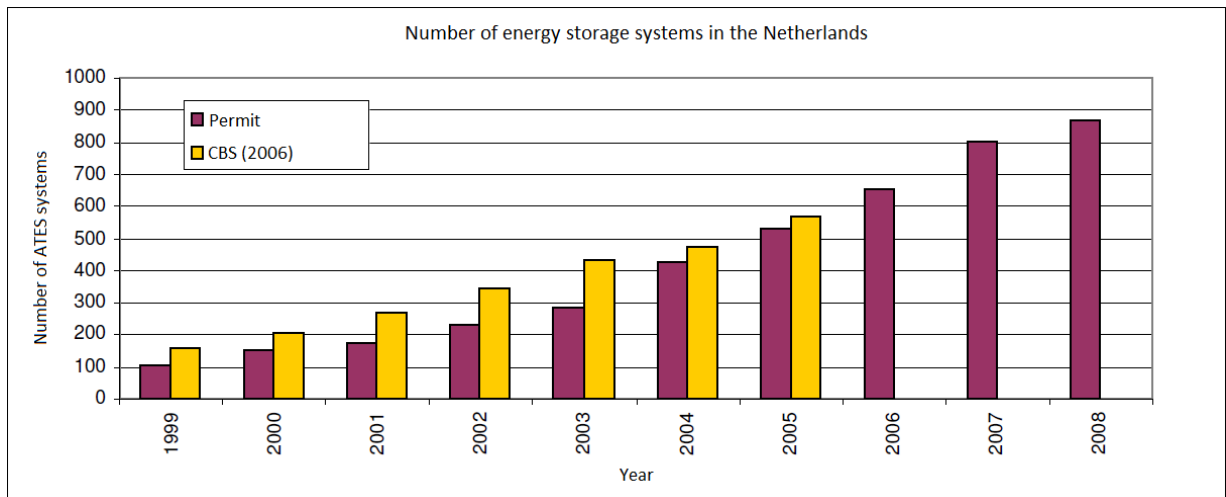
Figure 3: **Number of open energy storage systems in the Netherlands (Vermaas, 2008).**

1.4 Use in Amsterdam

The city of Amsterdam has set ambitious goals with regard to sustainable energy. In 2025 CO_2 emissions should be reduced by 40 % compared to the emission in 1990 (Ecofys, 2009). Part of this reduction can be established by ATES, while the potential is still far from fulfilled, as can be seen from the first graph in Figure 4.
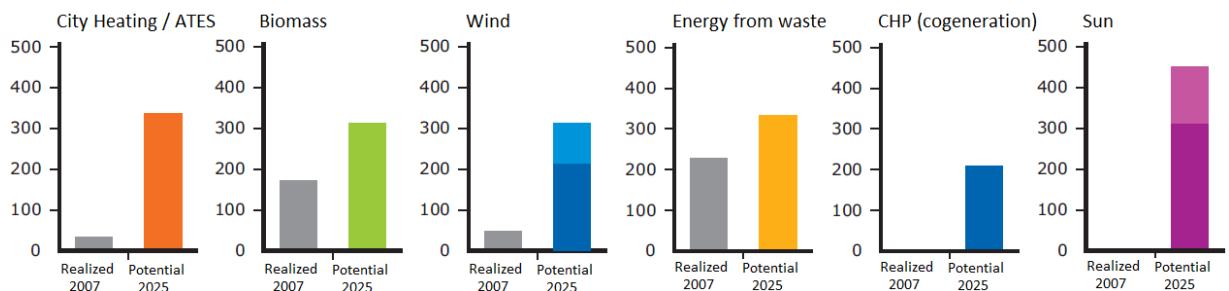
Figure 4: **CO_2 reduction by sustainable technologies in Amsterdam, realized in 2007 and potential for 2025 in avoided kilotons (Ecofys, 2009).**

Right now Amsterdam has a fair number of energy storage systems. The province has issued 85 permits until the end of 2008 (Figure 5). These systems are mainly located in newly developed areas like the Zuidas, Amsterdam South-East and Amsterdam North-West, but also some systems have been installed in the old centre of Amsterdam (Figure 6).
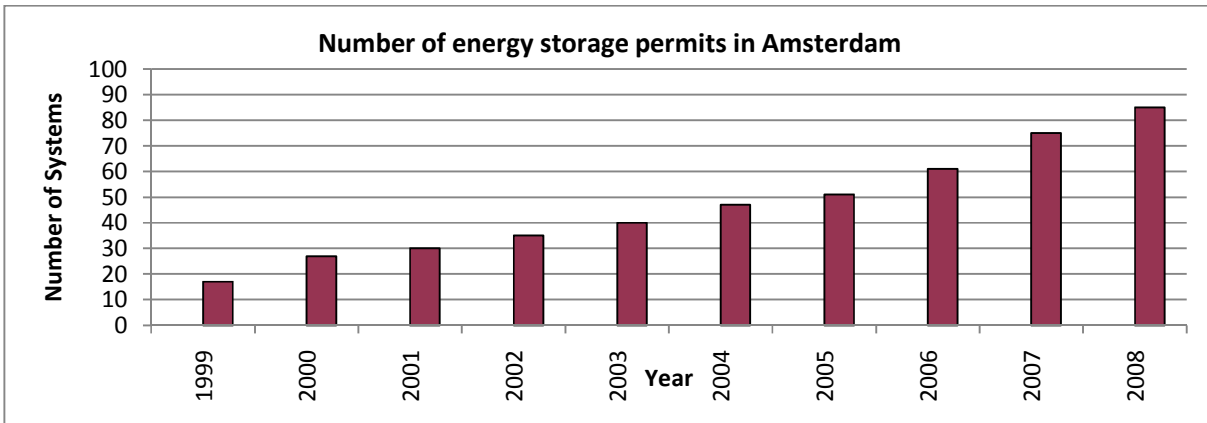
Figure 5: Number of permits issued by the province from 1999 until the end of 2008.
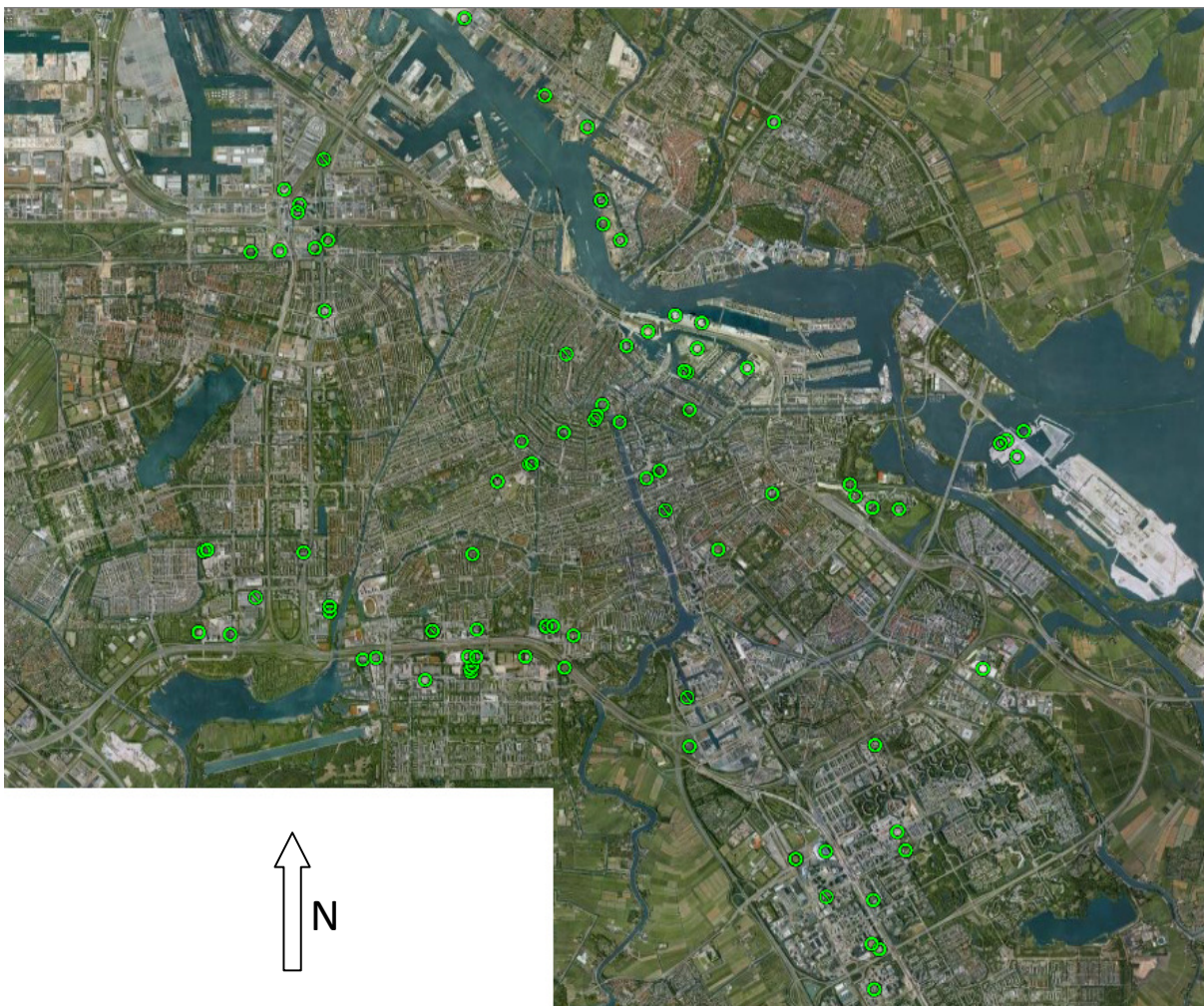
Figure 6: ATES systems with a permit in Amsterdam, from data of the province of North Holland. The systems that have a stripe in the circle are not in use any more.

Table 1 shows some generalized properties for energy storage systems in Amsterdam, as derived from the provided permit database. Only systems with a single doublet or a single monowell were used for the table. Systems with multiple wells are not included, as they are designed for specific projects, making them difficult to compare. These data allow a quick impression of some average properties of current ATES systems in Amsterdam. Not every property has data for all systems, which cause some distortion in the table. For example, because the province lacks data about the average discharge per hour for some of the smaller projects in their database, the maximum discharge per hour is smaller than the average discharge per hour for monowells.

These raw data allow computation of the length of the screens, the number of full load hours and the temperature difference between the infiltration temperatures of the cold and warm well, taking into account only the systems having data for all the properties used in the calculation. For example, the average number of full load hours is calculated by averaging the number of full loads hours for only those projects, for which the average yearly discharge as well as the average hourly discharge are supplied.

Table 1: Averaged properties of all ATES systems in Amsterdam with one doublet and one monowell.

Raw data:	1 Doublet	1 Monowell	
Number of projects	33	11	
Top of screen	79.2	71.6	m -NAP
Bottom of screen	157.0	146.3	m -NAP
Average discharge per hour, one way	152.5	55.0	m^3/h
Average discharge per year, both ways	298.5	137.6	1000 m^3/a
Maximum discharge per hour, one way	187.1	51.4	m^3/h
Maximum discharge per year, both ways	424.7	196.4	1000 m^3/a
Capacity warm	1373.4	383.5	MWh/a
Capacity cold	1387.4	383.5	MWh/a
Temperature warm well	17.7	15.2	^{o}C
Temperature cold well	7.1	8.9	^{o}C
Horizontal distance of screens	123.0	-	m

Calculated from this data:			
Nr. of full load hours for average discharge, both ways	1878.9	2800.0	hours
Nr. of full load hours for maximum discharge, both ways	2310.4	2978.3	hours
Temperature difference cold and warm well	10.6	6.3	^{o}C
Length of screen	77.7		m

1.5 Losses

The energy losses of subsurface ATES systems are caused by processes described in the following sections.

1.5.1 Advection due to Groundwater flow

Part of the injected energy is displaced from the well along with the natural groundwater flow. This flow varies with location; in the west of the Netherlands it is determined by the surrounding polders with their artificially maintained water levels. In Amsterdam the flow velocity is about 10 m/a on average.

When the energy is stored for half a year, the water displacement from the well will be 5 m. Because of retardation (see section 4.4), the thermal energy will move at about half the speed of the water, causing a displacement of only 2.5 m.

1.5.2 Mechanical Dispersion and Conduction

When the water infiltrates for the first time a sharp interface between the infiltrated water and the ambient water temperature will occur initially. Mechanical dispersion and heat conduction spread the heat over the boundary of the cold and warm water bubbles, making this transition smoother. Both these processes can be quantified by a single parameter, the effective thermal dispersion (see 4.4 Modeling heat transport).

$$D_w = \frac{k_{Tbulk}}{\theta \rho c_{Pfluid}} + \alpha \frac{q}{\theta} \approx 0.1 + \alpha \frac{q}{\theta}$$ [2]

Where: D_w is the effective thermal dispersion [m^2/d]; k_{Tbulk} is the thermal conductivity of water and particles [J/(d m ^{o}C)]; θ is the porosity [-]; ρ is the density of water [kg/m^3]; c_{Pfluid} is the specific heat capacity of the water [J/(kg^{o}C)]; α is the dispersivity [m]; and q is the specific discharge [m/d].

The first term incorporates heat conduction, which depends on the thermal conductivities of the aquifer material and water. Its value is approximately 0.1 m^2/d. The second term incorporates mechanical dispersion, which depends on the dispersivity of the subsurface and the velocity of the water. The dispersivity α may vary between 0.5 and 5 m (Gelhar, Welty, & Rehfeldt, 1992), while the velocity of the water strongly depends on the distance from the well. If the specific discharge is taken as 0.5 m/h and the radius of the well as 0.4 m, the right term of equation[2] varies from 171.43 m^2/d at the well with α=5, to 0.14 m^2/d at 50 m from the well and with α=0.5. So, for this discharge, the value of the second term is always larger than the first term. This means that for these values mechanical dispersion has more impact than conduction. When there is no or very little pumping from the well however, conduction will keep making the transition between warmer and colder water more smooth. This may be seen in terms of increasing standard deviation:

$$\sigma = \sqrt{2D_w t}$$ [3]

Where: σ is the standard deviation [m]; and t is time [d].

The one-dimensional solution for dispersion/diffusion, of an initially sharp front at $x=x_0$, where the concentration at both sides of the front can freely develop, can be approximated by equation [4]. We have a concentration C_0 for $x<x_0$ and $C=0$ for $x>x_0$ at $t\leq0$. When $x-x_0$ is equal to σ, the value for the concentration will be $0.16C_0$, which means that the largest part of the front is located between x_0-σ and x_0+σ. When only diffusion is taken into account, σ is 6 m for a storage time of 180 days. When also dispersion is taken into account, the heat front is spread more, depending on the chosen values for α and the velocity of water.

$$\frac{C}{C_0} = \frac{1}{2} erfc\left(\frac{(x-x_0)}{2\sqrt{D_x t}}\right) = \frac{1}{2} erfc\left(\frac{(x-x_0)}{\sqrt{2}\sigma}\right) \rightarrow (x-x_0) = \sigma \rightarrow \frac{C}{C_0} = \frac{1}{2} erfc\left(\frac{1}{\sqrt{2}}\right) = 0.1587 \qquad [4]$$

Where: C is the concentration at x [kg/m^3]; C_0 is the input concentration for $x<x_0$ at $t\leq0$ [kg/m^3]; $erfc$ is the complementary error function; x is the location at which the concentration is calculated [m]; and x_0 is the location of the interface between the two concentrations [m].

1.5.3   Losses due to interference

The losses described above act on a single well. On top of this there is interference between wells. The smaller the distance between cold and warm wells, the more they will influence each other in the zone between them. Cold wells will cool warm ones, and vice versa, causing the well temperatures to be closer to the ambient groundwater temperature, with less energy retrieved.

1.6   Administrative Context

Because energy storage is a relatively new technology, some problems relating to Dutch laws and legislation occur, especially in city centers with many office buildings. For an ATES system with a capacity of more than 10 m^3/h, a groundwater permit is required by the Province. The Province checks if the ATES system does not harm other systems and stakeholders. In practice this means that the first user will obtain the permit, excluding future use of the subsurface. This principle is explained by the saying: 'who comes first, pumps', which might not be desirable, as it may limit maximum beneficial use of the subsurface. When an ATES well is part of a collective system, aquifers can probably be used more effectively as the interference between different wells can be minimized in the design phase. This is one of the research questions in this report however, which will be answered later.

Therefore the Taskforce WKO (Taskforce WKO, 2009) proposes to organize the permits differently. They propose to divide the Netherlands in three kinds of areas: green, orange and red, see Figure 7:

- In the green areas no other interests are present. In these areas there is only a reporting obligation, and no permit is required.
- Next the orange areas are to be determined, where there are other interests. Such may be other ATES systems already present, or pollution that can be moved by pumping groundwater. Therefore, permits are needed in these areas. The subsurface of Amsterdam belongs mostly to the orange areas.
- Finally red areas are discerned, where the use of energy storage is undesirable. These areas can include the 25-year groundwater restriction zones around a drinking water pumping station, or nature areas that are sensitive to changes of the groundwater levels. In such red areas ATES systems are only permitted under exceptional circumstances and with very strict permit conditions.

With this proposed system the current permitting system would be simplified, especially for the green areas.

	Other interests	Vision	Regime	Areas
🟢	No relevant major interests	Who comes first, descides	General rules with reporting and modest control of local effects	Most unburdened rural and urban areas
🟡	There are other interests	The stress in the subsurface determines the extent of the approach	Permit, possibly coupled to a masterplan	Expected interference areas, drilling free zones and clean up locations
🟠	There are more important interests than energy storage	No ATES, except custom-made solutions	Permit	For example 25-year-zones

Figure 7:   The system proposed by the Taskforce WKO.

The Taskforce WKO also recommends that in orange and red areas, stakeholders cooperate to improve the overall benefit of the system. A third party, like a municipality or a water board, could make a master plan for a certain area, which would be taken into account by the permit authority. But first the province has to turn the plan into policy, to provide a legal base to reject permits that do not agree with the master plan.

Closed systems (BTES) are currently not regulated in the Groundwater law (Grondwaterwet), there are no permits or reporting duties. Only in groundwater protection areas there are some restrictions, stated in the provincial environmental regulation based on the environmental law. These restrictions regard drillings deeper than 2-3 m. Some negative environmental effects of BTES systems have been reported (Bonte, van den Berg, & van Wezel, 2008):

- The temperature variations are larger than in ATES systems, and therefore the influence on microbiological and chemical effects can be larger.
- BTES systems are smaller. With less money available, drillings may be done more carelessly, affecting confining layers.
- Many BTES systems use a coolant rather than water to transport the thermal energy. This leaking coolant may pollute groundwater, perhaps long after they were abandoned without proper disassembling.

For these reasons the Taskforce WKO recommends that closed systems are also taken into account in new regulations.

2. Research questions

In the previous chapter the rapid growth of the number of ATES systems was described. Previous research on ATES systems focused on ways of maximizing their efficiency. This thesis does the same, but also looks at this from a sustainability prospective. With ATES systems, energy can be saved and environmental goals can be met. However, there are some drawbacks associated with these systems. For instance, the subsurface is more and more perforated by various kinds of energy storage systems. Confining layers are breached, and, when not done with the utmost care, this can have negative effects on the groundwater system.

Many ATES systems are designed, assuming subsurface layers to be homogeneous. In reality zones with higher and lower hydraulic conductivity are present in the aquifer, which may affect the bubbles shape and mixing with native groundwater. It is questionable if this affects the efficiency of the system significantly. This thesis attempts to answer the question:

What is the influence of heterogeneity of the subsurface on the shape of the thermal energy bubbles, and on the performance of ATES systems?

ATES systems pump groundwater from a well and inject it back into another well. In this way, substances in the groundwater surrounding the well screens get mixed. This can have negative effects on drinking water production for example, or increase spreading of contaminations. Therefore the question is:

What is the influence of an ATES system on the salt gradient and how far does this influence reach?

Because of the current permitting system, not the entire potential of the subsurface is utilized. Existing ATES systems make beneficial use of the subsurface more difficult if not impossible for new requests. When stakeholders cooperate, the potential of the subsurface to store energy is assumed to increase. This thesis tries to identify the advantages of cooperation in developing ATES systems:

Are there advantages in cooperation of buildings in operating ATES, and, if so, what are these advantages?

We also investigate if abandoned ATES systems may affect current systems. The energy that is left in the subsurface can influence new systems, at least during the first years of use. This impact is thought to be small, as an ATES works like a battery that is charged and discharged. Therefore the retrieved energy depends more on the injected energy in the previous season, than on the initial ambient groundwater temperature. This hypothesis is examined:

Do old abandoned ATES systems have a significant impact on newly developed systems in the same area?

Another question related to groups of systems is how the wells can be optimally arranged. In many projects wells are arranged in such a way that cold and warm wells are in separate dedicated lanes parallel to the groundwater flow, see Figure 8 for an example. In this way, they influence each other as little as possible. Below Amsterdam, groundwater flow in the storage aquifer is quite small, 10 m/a. Therefore this 'lane' system might not be appropriate, given the severe limitations imposed by the current situation of streets, infrastructure and the location of businesses and other potential users. In

such situations arrangement in lanes may actually limit optimal overall use of the subsurface and might reduce the amount of energy saving that ATES systems can attribute. Hence any arrangement should take the current city structure into account. The following will be investigated:

What are the benefits of 'laning' of wells, and should this laning be applied to Amsterdam? Does laning influence the capacity for ATES in the subsurface of Amsterdam?
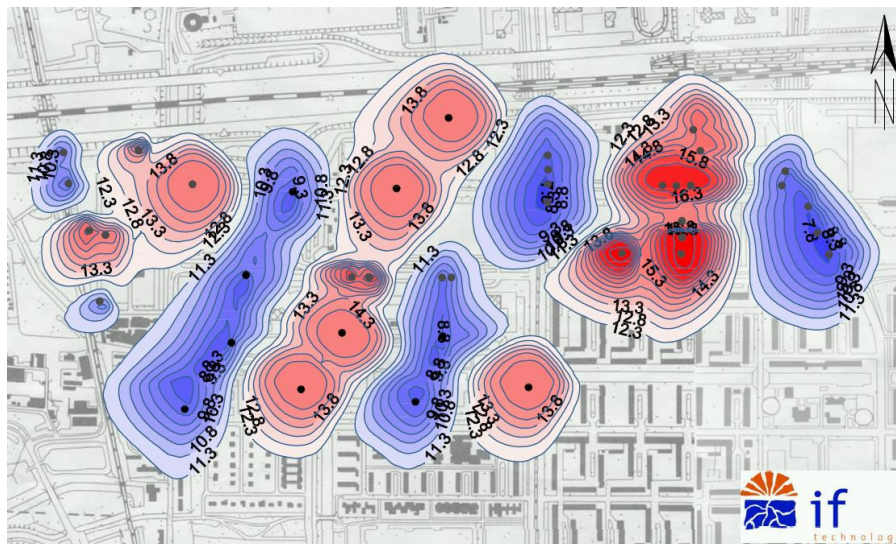
Figure 8:   **An example of placing the warm and cold wells parallelto the southwestern groundwater flow at the Zuidas in Amsterdam (IF Technology).**

Some other interesting questions could be posed concerning ATES systems, of which the use of high temperature storage is one. Right now most provinces do not allow storage of water over 25 ^{o}C, but it could be useful to store warmer water, to be used for heating without the intervention of a heat pump. The characteristics of this storage are quite different from a conventional ATES system however, as described below:

- Density effects will become larger, as the density dependency of water increases with temperature (see section 4.4.1).
- Viscosity effects will be more apparent and fingering of hot water in more conductive layers will take place.
- The speed of chemical and micro-biological processes increase dramatically with increasing temperature (IF Technology, 2004), causing other problems than with conventional ATES systems.
- Water of a very high temperature can be stored, but it is impossible to store water with a temperature below 0 ^{o}C. Therefore, more water needs to be pumped from the cold well to the warm well, than the other way, to achieve an energy balance. Then it is not possible to achieve a volume balance, which might present other problems.

For these differences, and because the optimization of conventional ATES systems offers sufficient options to examine, high temperature storage is not investigated further.

3. Approach

The research questions will be answered by a modeling exercise, using as much as possible the information of the subsurface and current experience. Two cases have been worked out for the centre of Amsterdam: the Stopera and the Dam Square (see chapter 5). For the Stopera case the model will be validated (see chapter 7) and questions about heterogeneity and salt mixing are answered. Then a combination of several systems is modeled to investigate optimal use of the subsurface for energy storage. The Dam Square and the surrounding buildings are investigated for this case. The systems will be analyzed using the SEAWAT code, which is explained in chapter 4. The generic simulation of a city with even more ATES doublets was done with a MATLAB model.

3.1 Heterogeneity

Heterogeneity can influence the performance of an ATES. The storage of heat is not in the form of a round bubble, but in a shape determined by the heterogeneities. In this thesis, heterogeneity is tested in two ways. The first one is vertical heterogeneity, where a more conductive layer is present in the storage aquifer. The other is heterogeneities in the horizontal plane, generated per layer.

All simulations regarding heterogeneity will be done for the Stopera wells. The Stopera is not a real ATES system however, but only a cold storage, see section 6.1. To simulate an ATES system with cold as well as warm water storage, the input temperatures are altered and the design discharges are used.

3.1.1 Case 1: variability in the layering

When a more conductive layer is present in the storage aquifer, a large part of the well discharge will flow through this conductive layer and transport the thermal energy further from the well than in other parts of the aquifer. Because of conductive transport the energy will be transported to the layer above or below this layer. When the season passes and the flow turns around to the well, this energy will only partly be extracted. As can be seen in chapter 6.1, both wells of the Stopera have a high conductive layer around NAP -130 m. The conductivity of this layer is estimated at 250 m/d and is modeled as 12 m thick. This layer is also modeled with a conductivity of 125 m/d, to see if the same effects take place, and how the results depends on the value for the hydraulic conductivity of the gravel layer. Finally, both simulations are repeated, but then with a blind pipe at the gravel layer, to find out if the negative effects of the gravel layer can be reduced in this way. This might be true, as no water will flow directly from the well to the gravel layer.

3.1.2 Case 2: generation of conductivity variability in the horizontal plane

The influence of heterogeneity in the horizontal plane is investigated by modeling random hydraulic conductivity fields for each layer in the model. Heterogeneities, i.e. spatial randomness, in the subsurface can be characterized by a variogram. The mean and standard deviation of two data sets can be equal, but the spatial variation can be very different. This spatial correlation is quantified by a variogram, whose definition is:

$$\gamma(h) = \frac{E\left[(Z(x+h)-Z(x))^2\right]}{2} = \frac{Var\left[Z(x+h)-Z(x)\right]}{2} \qquad [5]$$

Where: *γ* is the variogram [-]; *h* is the lag distance [m]; and *Z(x)* and *Z(x+h)* denote random variables.

γ(h) can be interpreted as the variance of the variable at the given lag distance *h* (Bachmaier & Backes, 2008). As the lag distance becomes larger, this variance will become larger. The shape of a variogram is determined by its sill, nugget and range. The sill is the limit as the lag distance goes to infinity and the nugget is the variance at lag zero. This represents true measurement variance, and is often zero. The range is the lag distance when the variogram reaches the sill. With these three variables, the exact shape of the variogram between the lag of zero and the range is still open. To use variograms in models we need to approach the shape by fitting a smooth curve through the data. These curves are called models, which are mathematical formulas describing the variogram using the nugget, range and sill. There are different models for variograms, and the most well-known are: spherical, exponential and Gaussian.

For this thesis, an exponential variogram was considered to suit best, because of its simplicity, and its frequent use in other research of the same type (Ferguson, 2007), to facilitate comparison with the literature. The formula for the exponential variogram is (Deutsch, 1997):

$$\gamma(h) = c \left[1 - \exp\left(-\frac{3h}{a} \right) \right]$$

[6]

Where: *c* is the sill [-]; and *a* is the range of the variogram [m].

The number 3 in equation [6] is determined by the definition of the range. Most literature use this number, which causes that the variogram at the range is 95% of the sill.

Several ranges will be tested. The range will take on values of 10, 50 and 200 m. The lowest value of 10 m is twice the grid size of 5 m. Smaller values are not possible to generate, as the nodes would have almost no correlation at all. A value of 200 m is at the scale of an energy storage system. The range between these values, 50 m, is in the middle to see what happens between these two extremes. The variograms will then have the forms described in Figure 9.
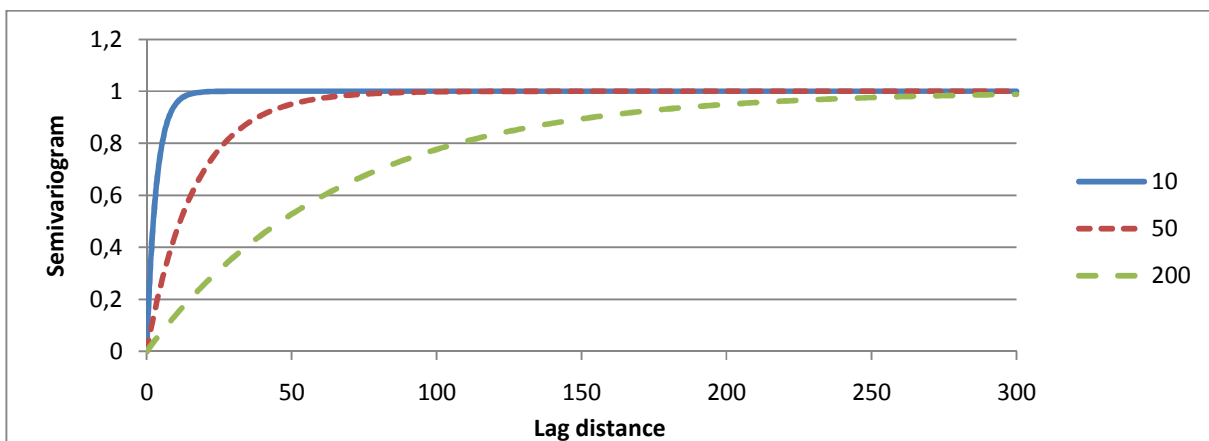
Figure 9:   Several exponential variograms, with a range of 10, 50 or 200 m, a sill of 1, and a nugget of 0.

The method of sequential Gaussian simulation will be followed with the GSLIB software (Deutsch, 1997) to create conductivity fields. Sequential Gaussian simulation can be described as follows (Deutsch, 1997):

- Define a random path that visits each node of the grid once. At each node retain a specified number of neighboring conditioning data, consisting of originally measured data and/or previously simulated grid nodes. In this case no measured data is used, and an unconditional simulation is performed with only previously simulated data.
- Use Standard Kriging with the variogram model to determine the mean and variance of the conditional distribution function of the random function Y(u) at location u.
- Draw a value y(u) from that conditional distribution function.
- Add the simulated value y(u) to the data set.
- Proceed to the next node, and loop until all nodes are simulated.

GSLIB only works with a regular grid. This means that Δx and Δy are constant in the entire grid. This is compatible with the SEAWAT model, where the grid, explained in section 4.5.2, is rectangular close to the wells. It is not rectangular at a certain distance of the wells anymore, but heterogeneities are not expected to have an influence at this distance. The resulting generated variance in the model can be seen in Figure 10.

The program GSLIB produces standard data with a standard normal distribution. Hydraulic conductivity data usually follows a lognormal distribution. To arrive at a lognormal distribution with parameters μ and σ, the following formula is used:

$$X = e^{\mu + \sigma * N}$$ [7]

Where: X is a random variate with a Log-normal distribution with parameters μ and σ; and N is a random variate drawn from the normal distribution with a mean of 0 and a standard deviation of 1.

The parameters μ and σ are determined by the mean and variance of the log-normal distribution according to the following formulas(Log-normal distribution, 2009):

$$\mu = \ln(E[X]) - \frac{1}{2}\ln\left(1 + \frac{Var[X]}{E[X]^2}\right)$$ [8]

$$\sigma = \sqrt{\ln\left(1 + \frac{Var[X]}{E[X]^2}\right)}$$ [9]

Where: $E[X]$ is the expected value, or mean, of the Lognormal distribution, which is equal to the average hydraulic conductivity; and $Var[X]$ is the variance of the Lognormal distribution, $Var(X)$ = standard deviation[2].

For the mean a value of the homogeneous model is used: 37 m/d for the storage aquifer. For the standard deviation half of the mean is used: 18.5 m/d. The resulting hydraulic conductivity fields are shown in Figure 11. The model layers are assumed to be independent of each other. New layers were

formed independent of the layers below. Therefore for each model layer, which is approximately 5 m thick, a conductivity field is created independently of the other model layers.
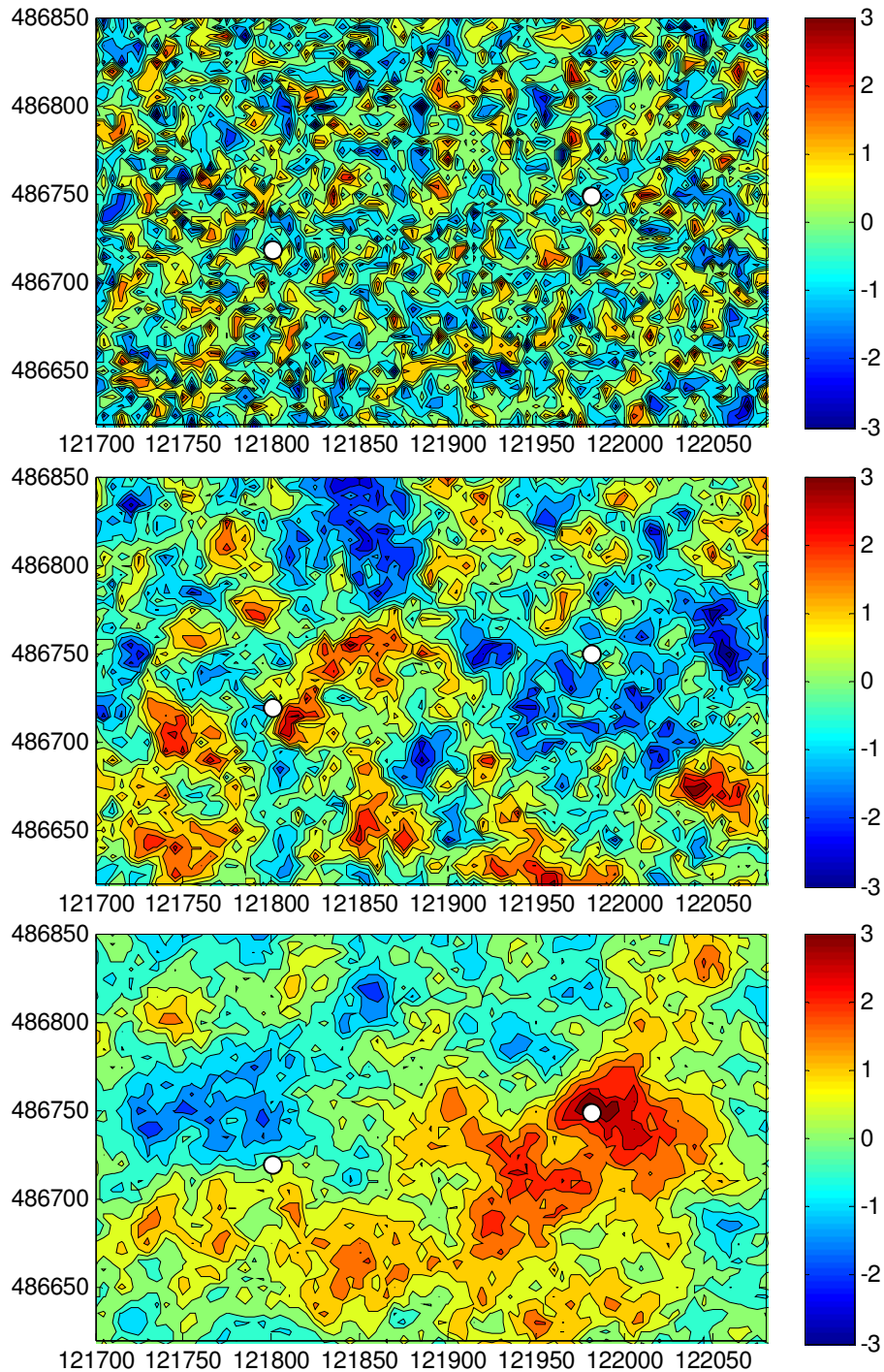
Figure 10: Spatially correlated fields as generated by Gslib, with a length-scale of 10, 50 or 200 m. Two white dots show the locations of the wells of the Stopera. The color bar gives the number of standard deviations from the mean.
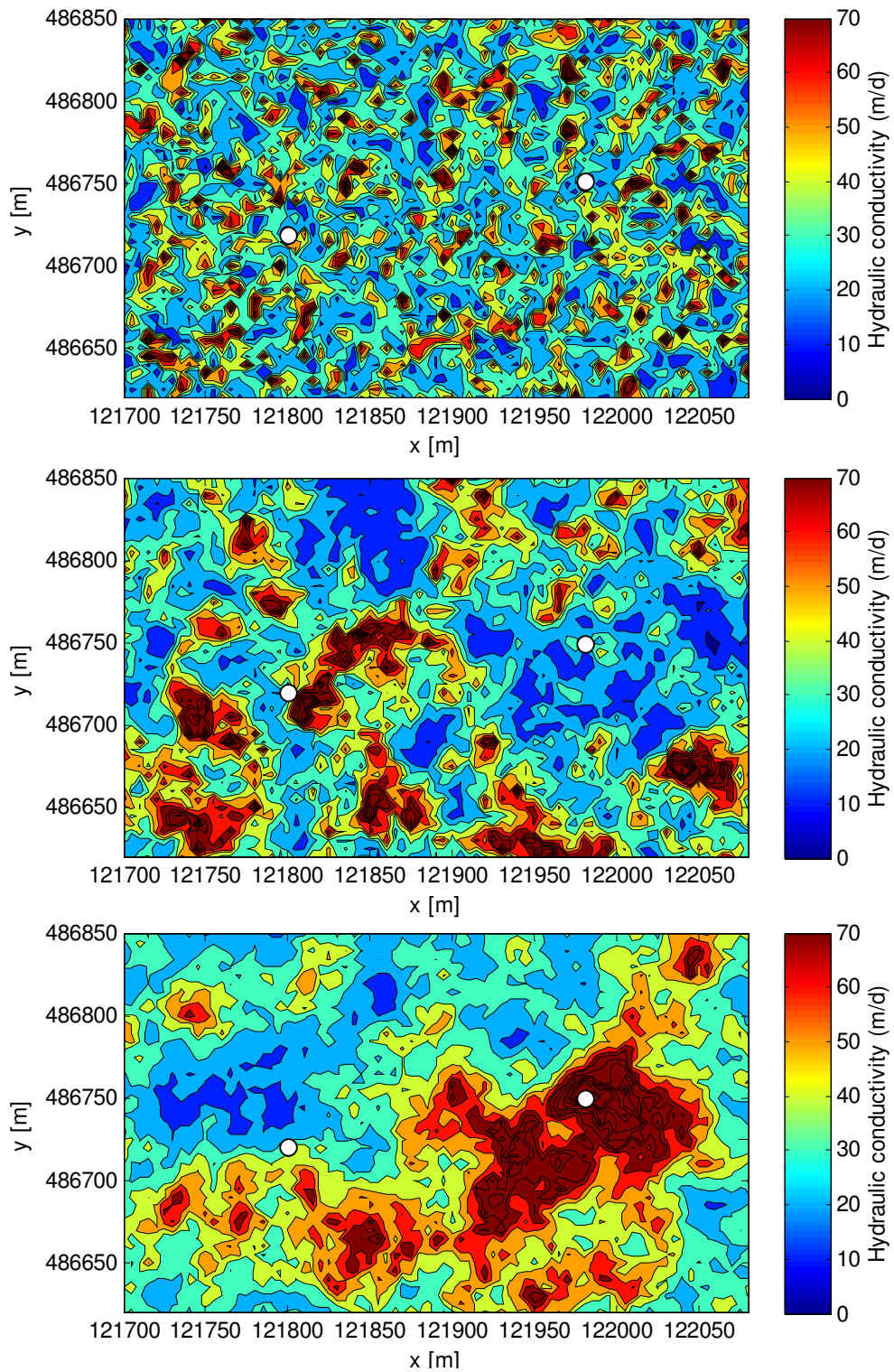
Figure 11: Spatially correlated hydraulic conductivity fields, calculated from the generated fields of Figure 10, with a length-scale of 10, 50 or 200 m. Two white dots show the locations of the wells of the Stopera.

3.2 Vertical mixing of the salinity

When an energy storage system pumps water to transport heat, it also transports solutes, of which salt is one. This can increase the salt concentration in some areas, making the groundwater less usable for drinking water production (Stuyfzand, Lebbink, & Nienhuis, 2008). The groundwater below Amsterdam is brackish; its chloride concentration increases from 0.15 to around 1 kg/m^3 at a depth of NAP -70 m. Still deeper, water is salt with chloride concentrations rising to around 10 kg/m^3 at NAP -200 m (see section 4.5.6).

The screens of energy storage wells in Amsterdam are located between NAP -70 and -200 m, right at the gradient. Therefore, these systems will inevitably mix the salt and the original vertical salt gradient will locally disappear. With the groundwater model, we quantified the area of influence for the wells of the Stopera, taking density and viscosity into account. The original discharges and temperatures of the register of the Stopera were used in this simulation, in order to quantify the mixing of the salinity for a system without an volume balance, and to attempt to simulate the increased salt concentration in the cold well, see section 5.1.

3.3 Multiple systems

One of the research questions is how the subsurface can be used as efficiently and beneficially as possible. With increasing demand for sustainable technologies, the number of ATES systems is booming the Netherlands, especially in the urban areas. The mutual influence of ATES systems increases with the number of systems installed. Therefore, ways have to be found in which the subsurface can be used to its maximum beneficial potential. The energy efficiency of several configurations of multiple systems will be calculated with a groundwater model. The Dam Square in the very centre of Amsterdam has been selected as a case study as it is not yet used for ATES systems while a dense configuration is anticipated for the near or medium term future. The case also serves as an example of how to configure ATES systems below century old intensively used city centers.

3.3.1 Different cases for the Dam Square

The first case is a mixed case where small buildings choose a monowell, and large buildings choose one or more doublets. This mixed situation is a realistic situation, which would develop without control by some governmental organization.

Energy storage for every building in a highly populated area is only possible if the parties cooperate. Therefore, the second case examines the situation where ATES systems of several buildings are clustered into groups, depending on their thermal energy demand and their location. For the Dam Square only three large cooperate systems remain, which only use doublets.

The third configuration is one in which each system takes care of its own energy supply through an ATES in the form of a monowell. If mono-wells are used for energy storage, placing of the well screens should preferably be done at pre-described depths. For the Amsterdam case for example, all warm well screens could be placed at NAP -70 to -110 m and all cold well screens from NAP -140 to -180 m. This way of organizing the subsurface is supposed to be flexible. The distance between different monowells can be small, as the wells will not affect each other negatively, at least not horizontally, when the wells pump

synchronized. Some arrangements have to be made however, to make sure that the injection temperatures of the different buildings are about the same, to prevent too much mutual influence of closely spaced monowells. Also, there can be problems, where the injected bubble of one well pushes away its neighbor. But overall monowells yield a more flexible situation than configurations with doublets, where the area around a well cannot be used by wells of another kind and more spacing is required. One of the drawbacks of monowells, however, is that their capacity is quite low, because of the vertical spacing required between the two screens (30-40 m), which cannot be used for injection or extraction. This causes large buildings to need many wells, a reason why these systems choose doublets.

The different cases are explained in more detail in section 5.2.

3.3.2   Heating of the subsurface by the Euronext system in the 1990s

Near the Dam, at the Beursplein, the Euronext building operated a cooling system for its computers from 1989 until 1999. Groundwater was used for this cooling, after which the heated water was injected again. The location of this thermal pollution, and its effects on the hypothetical ATES system of the grouped Dam Square system are investigated, using the SEAWAT model. More details can be found in section 5.3.

3.3.3   Comparing two configuration principles: with or without 'lanes'

The subsurface can be viewed in terms a little further from the geo-hydrological viewpoint, as a 'tragedy of the commons' (Hardin, 1968). This famous article describes a situation in which multiple individuals, acting independently, and solely and rationally consulting their own self-interest, will ultimately deplete a shared limited resource even when it is clear that it is not in anyone's long term interest for this to happen. To apply this theory, the subsurface could be seen as a common, where everybody desires to use it for energy storage. When this is not regulated, the subsurface would be filled, the storage capacity depleted, and ultimately many systems will not work properly anymore, causing society to reject energy storage. Therefore, some control needs to be applied, the only question is: how?

The forming of master plans for energy storage is hot issue given the rapid growth of the number of ATES in the Netherlands. To prevent mutual influence and maximize overall efficiency, such plans generally require warm and cold wells in dedicated warm and cold lanes, which are as much as possible aligned with the ambient groundwater flow. However, as development goes autonomously, the overall configuration will develop over time in a more random fashion, where each new system is optimized at the time for the situation then encountered, including the already existing ATES systems. Clearly, in the beginning, arranging systems was not necessary, and, in fact would have increased cost of early systems. Over time, as more systems are installed, the situation may reverse, and the arranging of systems in lanes might produce a more optimal situation. Therefore, it is important to compare the efficiency of forced 'laning' to a more 'laissez-faire' development.

To compare the two developments, a modeling exercise has been devised simulating a growth over time of the number of doublets in a generic fashion. All doublets are the same, consisting of two wells, requiring a given distance between warm and cold wells as well as between neighboring wells of the same type. The essence of the model is that buildings are placed randomly on a map, after which each

building tries to build an energy storage system, according to rules described below. This is done for two different simulations. The only difference between these simulations is that in one simulation the wells have to be placed in lanes, while in the other simulation buildings are free to place their wells wherever they want, as long as wells are not placed too close to each other.

In this simulation buildings and wells are placed according to the following rules:

1) 100 Buildings are placed randomly on the map in an area of 500 by 500 m, representing a city centre. When it is close (<10 m) to another building, this random search is repeated until a suitable location is found. So all buildings are placed first, before any ATES systems are planned, to simulate an existing city. From here, a randomly chosen individual building tries to install an ATES.

2) The warm well is placed, randomly on a radius of 50 m from the building. This random placement on the radius is to account for the random facts determining the location of the wells, like topography, street patterns, economic activities etc. If the thus placed warm well is too close to any building (<10 m), to another warm well (<33 m), or to a cold well (<100 m), the warm well is relocated on the radius of 50 m. This continues until the entire search radius, which is divided in 32 parts, is searched randomly, until a suitable location is found. If this is still not possible, the radius is increased by 10 m, and this radius is searched again. This continues until a distance of 150 m from the building. If it is still not possible to find a location, then it is assumed there is no possibility to place the warm well, and the building is unable to use energy storage.

3) After the warm well, the cold well is placed. Again a radius around the building of 50 m is examined. If the warm well was placed at a distance greater than this 50 m, the cold well can be placed closer to the building. So if the warm well was placed at 80 m form the building, the cold well can be placed 20 m from the building, and a radius of 20 m around the building is searched for a good location. The cold well needs to be at a distance of at least 10 m from any building, 33 m from cold wells, and 100 m from warm wells. If this is not possible, the radius is stepwise increased by 10 m until 150 m from the building, and stops if a good location is found. If this is not possible, the building is unable to use energy storage.

4) After the procedure above has been run through, the distance between the wells and the building can be calculated. This distance has to be minimized. Therefore the procedure above is repeated, but then for other distances as the initial distance from the warm well to the building, which was set to 50 m in point 2). So the procedure above is repeated for distances of 10 to 40 m between the building and the warm well. The total distance between the wells and the building is again calculated. If this distance is smaller, the new locations for the wells will be adopted.

5) Until now both simulations have the same restrictions. But for the simulation with lanes for the cold and warm wells, the lanes form an extra requirement. If a warm well is placed outside of a warm lane, the well is relocated, according to the procedures above. The same holds for a cold well. The lanes are 50 m wide, and the edge of a warm lane is 100 m from a cold lane. In this way, the distance between a warm and a cold well is always more than 100 m.

6) All 100 buildings want to use energy storage. The procedures in points 2) to 5) are repeated for every building, taking all buildings and all previously placed ATES wells into account.

7) The capacity of each well is taken to be a little higher than the average capacity in Amsterdam, as shown in section 1.4: 200000 m^3/a. This value causes the thermal radius to be 33 m, which is the reason why cold and warm wells have to be placed 100 m from each other, being three times the thermal radius, see section 4.5.7. Also, when wells of the same type are placed at a distance of at least one time the thermal radius, 33 m, the wells are thought not to increase each other's thermal bubble.

The resulting cold and warm well location can be evaluated on several criteria: the number of buildings that were able to find a location for the wells of their ATES system, the average distance between a building and its wells, and the energy efficiency of the wells. For this last criterion a groundwater model with fewer layers is used, to reduce calculation time.

4. Modeling of aquifer thermal energy storage

Since the start of the research in energy storage, models have been developed and used. Analytical solutions have been developed, for example for a confined aquifer (Shaw-Yang & Hund-Der, 2008). Also, a dimensionless approach has been used (Doughty, Hellstrom, & Fu Tsang, 1982). With increasing computational power, the opportunities of numerical modeling are growing, eliminating some of the limitations of analytical solutions. With these numerical models for instance it is possible to simulate more than one ATES system and at the same time take into account effects of viscosity and density variations, things that are generally not possible with analytical solutions. To answer the research questions stated in this report a numerical model was used. The selected model is SEAWAT, which is a fusion of MODFLOW an MT3DMS with density and viscosity added.

For the modeling with SEAWAT, no commercial Graphical User Interface (GUI) will be used. These GUIs limit the possibilities of the user and are expensive. Instead, MATLAB is used to write input files and to process the SEAWAT-output, in a way explained in Appendix 1. The MATLAB code has been written by prof. dr. ir. T. N. Olsthoorn (Olsthoorn, 2009), with some small enhancements. These enhancements are the inclusion of SEAWAT's variable viscosity (VSC) package, and some changes to allow simulation of multiple species. The MATLAB code was tested by calculating the example, taken from the SEAWAT Version 4 manual (Langevin, Thorne, Dausman, Sukop, & Guo, 2008). The results are shown in Appendix 2.

With the MATLAB code it is also possible to link one simulation to a previous simulation. This is used to model the mixing of the salt concentration occurring along the extraction well screens. The heads, temperature and the salt concentration at the end of one simulation are used as initial heads and concentrations for the next simulation. This is needed because the salt concentration of the injected water depends on the salt concentration of the extracted water. In only MODFLOW or SEAWAT this is not possible for multiple cells, but it is using MATLAB to write the input files.

4.1 MODFLOW

MODFLOW is a computer program that solves the three-dimensional groundwater flow equation for a porous medium by using a finite-difference formulation (Harbaugh, Banta, Hill, & McDonald, 2000). The code solves the following partial differential equation on a rectangular finite difference grid, subject to its boundary conditions:

$$\nabla\left(K\nabla h\right) = S_s \frac{\partial h}{\partial t} - W \qquad\qquad [10]$$

Where: ∇ is the gradient is x, y and z direction; K is the hydraulic conductivity tensor [m/d]; h is the hydraulic head [m]; W is a volumetric flux per unit volume representing sources and/or sinks [d^{-1}]; S_s is the specific storage of the porous material [m^{-1}]; and t is time [d].

For this thesis MODFLOW 2000 was used, as this is the version incorporated in SEAWAT.

4.2   MT3DMS

MT3DMS is a modular three-dimensional multi-species transport model for the simulation of advection, dispersion, and some sorption and linear reactions of constituents in the groundwater (Zheng & Wang, 1999). The transport equation being solved, with linear sorption is:

$$\left(1+\frac{\rho_b K_d}{\theta}\right)\frac{\partial(\theta C)}{\partial t}=\nabla\cdot\left[\theta\left(D_m+\alpha\frac{q}{\theta}\right)\cdot\nabla C\right]-\nabla\cdot(qC)-q_s'C_s \qquad [11]$$

Where: ρ_b is the bulk density , the mass of the solids divided by the total volume [kg/m^3]; K_d is the distribution coefficient [m^3/kg]; θ is porosity [-]; C is the concentration [kg/m^3]; D_m is the molecular diffusion coefficient [m^2/d]; α is the dispersivity tensor [m]; q is specific discharge[m/d]; q_s is the specific discharge of sinks or sources[m/d]; and C_s is the sink or source concentration [kg/m^3].

This equation expresses the rate of change of concentration in terms of dispersion, advection and sinks or sources. The rate of change is multiplied by a species-specific retardation factor, to include the effect of sorption, where there is a mass exchange of the species between the groundwater and the porous medium.

For this thesis MT3DMS version 5.2 is used. This is the latest version and also the one implemented in SEAWAT. An important improvement of this version is that different diffusion coefficients for each species can be entered, which is essential to simulate diffusion and thermal conduction simultaneously, as will be explained in section 4.4.

4.3   SEAWAT

SEAWAT combines these two models in such a way that it couples MODFLOW and MT3DMS at each time step. The flow will then be influenced by density differences of the groundwater. In this way, SEAWAT can be used to simulate three-dimensional, variable-density, saturated groundwater flow, including effects of viscosity changes with temperature (Langevin, Thorne, Dausman, Sukop, & Guo, 2008). SEAWAT uses the same input files as MT3DMS and MODFLOW and is, therefore, relatively easy to implement in existing models and to apply by experienced users of these models. The altered flow equation becomes:

$$\nabla\cdot\left[\rho\frac{\mu_0}{\mu}K_0\left(\nabla h_0+\frac{\rho-\rho_0}{\rho_0}\nabla z\right)\right]=\rho S_{s,0}\frac{\partial h_0}{\partial t}+\theta\frac{\partial\rho}{\partial C}\frac{\partial C}{\partial t}-\rho_s q_s' \qquad [12]$$

Where: ρ is the water density [kg/m^3]; μ_0 is the dynamic viscosity at the reference concentration and temperature [kg/(ms)]; μ is the dynamic viscosity [kg/(ms)]; K_0 is the hydraulic conductivity tensor of material saturated with the reference fluid [m/d]; h_0 is the hydraulic head measured in terms of the reference fluid of a specified concentration and temperature [m]; ρ_0 is the water density at the reference concentration and temperature [kg/m^3]; z is the elevation head [m]; $S_{s,0}$ is the specific storage, defined as the volume of water released from storage per unit decline of h_0 [m^{-1}]; t is time [d]; and ρ_s is the density of the source or sink [kg/m^3].

When equation [10] and [12] are compared, one can see that the first term of equation [12] corrects the hydraulic head for varying density. The term μ_0/μ includes viscosity changes of the water, which affects the hydraulic conductivity.

SEAWAT reads and writes so-called point water heads, but calculates the flow in fresh water heads. The different kinds of head are explained in Figure 12. Point water heads are the heads as they would actually be measured in a well, i.e. its tube is filled with the water surrounding the well screen. From these point water heads, fresh water heads are calculated. A fresh water head is the head in the well, when its tube would be filled with fresh water, while maintaining the same pressure at the well screen.

After this conversion the flow is calculated with the variable density flow equation [12]. The calculated fresh water heads are transferred into point water heads again upon output. The definition of fresh water head at a certain point is:

$$h_0 = z + \frac{p}{\rho_0 g}$$

[13]

Where: p is the fluid pressure [kg/(ms^2)]; and g is the gravitational acceleration [m/s^2].

Fresh water heads can be calculated from point water heads using:

$$h_0 = \frac{\rho}{\rho_0} h - \frac{\rho - \rho_0}{\rho_0} z$$

[14]
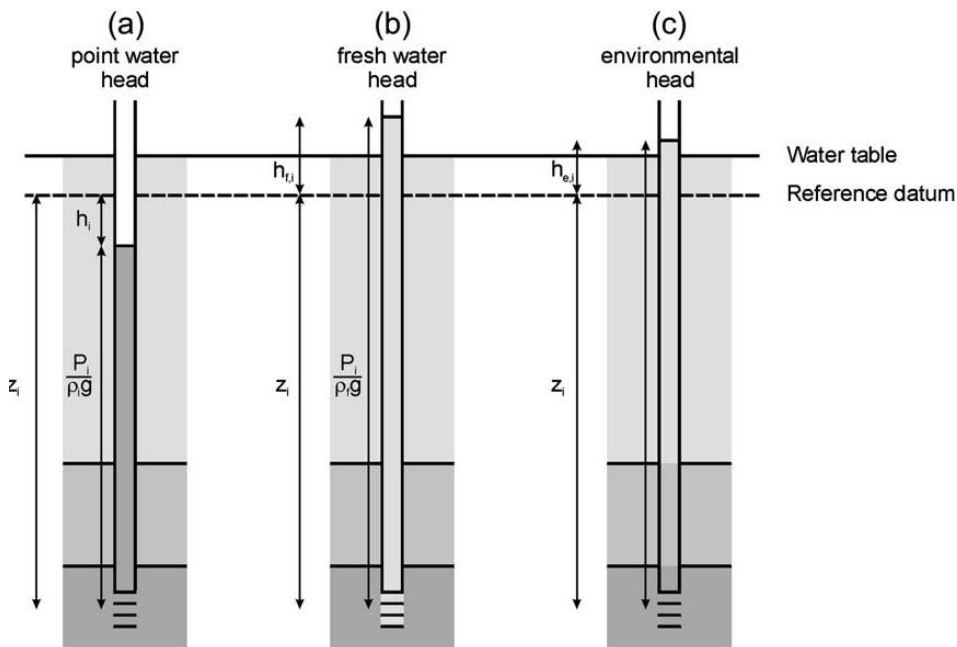
Figure 12: **Explanation of different kinds of head (Post, Kooi, & Simmons, 2007). Environmental head will be used later in section 4.5.4.1.**

4.4 Modeling heat transport

In this study the SEAWAT model was used to calculate the effects of an subsurface energy storage system. The modeling will be done with two species: salt and temperature. Equation [11] is used to calculate the transport of salt. The transport of heat is mathematically similar to the transport of a normal MT3DMS species. This is caused by the fact that the transport of heat is described by Fourier's law [15], which is mathematically equal to Fick's First law of diffusion [16].

Fourier's law states that the heat flow is proportional to the negative gradient in the temperature. The heat flux is the amount of energy flowing through a particular surface per unit area per unit time:

$$\phi_q = -k\nabla T \qquad [15]$$

Where: φ_q is the local heat flux [W m^{-2}]; k is the material's thermal conductivity [W m^{-1} ^{o}C^{-1}]; and T is the temperature [^{o}C].

Fick's First law states that the diffusion flux is proportional to the negative gradient in concentration. The diffusion flux is the amount of substance flowing through a particular surface per unit area per unit time:

$$\phi_m = -D_m\nabla C \qquad [16]$$

Where: φ_m is the diffusion mass flux [kg m^{-2} d^{-1}].

The heat transport equation can be rewritten in the following form (Thorne, Langevin, & Sukop, 2006):

$$\left(1 + \frac{1-\theta}{\theta}\frac{\rho_s}{\rho}\frac{c_{Psolid}}{c_{Pfluid}}\right)\frac{\partial(\theta T)}{\partial t} = \nabla\cdot\left[\theta\left(\frac{k_{Tbulk}}{\theta\rho c_{Pfluid}} + \alpha\frac{q}{\theta}\right)\cdot\nabla T\right] - \nabla\cdot(qT) - q_s'T_s \qquad [17]$$

Where: ρ_s is the density of the solid, the mass of the solid divided by the volume of the solid [kg/m^3]; c_{Psolid} is the specific heat capacity of the solid [J/(kg ^{o}C)]; c_{Pfluid} is the specific heat capacity of water [J/(kg ^{o}C)]; k_{Tbulk} is the bulk thermal conductivity of the aquifer material [W/m^2]; and T_s is the sink/source temperature [^{o}C].

Comparing equation [17] and [11], we see two differences: The retardation factor consists of other parameters and diffusion has been replaced by conduction. Equation [17] can be rewritten as follows, using $\rho_b = \rho_s (1-\theta)$,

$$K_{d\_temp} = \frac{c_{Psolid}}{\rho c_{Pfluid}} \qquad [18]$$

and

$$D_{m\_temp} = \frac{k_{Tbulk}}{\theta\rho c_{Pfluid}} \qquad [19]$$

into

$$\left(1+\frac{\rho_b K_{d\_temp}}{\theta}\right)\frac{\partial(\theta T)}{\partial t} = \nabla \cdot \left[\theta\left(D_{m\_temp}+\alpha\frac{q}{\theta}\right)\cdot \nabla T\right] - \nabla \cdot (qT) - q_s' T_s \qquad [20]$$

Where: D_{m_temp} is the thermal conduction term [m^2/d]; and K_{d_temp} is the thermal distribution factor [m^3/kg].

Equation [20] is similar to equation [11]; therefore SEAWAT can model heat transport in the same way as solute transport. The only difference is that the constants K_d and D_m will have different values.

4.4.1 Density dependency on temperature

The density of fresh water reaches its maximum at 4 ^{o}C. When the temperature rises above or drops below this temperature, the density will decrease. The rate at which the density decreases, increases with the difference between the temperature and this 4 ^{o}C, and therefore the relationship between density and temperature is non-linear (The Engineering Toolbox, 2009), as can be seen in Figure 13.

In SEAWAT however, the density can only be coupled to temperature following a linear relationship. Therefore, an approximation has to be made valid for the expected temperature values. This approximation has to represent the temperatures in an energy storage, which ranges from 9 to 17 ^{o}C in this thesis. The approximation is showed in Figure 13 as well.
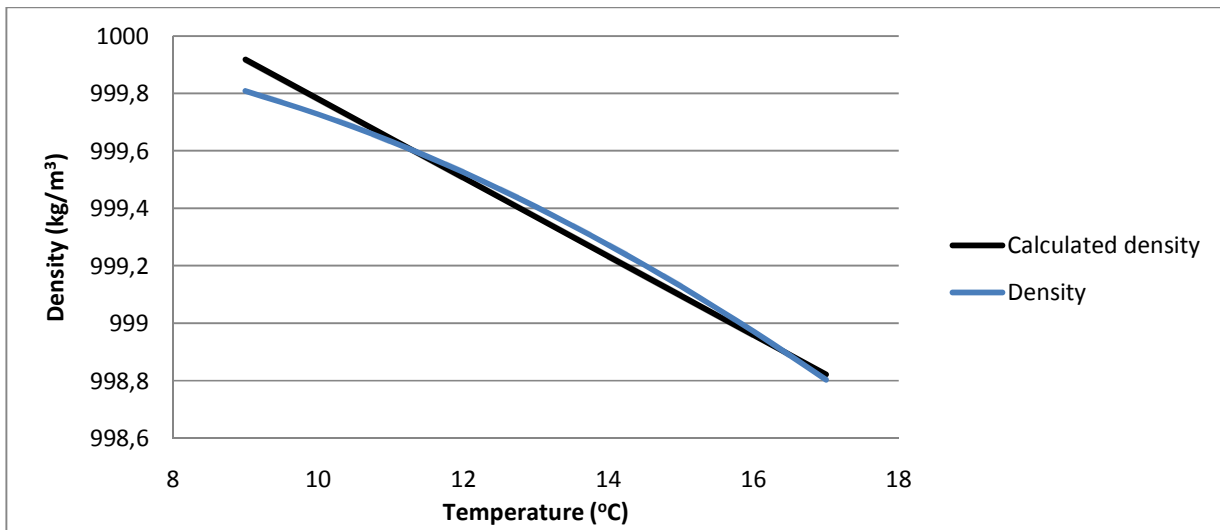
Figure 13: The relationship between temperature and density for fresh water, together with the approximation in SEAWAT.

4.4.2 Density dependency on salt concentration

The density dependence of water on salinity, over the ranges encountered in groundwater, is essentially linear. Therefore it is straightforward to implement this in SEAWAT. The dependency of the density of water of 13 ^{o}C on the salinity of water is shown in Figure 14. The salinities which are expected in the subsurface of Amsterdam from NAP 0 to -200 m range from 0 to 10 kg/m^3 (see section 4.5.6).
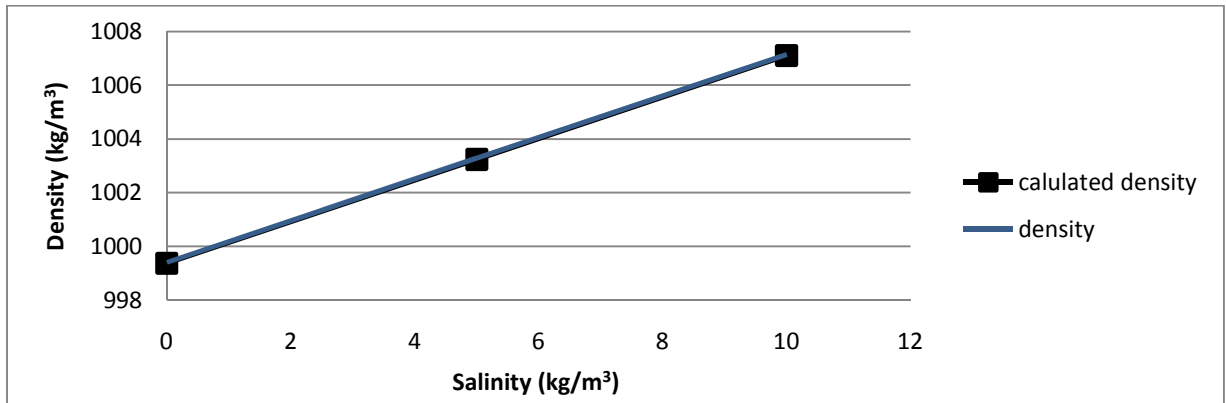
Figure 14: The relationship between density and salinity of water of 13°C, together with the calculated density in SEAWAT.

The equation of state of the density of water, specifically for the ranges used in this report, can be approximated by the addition of the temperature effects and the salinity effects by the following formula:

$$\rho = \rho_0 + \frac{\partial \rho}{\partial T}(T - T_0) + \frac{\partial \rho}{\partial C}(C - C_0) = 1000 - 0.137(\text{T} - 8.4) + 0.773(C - 0) \qquad [21]$$

Where: T_0 is the reference water temperature [°C]; and C_0 is the reference salinity concentration [kg/m³].

These calculated values have been compared to measured density values (Encyclopædia Britannica Online, 2009). The result is shown in Figure 15. For higher salinity values, the density drops a little more with increasing temperatures than for lower salinity values. This difference, however, is much less than the error caused by the temperature dependency of the density.
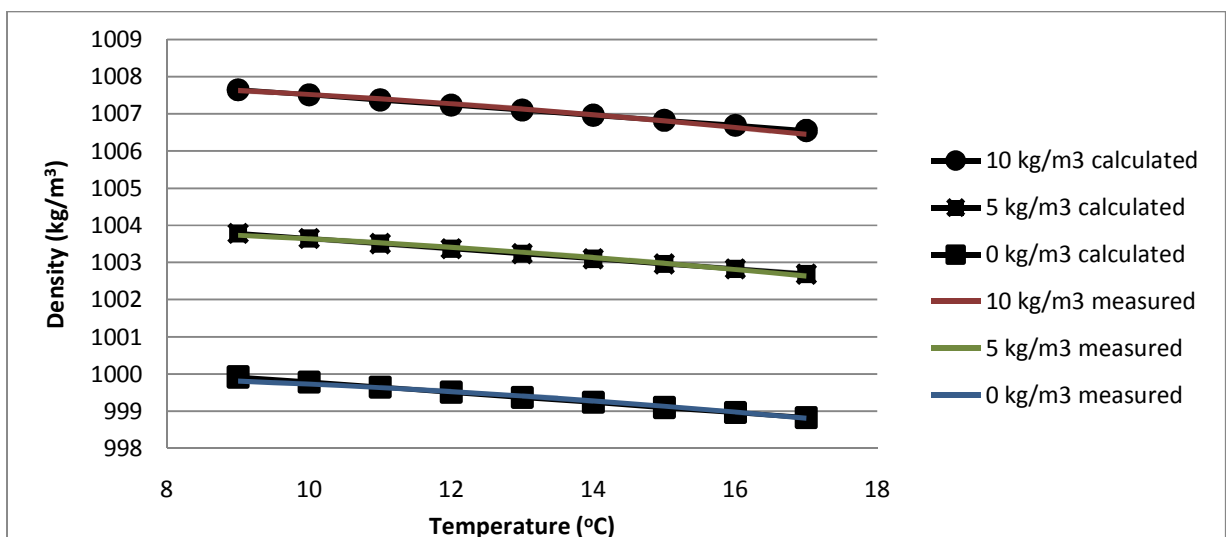
Figure 15: The relationship between density, temperature and salinity for water at atmospheric pressure.

4.4.3 Viscosity dependency on temperature

The viscosity of water decreases with increasing temperature. Therefore, water will flow more easily and hence faster with increasing temperature. SEAWAT supports several formulas to model this relation. The two most sophisticated formulas are those of Voss and Pawlowski. Figure 16, shows a comparison of these two formulas with measurements (The Engineering Toolbox, 2009). The error in the formula of Pawlowski is less in most points and especially in the temperature range considered in this thesis (5-15 ^{o}C). Therefore the formula of Pawlowski is chosen to represent the dependence of viscosity on water temperature. The formula of Pawlowski is:

$$\mu(T) = 10^{-3}\left(1 + 0.015512(T - 20)\right)^{-1.572}$$

[22]
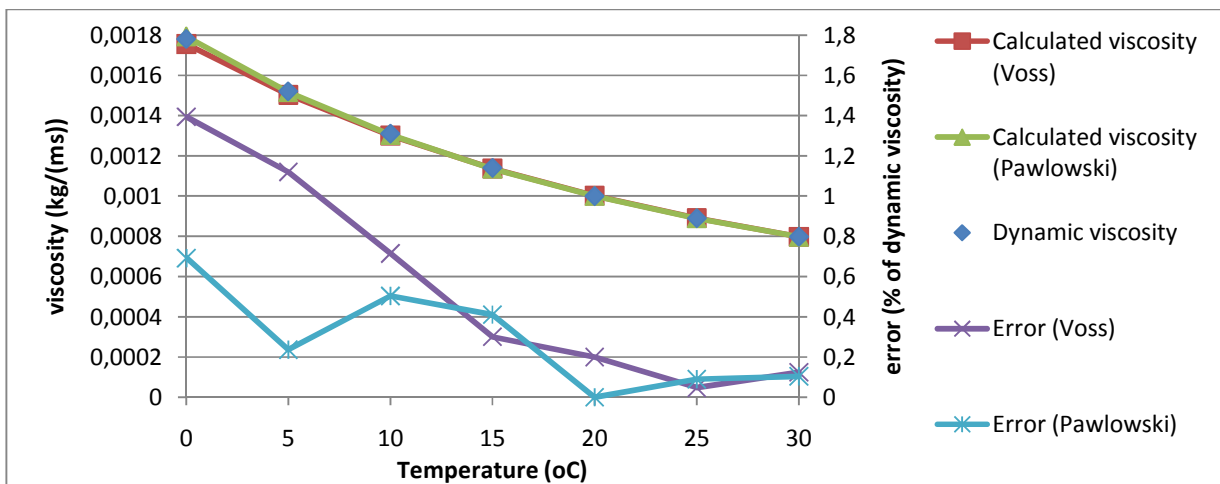
Figure 16: **The relationship between viscosity and temperature, calculated using two different formulas and compared with measurements. The relative error between these formulas and the measurements is also shown. The dimension of viscosity is Ns/m^2 = kg/(ms)**

4.4.4 Viscosity dependency on salt concentration

The dependency of viscosity on the salt concentration of the water can be neglected. There is some dependency, but this is a few orders of magnitude smaller than the dependency on the temperature.

4.5 Elements of the model

4.5.1 Mathematical solution technique

MT3DMS, where SEAWAT is based on, contains several solution techniques for calculating transport of solutes. These can be categorized into three groups: finite difference methods (explicit and implicit), particle tracking methods (MOC, MMOC and HMOC) and the TVD method. The methods each have their own disadvantages and advantages (Schäfer), described in Table 2.

The TVD method stands for 'Total Variation Diminishing'-method. This method is a higher order finite difference method, which minimizes numerical dispersion, but can introduce oscillations in the solution. Therefore, numerical procedures, called flux delimiters, are used to eliminate these oscillations. The TVD-scheme used by MT3DMS is a third-order scheme based on the ULTIMATE algorithm. A universal flux limiting procedure is used to minimize oscillations.

Table 2:   Different solution techniques for MT3DMS and some of their properties.

	FD Explicit	FD Implicit	MOC	MMOC	HMOC	TVD
Computational effort or storage demand	Low	Medium	Large	Low	Large	Large
Numerical dispersion or oscillations	Large	Large	Null	Medium	Small	Small
Mass balance	Exact	Exact	Not Exact	Not Exact	Not Exact	Exact
Maximum time step	Small	Large	Large	Large	Large	Small

The TVD method was selected the most optimal method for this study for several reasons:

- The main reason is limitation of numerical dispersion with salt displacement in radial flow with small Peclet numbers near the wells. The temperature will have a large diffusivity, so numerical dispersion is not expected to be a big problem. For salt however, where the diffusivity is small, large numerical dispersion could be a problem. Therefore a solution method is chosen with small numerical dispersion.
- With the model the recoverable energy will be computed in combination with the efficiency of the energy storage system. Therefore the available energy and energy fluxes should follow a mass balance, and an exact mass balance is desired, which requires a finite difference solution.
- The maximum time step size should must be limited for accuracy reasons, and therefore does not limit the solution technique. The model will not be used for calculating very long time-series in the order of centuries, and so very large time steps are not needed.

4.5.2   Grid

The size of the grid cells varies to accommodate detail near the location of the cells. In the horizontal surface the cells will have a constant size close to the wells, within 100 m, of 5 by 5 m. In this area are the largest flow and temperature differences, and therefore needs to be calculated more precisely than in the rest of the modeled area. Further away from the wells, the cell size increases stepwise by a factor of 1.2. In chapter 5 the calculation grids for the different cases are shown. For the calculations with the Dam Square (3.3.1) and the simulation of a city (3.3.3), the minimum cell size was increased to 10 by 10 m, as otherwise the calculation would take too long.

The layers in the model have a maximum thickness of 5 m. If the thickness of one aquifer or aquitard is more than 5 m, the thickness of this aquifer or aquitard is equally divided by the largest division below 5. So if there is an aquifer of 12 m thick, this will result in three layers of 4 m.

To model the simulations of a city fewer layers will be used, in order to reduce calculation time so that multiple simulations can be calculated. This simplification produces a subsurface with only five layers, where the wells are located in just one model layer, as shown in Table 3.

From NAP	Until NAP	Thickness	Horizontal hydraulic conductivity	Screen of ATES
0	-65	65	0.004	No
-65	-80	15	37	No
-80	-160	80	37	Yes
-160	-200	40	37	No
-200	-230	30	5	No

4.5.3   Time steps

The time step in the calculations was determined by the courant number, which is set to 1. This means that a water drop will never travel more than 1 cell per time step anywhere in the model region. In this way, the results stay accurate. When the TVD method is used, the courant number has to be below 1 anyway, because of stability constraints. On top of the courant constraint, a transport step has a maximum value of 1 day, so the accuracy of the solution will remain high, even when none of the wells is pumping.

4.5.4   Boundary Conditions

4.5.4.1   Head boundaries

Head boundaries are placed at the four vertical boundary surfaces of the model. The boundary conditions should be implemented in such a way, that there is no vertical flow at the boundaries. In other words, the flow should be hydrostatic, q_z=0. This is accomplished when the change of fresh water head with depth cancels out with the buoyancy term from the left side of equation [12]:

$$buoyancy\_term = \frac{\rho - \rho_0}{\rho_0} \nabla z \qquad\qquad [23]$$

This is done by giving the boundary a constant environmental head. Environmental water head is the head in a well, when its tube would be filled with the water along the vertical above that point (Lusczynski, 1961), see Figure 12. Therefore the buoyancy term cancels out, and the normal flow equation [10] can be used in terms of environmental head.

4.5.4.2   Temperature boundaries

The four vertical boundary surfaces of the model have a temperature boundary condition, implemented in the following way: only advective transport (no dispersive/diffusive transport) is allowed across the boundary (ITYPE = 1 in the SSM input file). In this way inflowing water will have a temperature according to the boundary condition. If water is flowing out of the model over the boundary, the temperature at the boundary will be the same as this out flowing water, and not of the boundary condition.

The boundary causes an error, when the flow turns around. This is explained in the case of an energy storage system for warm water: First warmer water is flowing out of the model. When the flow is turning around, and water is flowing into the model, this water will have a temperature equal to the temperature boundary. In this way some heat may lost to the boundary. Therefore the boundary should

be placed far enough from the wells, so that the temperature at the boundaries is not affected by the wells. As the boundaries are at least 1000 m from the wells, this condition is met in this study.

4.5.4.3 Salt concentration boundaries
The type and location of the salt concentration boundary conditions are the same as for the temperature boundaries.

4.5.5 Initial temperatures
The initial temperatures of the aquifer are taken from a temperature map of the shallow subsurface in the Netherlands (van Dalfsen, 1981), modified with extra measurements by IF Technology. Van Dalfsen created maps for every 25 m until 250 m below the surface. From these maps and from measurements at the Stopera and Euronext it is concluded that the temperature of the subsurface is higher beneath Amsterdam than in its surroundings. The temperature in Amsterdam rises from 12 $^{\circ}$C at the surface until 14.5 $^{\circ}$C at 250 m depth. To simplify the modeling and the analysis of results, a constant initial temperature of 13 $^{\circ}$C was adapted everywhere in the subsurface. In this way, the charged and supplied amount of energy can be calculated with respect to this ambient groundwater temperature. Otherwise the charged and supplied amount of energy would also depend on the depth of injection or extraction.

4.5.6 Initial Salt Concentrations
The salt concentrations of groundwater below the center of Amsterdam were taken from the groundwater map of the Netherlands (Speelman & Houtman, 1979), combined with measurements from nearby wells. From the map and the data a certain relationship between the salt concentration and depth is adapted, shown in Figure 17. The salt concentration is assumed to be constant at 1 kg/m^3 until a depth of 70 m, from where the salt concentration increases linearly until 10 kg/m^3 at 200 m depth.
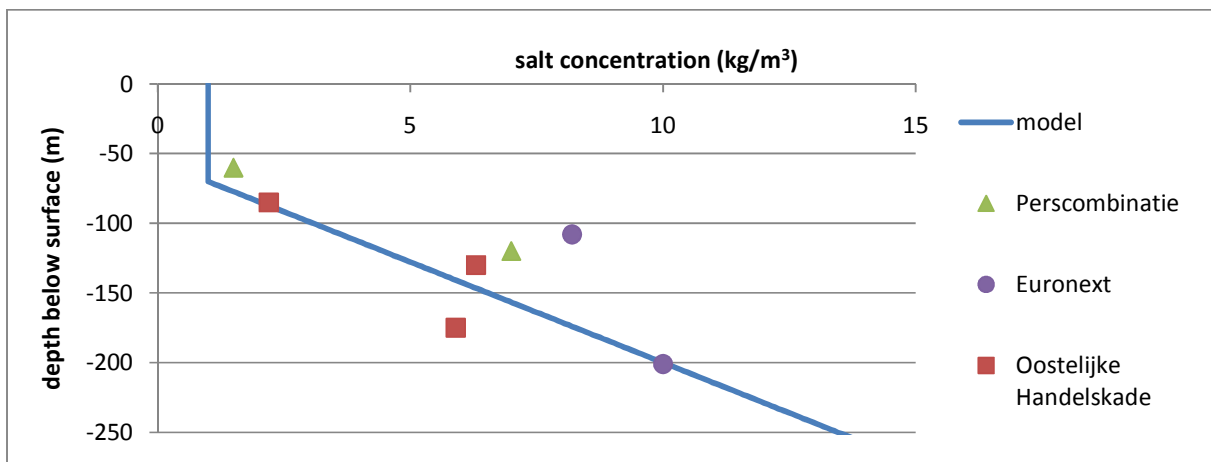
Figure 17: The adopted and measured salt concentrations in the subsurface of the center of Amsterdam.

4.5.7 Wells
A well screen in the model is divided over multiple cells along the vertical axis. For instance those of the Stopera are 70 m long, while the maximum layer thickness is 5 m. These wells, therefore consist of more than 14 cells. There are several ways to implement such multiple node wells. The discharge of the well can be apportioned among the nodes on the basis of the transmissivities, according to equation [24]:

$$Q_{i,j,k} = T_{i,j,k} \frac{Q}{T_{sum}}$$ [24]

Where: $Q_{i,j,k}$ is the pumping rate from an individual cell on row i, column j and layer k [m^3/d]; Q is the total pumping rate from the well [m^3/d]; $T_{i,j,k}$ is the transmissivity of the cell penetrated by the well on row i, column j and layer k [m^2/d]; and T_{sum} is the sum of the transmissivities of all cells penetrated by the well [m^2/d].

The use of the Multi-Node Well (MNW) package (Halford & Hanson, 2002) would be a better choice to implement the ATES wells. In this package the hydraulic head in the well is recalculated for every node of the well, by adjusting the flows from each node in an extra iteration cycle, until the hydraulic head in the entire well is constant. In this way a more realistic allocation of the total pumping flow among the different cells is possible, because not only transmissivity differences are taken into account, but also storage differences and differences in hydraulic head between layers. Not only are the properties of the cell in which the well is located used to calculate the flow to that cell, but also the properties of the surrounding cells.

Unfortunately, there are some problems when combining the MNW-package with SEAWAT. The package only works in fresh water zones, as the package does not take variable density flow into account. On top of that, there was an error in the SEAWAT program. The MNW flows used by MT3DMS were a time step off, causing the transport to lag behind the flow solution by one time step. This error has been corrected in the latest SEAWAT version though. For these reasons it was impossible to combine the MNW-package directly with SEAWAT for variable density flow. The MNW package was used with only MODFLOW to see if the approximation of equation [24] was correct. This turned out to be the case, as the MNW package calculated only slightly different discharges per node. For the calculation of the horizontal heterogeneities however, equation [24] might not be correct, since this equation only deals with the hydraulic conductivity at the cell in which the well resides. Therefore, the MNW package was used in combination with MODFLOW to determine the flows from each cell of a well. These flows were then applied in the WELL package, which was used in the simulations with SEAWAT with variable density flow.

For the Dam Square case, a certain distribution of the yearly energy demand over the months has been adopted. This division is based on the average monthly temperature. Heating is needed if the temperature drops below 15 ^{o}C and cooling is needed if the average monthly temperature exceeds 5°C. The amount of cooling or heating depends on the squared difference between these temperatures and the average monthly temperature. In this way, a realistic situation occurs, where most of the heating or cooling takes place in winter and summer months, and cooling and heating can take place at the same time in spring and autumn months. This division also causes a difference between buildings, depending on the ratio of yearly needed heating and cooling, which is building specific. A building needing more cooling will supply cold water in October, while charging warm water into the warm well. Another building requiring more heating will be supplying warm water, while loading cold water into the cold well in that same month of October. The result can be seen in Figure 18.
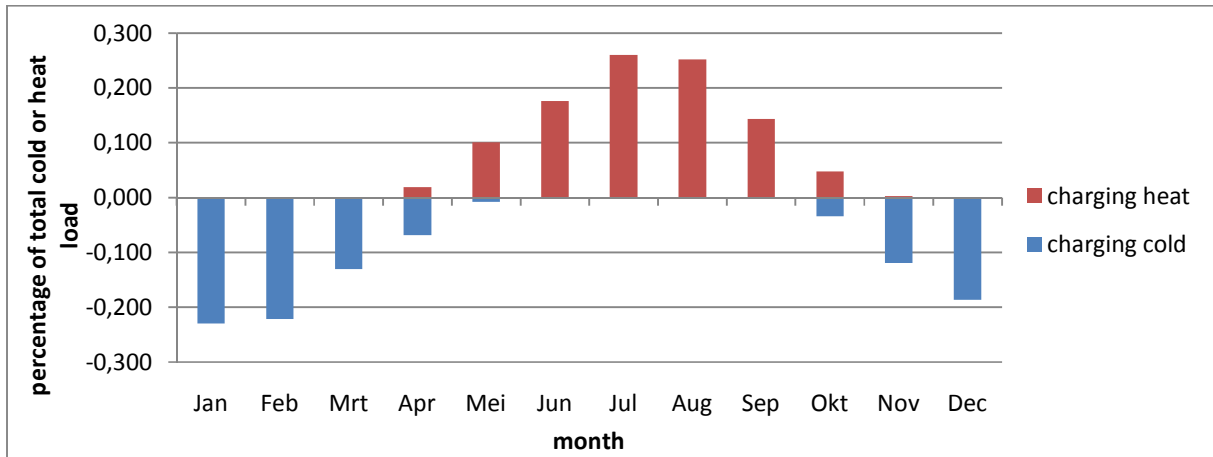
Figure 18: The division of heat and cold loading during the year.

The well data is registered by ATES operators in monthly values, as required in their permits. During one month it is possible that a well injects and extracts at different days. On the monthly scale this implies that a well has been pumping and injecting in the same time span. The way this discharge is divided over the days of a month is unknown from the registration. Therefore, a constant discharge is assumed by dividing the discharge of a well by the number of days in a month. This monthly discharge is obtained by subtracting the discharged water from the injected water, which makes that for each well there is either injection or discharge in a given month. For most months this is not a problem, since the monthly injected amount of water for a single well is much larger than the discharged amount of water, or the other way around (in summer or winter). But during months where the discharge and injection are of the same order (in spring or autumn) an error may occur, which, however, does not have a substantial effect.

For the design of wells, which needs to be done for the case of the Dam Square, several formulas are used. In the next section these formulas are given. According to the directives of the Dutch Society of Subsurface Energy storage, the 'Nederlandse Vereniging voor Ondergrondse Energieopslagsystemen' (N.V.O.E., 2006), the amount of water that needs to be pumped to produce a certain amount of energy can be calculated with the following equation:

$$Q = \frac{P_t}{c_{P_{fluid}} \rho \Delta T}$$

[25]

Where: P_t is the required capacity [W].

Equation [26] shows the equation for the thermal radius of an energy storage system. In general there should be a distance of three times the thermal radius between the wells of a doublet. This formula is valid as long as the system has a thermal balance and thermal shortcutting should be avoided. For monowells, thermal shortcutting does not have to be avoided, but instead sufficient vertical distance between the two screens is to be taken into their design. Therefore, for monowells the thermal radius does not have to be considered.

$$r_{th} = \sqrt{\frac{c_w Q u_{eq}}{c_a H \pi}}$$

[26]

Where: r_{th} is the thermal radius of the stored cold or heat [m]; c_w is the heat capacity of water [J/(m^3 ^{o}C)]; Q is the discharge in the well [m^3/h]; u_{eq} is the number of full-load hours [h]; c_a is the heat capacity of the aquifer [J/(m^3 ^{o}C)]; and H is the length of the screen [m].

The values for c_w and c_a can be found by multiplying the specific heat capacities from section 6.3 by their density.

In a Novem-study (IF Technology, 2001) a design standard for infiltration wells is given to limit well-clogging, according to the following formula:

$$v_{des\_i} = 1000 \left(\frac{K}{150} \right)^{0.6} \sqrt{\frac{v_v}{2 MFI_{mea} u_{eq}}}$$

[27]

Where: v_{des_i} is the design injection Darcy speed [m/h]; K is the conductivity of the aquifer [m/d]; v_v is the specific clogging speed [m/year]; MFI_{mea} is the measured Membrane filter index[s/l^2]; and u_{eq} is the number of equivalent full load hours per year [h].

The *MFI* can be taken as 2 s/l^2, if no other information is available, and the specific clogging speed is set to 0.1 m/year. For extraction wells the equation is:

$$v_{des\_e} = \frac{K}{12}$$

[28]

Where: v_{des_e} is the design extraction Darcy speed [m/h]; and K is the hydraulic conductivity [m/d].

The surface of the well can be found by:

$$Q = v_{des} A$$

[29]

Where: A is the surface of the borehole wall: $A = \pi * D * H$ [m^2]; and D is the diameter of the borehole [m].

For a well with a diameter of 800 mm, a screen with a length of 110 m in an aquifer with a hydraulic conductivity of 37 m/d and a porosity of 0.35, the maximum injection discharge in a well is 546 m^3/h. This discharge is large, caused by the large screen length. Water pumps with this capacity are not used normally. The maximum discharge is therefore set to the largest standard system (De Ruiter Boringen en Bemalingen bv): 200 m^3/h.

4.5.8 Ambient groundwater flow

No data about the groundwater flow at depths of -100 to -200 m was found in the groundwater maps of the Netherlands. These only contain head gradients for the first aquifer. According to the NVOE directives the gradient in Amsterdam is 0.2 ‰ in West/Southwest direction. This gradient was taken into

account in the model, by incorporating it in the head boundary and initial conditions. Together with a hydraulic conductivity of 37 m/d (see section 6.1), this causes the following flow velocity:

$$v = \frac{K\,i}{\theta}365 = \frac{37\,x\,0.00025}{0.35}365 = 9.6$$ [30]

Where: v is the flow velocity [m/a]; and i is the hydraulic gradient [-].

This is a low value compared to other locations in the Netherlands (N.V.O.E., 2006).

4.5.9 Other parameters
The other parameters that are used in the model are shown in Table 4.

Table 4:   Parameters for the SEAWAT model.

Hydraulic conductivity	K_x, K_y, K_z	See section 6.1	m/d
Thermal conductivity	k	See section 6.2	W/(m°C)
Thermal retardation factor	R	See section 6.3	(-)
Bulk density of the aquifer medium	ρ_s	1700	Kg/m^3
Effective molecular diffusion coefficient	$D_{m\_salinity}$	1.0 x 10^{-10}	m^2/d
Longitudinal dispersivity	α_L	5 (Gelhar, Welty, & Rehfeldt, 1992)	m
Horizontal Transverse dispersivity	α_{TH}	0.5	m
Vertical Transverse dispersivity	α_{TV}	0.05	m
Specific storage	S_s	0.0001 (ρ_wg(nβ+α)) (Fitts, 2002)	m
Specific yield	S_y	0.2 (Johnson, 1967)	m
Porosity	θ	0.35	-

4.6 Hydraulic effects of ATES systems
The hydraulic effects of ATES systems are their combined influence on groundwater heads is expressed in drawdown. The drawdown can be calculated in several ways. The steady state drawdown of a single well can be calculated with the Thiem equation [31]. For transient flow, Theis's solution [32] can be used.

$$h - h_0 = -\frac{Q}{2\pi T}\ln\left(\frac{r}{r_0}\right)$$ [31]

Where: h_0 is the known drawdown at a certain point r_0 away from the well [m]; Q is positive when infiltrating [m^3/d]; T is the transmissivity of the aquifer [m^2/d]; r_0 is the radius of a point where h_0 is measured [m]; and r is the distance where the drawdown is calculated [m].

$$h - h_0 = \frac{Q}{4\pi T}E_1\left(\frac{r^2 S}{4T(t - t_0)}\right)$$ [32]

Where: E_1 is the well function or exponential integral; T is the transmissivity [m^2/d]; and S is the storativity [-].

The steady state effects of the two wells of an ATES doublet can be computed by superposition:

$$h - h_0 = \frac{Q}{2\pi T} \ln\left(\frac{r_1}{r_2}\right)$$

[33]

Where: r_1 is the distance to the pumping well, with a discharge of $-Q$ [m]; and r_2 is the distance to the injecting well of the same doublet, having a discharge $+Q$ [m].

At distances larger than about twice the distance between the two wells, they cancel each other out, and there will be almost no difference in groundwater level caused by the wells. As an example, the drawdown for the Stopera wells is shown in Figure 19. This drawdown is calculated with a discharge of 260 m^3/h.
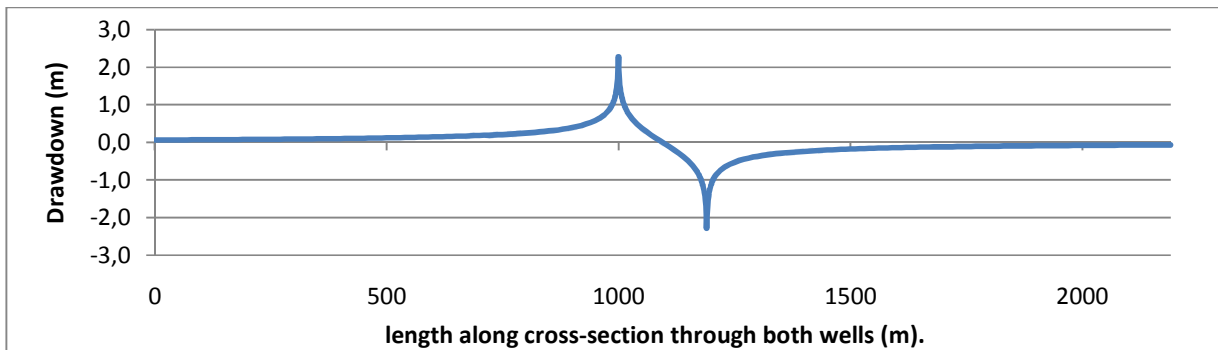
Figure 19: Drawdown of the wells of the Stopera in a cross-section through both wells, for the maximum discharge of 260 m^3/uur.

4.7 Energy efficiency computations

There are several ways to calculate energy and efficiency of ATES systems, depending from which viewpoint this is considered. When an energy specialist examines an ATES he wants to know how much energy was delivered to a building, and how much energy the building charges into an ATES, which can be calculated using the formulas in section 4.7.1. From these the efficiency from the buildings perspective can be determined.

A geohydrologist wants to know how much energy was injected and extracted in and from the wells, which can be calculated using the formulas in section 4.7.2. The difference between the injected and extracted energy is caused by losses (see section 1.5), which bring the temperature of the water back to the ambient groundwater temperature. Therefore, energy is defined with regard to the ambient groundwater temperature. When all energy is lost, the water will have the ambient groundwater temperature, and the supplied energy is zero, and so the efficiency will be zero as well. When there are no losses, the extracted temperature is the same as the injected temperature, and the supplied amount of energy is equal to the charged amount of energy, provided the pumped volume is equal, and the efficiency will be one. This computation is also useful as the ATES permit and sustainability require an energy balance in order to maintain the original groundwater temperature over time.

A different way to express efficiency may be in terms of exergy, see section 4.7.3. The results of these calculations are more difficult to interpret, however. Also, the development in time of the efficiency and the comparison of different ATES setups did not provide any different results between energy and exergy. The only difference is that the exergy efficiency is always lower than the energy efficiency. Therefore, in the rest of this thesis, the energy efficiency from the viewpoint of the wells, with regard to the ambient groundwater temperature, is used.

Because the wells consist of several calculation cells, the temperature of the water extracted from a well is the weighted average of the temperature of the different model screen cells. The weights are determined by the flow from each cell relative to the total well flow. The temperature of a well is calculated according to:

$$T_e = \sum \left(Q_{i,j,k} \frac{T_{i,j,k}}{Q} \right)$$
[34]

4.7.1 Energy to and from the buildings

From the modeled temperatures, energy flowing to and from the building can be calculated from the temperature difference of the extracted water from one well and the injected water into the other, with the following formulas:

$$E_c^b = Q_c c_p \rho (T_e^w - T_i^k) * dt$$
[35]

$$E_s^b = Q_s c_p \rho (T_i^w - T_e^k) * dt$$
[36]

Where: E_c^b and E_s^b are charged and supplied amount of energy from and to the building [J]; Q_c and Q_s are the discharges, used for charging and supplying [m^3/d]; T_i^w and T_e^w are the temperatures of the injected and extracted water in and from the warm well [^{o}C]; T_i^k and T_e^k are the temperatures of the injected and extracted water into and from the cold well [^{o}C]; and dt is the model time step [d].

4.7.2 Energy to and from the wells

Equation [35] and [36] express the energy charged and supplied from and to the building. If the energy supplied and charged from or to a well is taken into account, the efficiency of a single well can be calculated. This efficiency can be used to evaluate the influence of certain well characteristics or certain configurations of wells. The charged and supplied energy amount of energy can be calculated, relative to the original groundwater temperature, with the following formulas:

$$E_c^w = Q_{in} c_p \rho (T_{in} - T_0) dt$$
[37]

$$E_s^w = Q_{ext} c_p \rho (T_{ext} - T_0) dt$$
[38]

Where: Q_{in} and Q_{ext} are the injected and the extracted discharges [m^3/h]; T_{in} and T_{ext} are the temperature of the injected and extracted water [^{o}C]; and T_0 is the original groundwater temperature [^{o}C].

4.7.3 Exergy

Instead of energy analysis, the performance of an ATES system can also be evaluated using exergy (Rosen, 1999). Exergy analysis is called a second-law analysis, as it is based on the second law of thermodynamics. Exergy is the potential of a system to cause a change as it achieves equilibrium with its environment. It is zero when equilibrium is reached. When using exergy instead of energy, not only the energy of the supplied water is taken into account, but also the temperature at which it is supplied. The difference can best be explained using an example. Suppose an ATES system stores water at 20 $^\circ$C against an ambient temperature of 10 $^\circ$C and retrieves it at 15 $^\circ$C. Another system also stores water at 20 $^\circ$C against an ambient temperature of 10 $^\circ$C, but retrieves it at 11 $^\circ$C and pumps 5 times more water than the first system. The amount of pumped energy is the same in both systems. Nevertheless, the temperature of the second system is far less useful, as much more energy for water and heat pumps is needed to retrieve the energy from the water. Besides, when you have to pump five times more water, you are also dispersing thermal energy in the subsurface and thereby will change groundwater temperature over larger volumes. Also, more mutual interference must then be anticipated. With an exergy analysis this temperature quality is taken into account. The amount of retrieved exergy is much more for the first system than for the second.

The formulas for the charged and supplied amount of exergy are shown in equation [39] and [40]. The first term is the same as the charged or supplied amount of energy, while the second term gives the loss of the quality of energy.

$$\varepsilon_c = Q_{in} c_p \rho \left((T_{in} - T_0) - (T_0 + 273) \ln\left(\frac{T_{in} + 273}{T_0 + 273} \right) \right) dt \qquad [39]$$

$$\varepsilon_s = Q_{ext} c_p \rho \left((T_{ext} - T_0) - (T_0 + 273) \ln\left(\frac{T_{ext} + 273}{T_0 + 273} \right) \right) dt \qquad [40]$$

Where: ε_c and ε_s are the charged and supplied amount of exergy [J].

4.7.4 Efficiency

For both energy and exergy the efficiency of the wells can be calculated by the following equations:

$$\eta_E = \frac{E_s}{E_c} \qquad [41]$$

$$\eta_\varepsilon = \frac{\varepsilon_s}{\varepsilon_c} \qquad [42]$$

Where: η_E and η_ε are the energy and exergy efficiency [-].

5. Cases

5.1 Stopera

The Stopera ATES system was selected to be used for the examination of a single system. The Stopera is a complex building that houses both the city hall of Amsterdam and the 'Muziektheater', the principle opera house of the Netherlands. The location of the Stopera is in the heart of the old city centre of Amsterdam and a photo can be seen in Figure 20. It is a well known

Figure 20: The Stopera.

building to the people of Amsterdam, possibly because it differs significantly in style from its surroundings. The building was finished in 1986 and since October 2002 an aquifer thermal energy storage system is operating below the building. This project was chosen as the example project, because quite a lot of data is available, as the project is relatively old compared to other energy storage systems in the Netherlands. Also, the Stopera is close to the Dam Square, which is used for the second part of this research. Therefore, the geo-hydrologic conditions of these two projects are similar.

Figure 21 shows the charged and extracted amounts of energy to and from the aquifer. During winter the system is charging cold water to the aquifer and during summer it extracts cold water from the aquifer. The water that is heated up, as a result of cooling the building in summer, is injected in the warm well at a temperature close to the original groundwater temperature. So this system is not a complete energy storage, but only a cold storage.
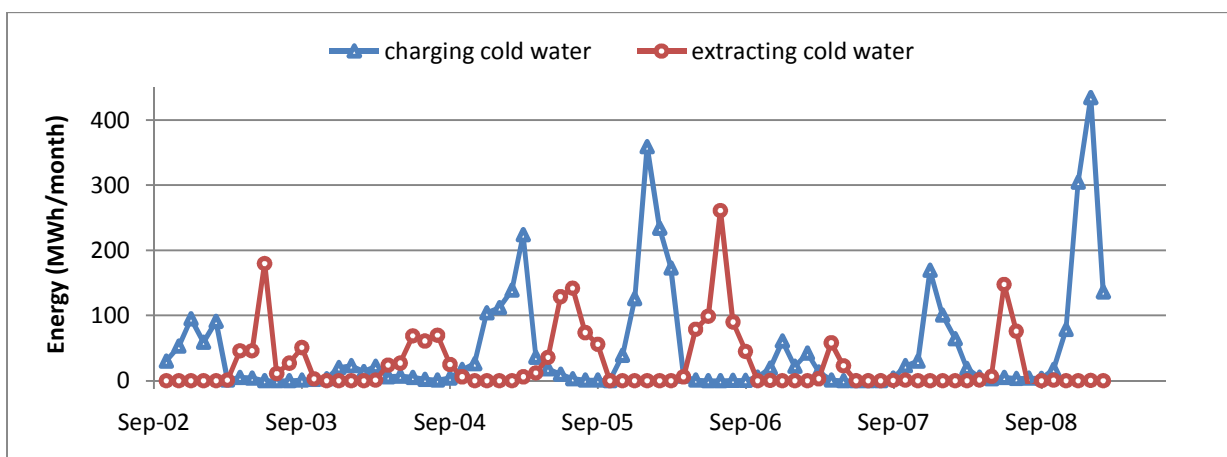

Figure 21: Monthly charged and supplied amounts of energy for the Stopera.

In most years more thermal energy is charged than extracted. This is logical, because it is impossible to extract energy that has not been charged. The difference between these two amounts is caused by the losses due to convection, dispersion and ambient groundwater flow. However, the charged and extracted amounts of energy do not differ very much. The supplied amount is on average 75% of the charged amount, which is high. This is caused by the amount of pumped water. Each year this amount is much larger for supplying than for charging of cold water, as can be seen in Figure 22. This means that the entire cold bubble is pumped up again, and almost no cold water remains in the subsurface. At the end of summer the temperature at the cold well is almost equal to the ambient groundwater temperature. Therefore the amount of energy that can be gained from the pumped water is very little. This also shows in an exergy analysis, and the exergy efficiency is substantially lower than 75 %.
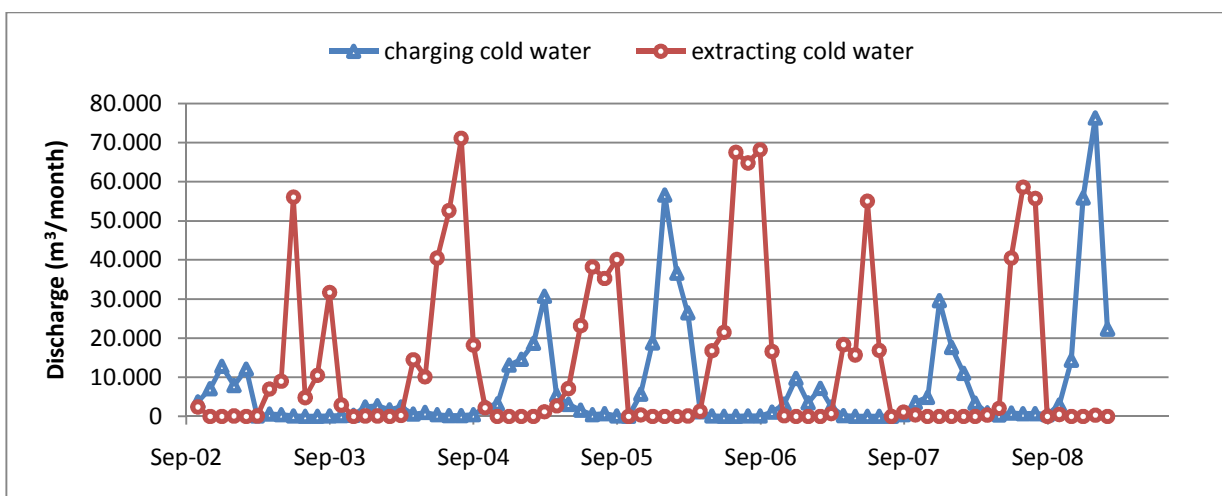

Figure 22:   Monthly pumped amount of water for charging and supplying of cold.

In the winter of 2003/2004 there were some problems with the system, which caused that only a small amount of cold water could be charged. That is why 2004 is the only year that more cold water was supplied than charged. This was possible because of the huge volume that was pumped to get all the remaining cold water from the subsurface. During the winter of 2008/2009 a lot of cold water could be charged, probably because of the relatively strong winter.

There have been taken several water quality samples from the cold well of the Stopera, approximately once a year. From these samples the calcium, potassium, magnesium, manganese, sodium, iron, ammonium, bicarbonate, chloride, nitrate and sulfate concentration have been measured. Some of these concentrations seem to be increasing, namely chloride, calcium and magnesium, as can be seen in Figure 23.

The locations of the cold and warm well are shown if Figure 24, and the calculation grid for the Stopera case is shown in Figure 25.
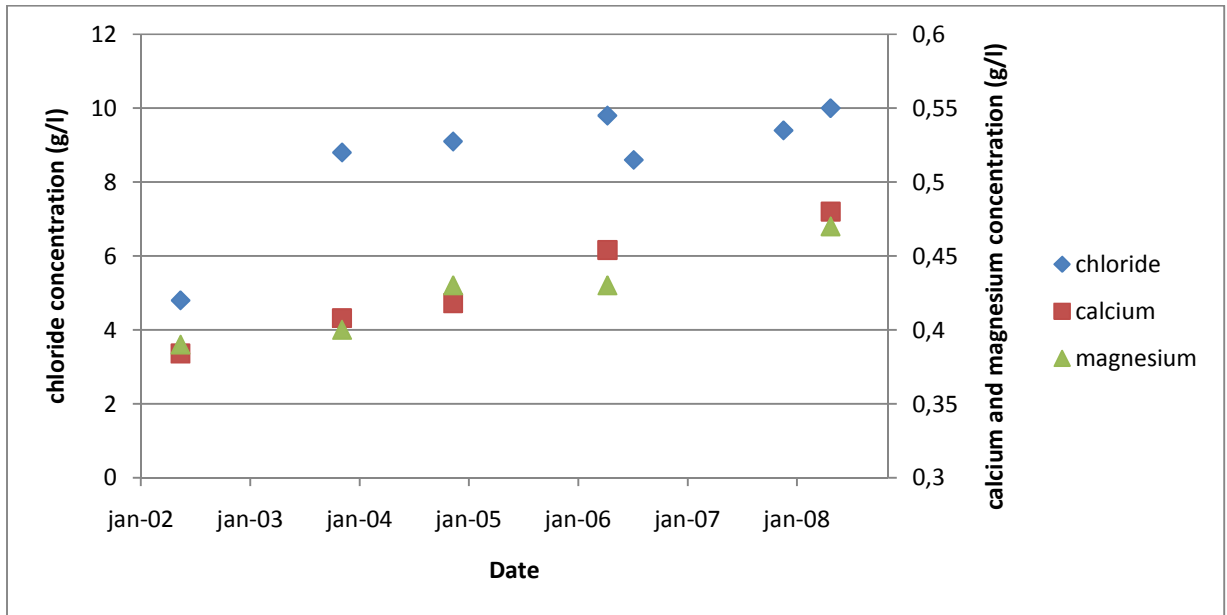
Figure 23: Chloride, calcium and magnesium concentration, as measured from the cold well of the Stopera.
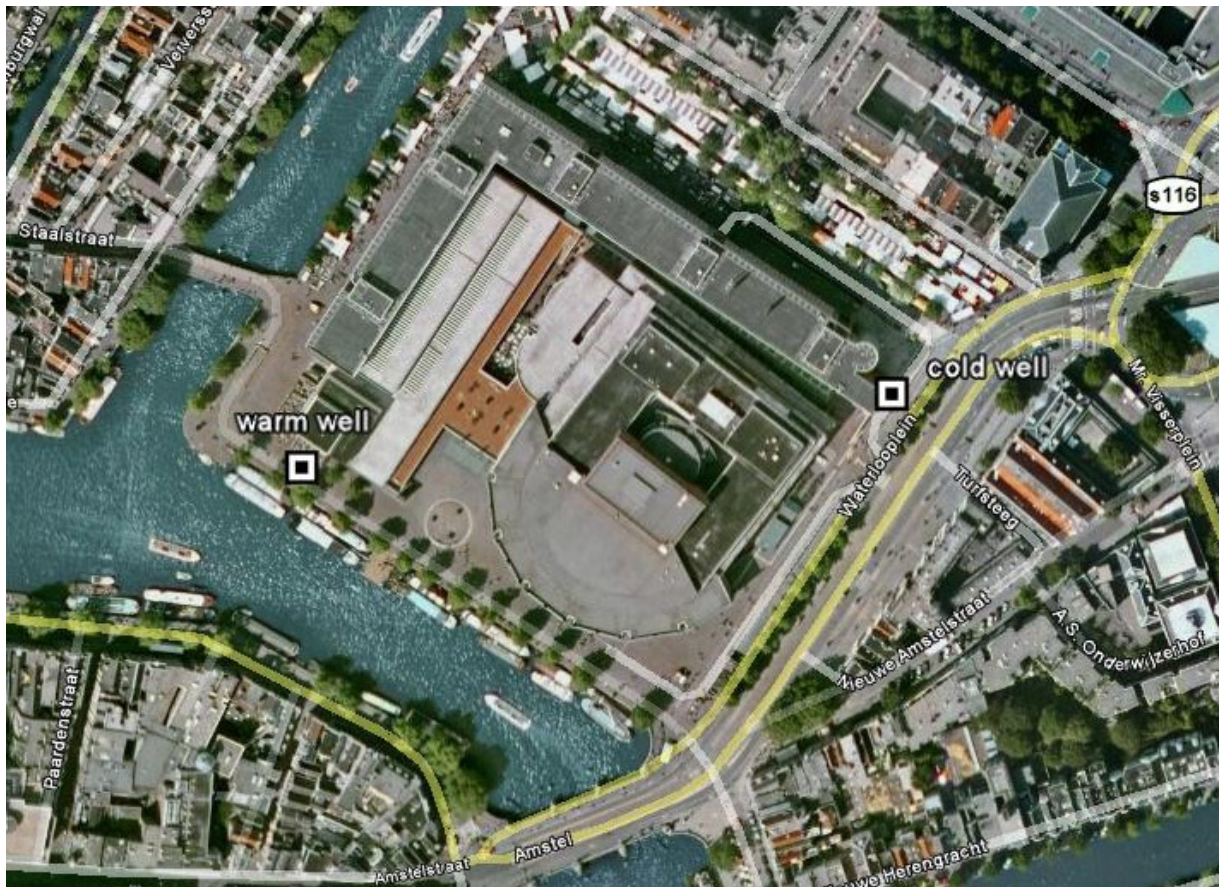

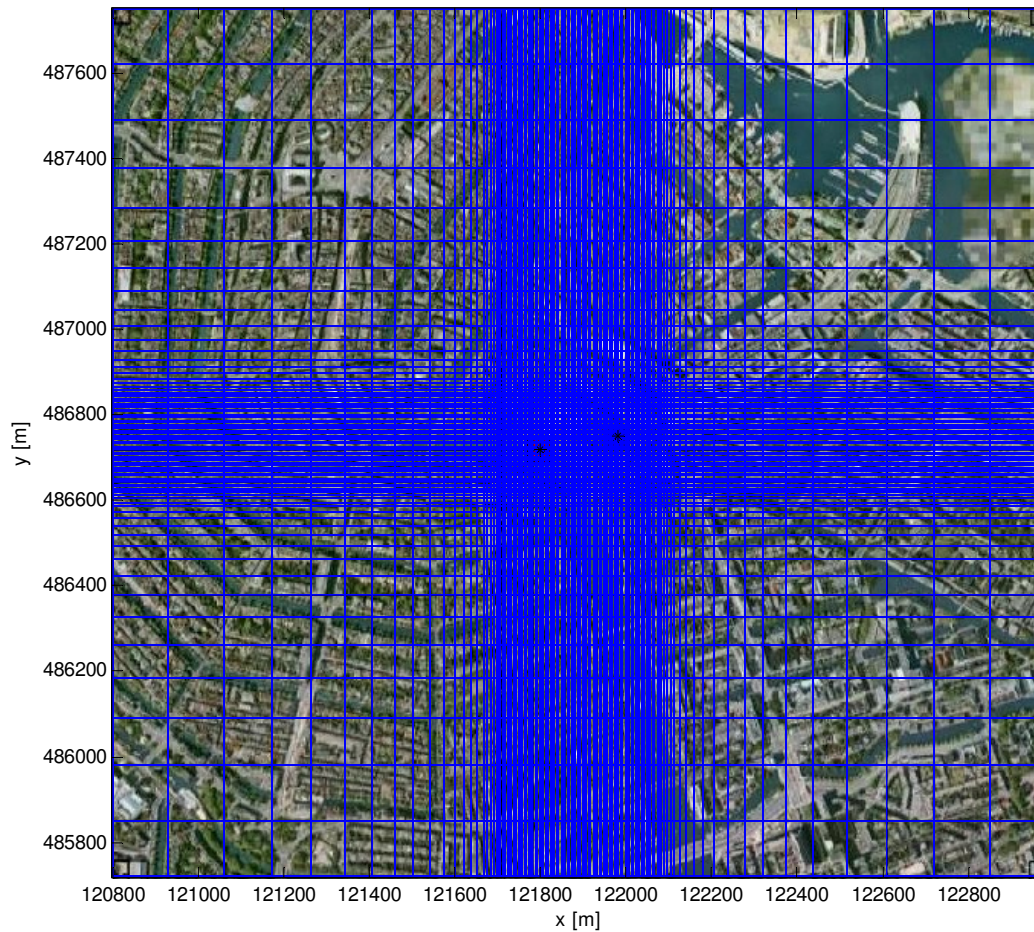Figure 24: Location of the warm and cold wells of the Stopera.

Figure 25: Calculation grid for the Stopera. Close to the wells (*) cell sizes are 5 m, and they become larger further away from the wells.

5.2 The Dam Square

The Dam Square is a famous place in the historic centre of Amsterdam, and is a tourist attraction, see Figure 26. Several old buildings surround this touristic place, of which the Beurs van Berlage, the Bijenkorf, hotel Krasnapolski, the Paleis op de Dam, the Oude Kerk and the Nieuwe Kerk are well-known. These buildings took part in a project organized by the municipality of Amsterdam to investigate energy storage for this part of the city. Waternet is investigating the possibilities together with the energy company Cofely. The project is still in an early stage, and most building owners still need to decide if they want to participate. An investigation has already been done by the municipality regarding the required capacities. Figure 27 shows the required cooling and heating capacities of the buildings. In this graph the required heat capacity is already lowered by $1/4^{th}$, as this part of the heat is assumed to be added by electricity to the heat pumps. The required capacity shown here is the capacity required from the subsoil. Euronext and the Magna Plaza Shopping Centre are the only buildings that need more cold than heat. The fact that only few buildings need more cooling than heating is caused by the age of the buildings; old buildings are generally less well isolated.
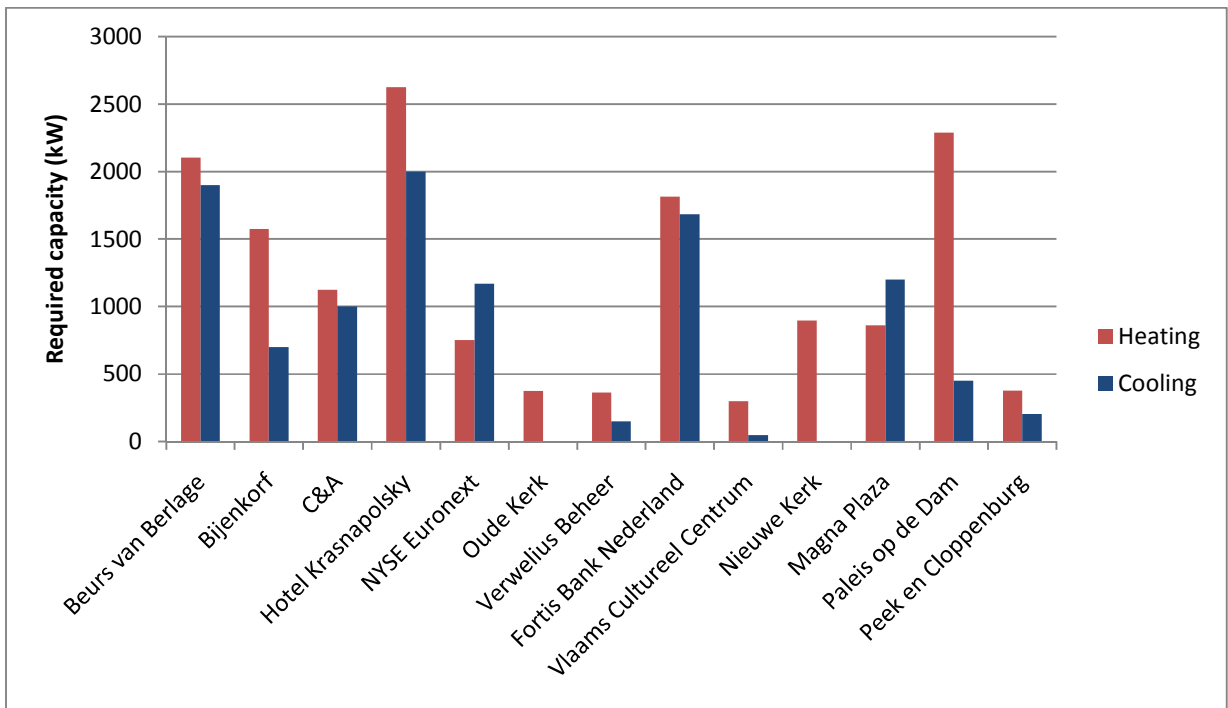
Figure 26:   The Dam Square

Figure 27:   Required capacity of the buildings who want to participate in energy storage around the Dam Square.

5.2.1 Assumptions for design of energy systems at the Dam Square

Three cases are simulated, described in the following sections. The wells are placed, in the available space, as close to the buildings as possible, without interfering with other wells. The locations are shown in Appendix 6 for the three cases. For the design of the wells of the Dam Square, several criteria have been set up and assumptions made. These are:

- The energy required for heating of the building will be upgraded to a higher temperature level by a heat pump. The heat pump is assumed to have a COP of 4. This means that 1 J of electricity is needed to produce 4 J of heat. So 3 J are taken from the groundwater to produce 4 J of heating energy, and ¾th of a buildings required heating energy needs to come from the ATES.
- The required capacities from the subsurface are taken from the forms that have been filled in by the buildings that want to participate in energy storage around the Dam Square.
- The number of full load-hours is equal to 1200 h/a for cooling as well as for heating, with which the annual energy demand can be established.
- The demand for energy follows the pattern shown in Figure 18 throughout the year.
- Water is injected in the warm well with a temperature of 17 $^{\circ}$C and in the cold well with a temperature of 9 $^{\circ}$C. So in both wells the difference between the injected water and the natural groundwater temperature of 13 $^{\circ}$C is 4 $^{\circ}$C and the difference between the two wells is 8 $^{\circ}$C. Of this 8 $^{\circ}$C, 6 $^{\circ}$C is assumed to remain on average as the water is pumped up again. So on average, water of 11 $^{\circ}$C is assumed to be pumped from the cold well, and water of 15 $^{\circ}$C is assumed to be pumped from the warm well. In reality there will be a pattern, where at the start of the season the retrieved water has a temperature equal to the injected water, and this temperature will gradually approach the ambient groundwater temperature as the season progresses. For the design of the wells, this pattern is not known in advance, and the conservative assumption above can be used.
- The screens can be placed from NAP -70 to -180 m. This upper limit is the same as the average of the buildings in Amsterdam, see section 1.4. The lower limit is determined by the location of the top of the less permeable sand layer from NAP -180 to -200 m. Some other ATES-projects in Amsterdam, like the former Euronext system, show some clay in this layer.
- The length of the screens and the distance between them are determined by the formulas in section 4.5.7. Monowells have a vertical distance from the cold well to the warm well of 30 m, leaving 40 m for each screen.
- The diameter of the borehole of all wells is set to 800 mm.
- According to the handbook of the N.V.O.E. (N.V.O.E., 2006), flat warm and cold bubbles are generally more efficient than high and narrow bubbles. This is because the losses due to groundwater flow are usually larger than losses as a result of conduction to upper and lower layers. For Amsterdam this might not be true, and therefore all wells are designed in a way that the thermal radius is always equal, in order to really compare the different configurations. When the full thickness of the aquifer is used, while the maximum discharge is 200 m^3/h, the thermal radius is 31 m. When less water needs to be pumped, the screen will be shorter, so that the thermal radius is still 31 m. This screens will always be in the top of the range NAP -70 to -180 m, as the drilling costs are than kept to a minimum.

5.2.2 Case 1: all buildings decide for themselves

In this 'mixed' case each building owner decides independently what kind of ATES they install and where to place their wells. Small buildings decide for a monowell, and larger buildings choose a doublet. The buildings of Verwelius Beheer, the Paleis on the Dam, Peek en Kloppenburg, and the Vlaams Cultureel Centrum can store enough thermal energy in a monowell. The other buildings decide for a doublet. The calculation grid for the mixed case in SEAWAT is shown in Figure 28. The other cases have a similar grid.
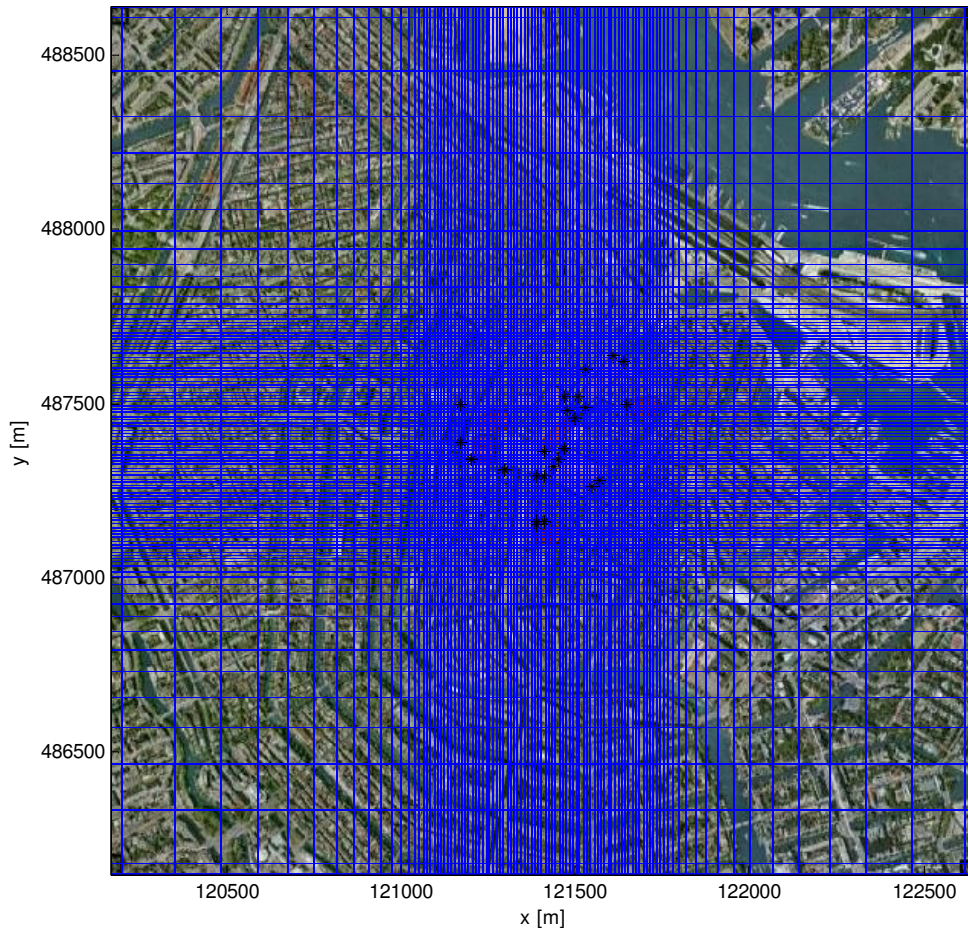

Figure 28: Calculation grid for the mixed case. Close to the wells (*) cell sizes are 10 m, and they become larger further away from the wells.

5.2.3 Case 2: The buildings are grouped

In the 'grouped' case the buildings surrounding the Dam Square are combined into three groups, depending on their relative location. Table 5 lists the buildings and the groups they have been put in. The number of wells for the 3 cases is also shown.

Because the NYSE Euronext needs more cold, the buildings in group 1 can store more heat, while there is still an energy balance. The same can be said about the Magna Plaza Shopping centre in group 3. Because only these two buildings need more cold than heat, the benefits of grouping are limited in this

case. When no buildings are grouped, the energy that can be stored is 11700 MWh, and when buildings are grouped the energy that can be stored is 12600 MWh.

	Only monowells	Mixed case		Grouped case
Naam	Nr. of monowells	Nr. of monowells or doublets	Group	Nr. of doublets
Beurs van Berlage	4	4	1	12
Bijenkorf	2	2		
C&A Nederland kavel	3	2		
Hotel Krasnapolsky	5	4		
NYSE Euronext	2	2		
Oude Kerk	0	0		
Verwelius Beheer	1	1		
Fortis Bank Nederland	4	4	2	4
Vlaams Cultureel Centrum	1	1		
Nieuwe Kerk	0	0	3	4
Magna Plaza Shopping	2	2		
Paleis op de Dam	1	1		
Peek en Cloppenburg	1	1		

Total	26	24	Total	20

5.2.4   Case 3: all buildings use monowells
For this case each building uses only monowells. Because of the smaller capacity of monowells, large buildings will use several monowells.

5.3   NYSE Euronext
The NYSE Euronext building used thermal energy storage from 1989 until 1999. It used the original groundwater temperature to cool the computers in the building with a nearly constant discharge of 40000 m^3/month throughout the year. Three injection wells were located at the southwest-side of the Beursplein in the bottom of the aquifer at NAP -140 to -180 m, and two extraction wells were located in the northeast side of the Beursplein in the top of the aquifer at NAP -80 to -100 m. The original idea was that the extraction wells were vertically spaced at a sufficient distance from the injection wells below, so that the extraction wells were not influenced by the injected water. This design did not take density flow into account however, as the warmer injected water would raise and would heat the water surrounding the extraction wells. Therefore another extraction well was placed in 1993, near the Old Church, upstream of the Beursplein, but still at a depth of NAP -80 to -100 m. After some months also the water in this well began to rise in temperature, and in 1999 NYSE Euronext decided to abandon the system and fill the wells with material similar to the original subsurface.

6. Soil characteristics

The storage aquifer for ATES in Amsterdam belongs to the Formations of Peize and Waalre, which intertwine. The Peize Formation consist of fluvial deposits from the river Eridanos, which originated from what is now called the Baltic Sea. The Waalre Formation was formed by deposits from the Rhine (Berendsen, De vorming van het land: inleiding in de geologie en de geomorfologie, 2004).

6.1 Hydraulic conductivity

One of the most influential parameters in any groundwater model is the hydraulic conductivity. For this study the saturated hydraulic conductivity was estimated using drilling descriptions and the capacity tests from the Stopera. The capacity test is described in Appendix 5. The resulting hydraulic conductivity for the warm well is 32 m/d, and for the cold well the calibrated value is 42 m/d. These values are averaged, and a resulting value of 37 m/d is used for the average hydraulic conductivity of the model.

Several sources were consulted to arrive at a build-up of the subsurface below the Dam, of which some are mentioned here. According to the groundwater map of the Netherlands (Speelman & Houtman, 1979) the geohydrological basis is estimated at NAP -300 m, by the Formation of Oosterhout. According to REGIS (TNO, 2009) the subsurface of Amsterdam consists of the following layers, shown in Figure 29:

- The hydrological basis is formed by the Maassluis complex with its top at NAP -220 to -240 m. It has a vertical hydraulic conductivity of 0.001 m/d. Therefore, the top of this layer is taken as the hydrological basis for the model.
- On top of this layer is the Peize-Waalre Sand 8, with its top between NAP -200 and -210 m.
- The main part of the ATES screens in Amsterdam are located in Peize-Waalre Sand 6. This Formation has its top at NAP -120 to -130 m and its bottom at NAP -200 to -210 m. Its hydraulic conductivity ranges from 12.5 to 20 m/d below Amsterdam, according to REGIS. This value is too low, when compared to other data like the drilling descriptions and capacity tests, and will therefore be ignored.
- On top of this layer is Peize-Waalre Sand 5, Sand 4, Sand 3, Sand 2, all with a thickness of just a few meters and with an overall top of around NAP -70 m.
- On top of these layers are many others, of which the Drente Uitdam Clay 1, from NAP -50 to -70 m, and the Eem Clay 2, from NAP -30 to -50 m, are the thickest.

From the design report of the Stopera (IF Technology, 1999) the following values are gathered:

- Vertical hydraulic conductivity in the upper layer is 0.005 m/d for peat and 0.01 m/d for clay.
- The resistance of the 1st aquitard, with which the clay layer from NAP -28 to -65 m is meant, is set to 10000 days.
- From NAP -65 to -180 m the hydraulic conductivity is 35 m/day.
- From NAP -180 to -220 m the hydraulic conductivity is 5 m/d.
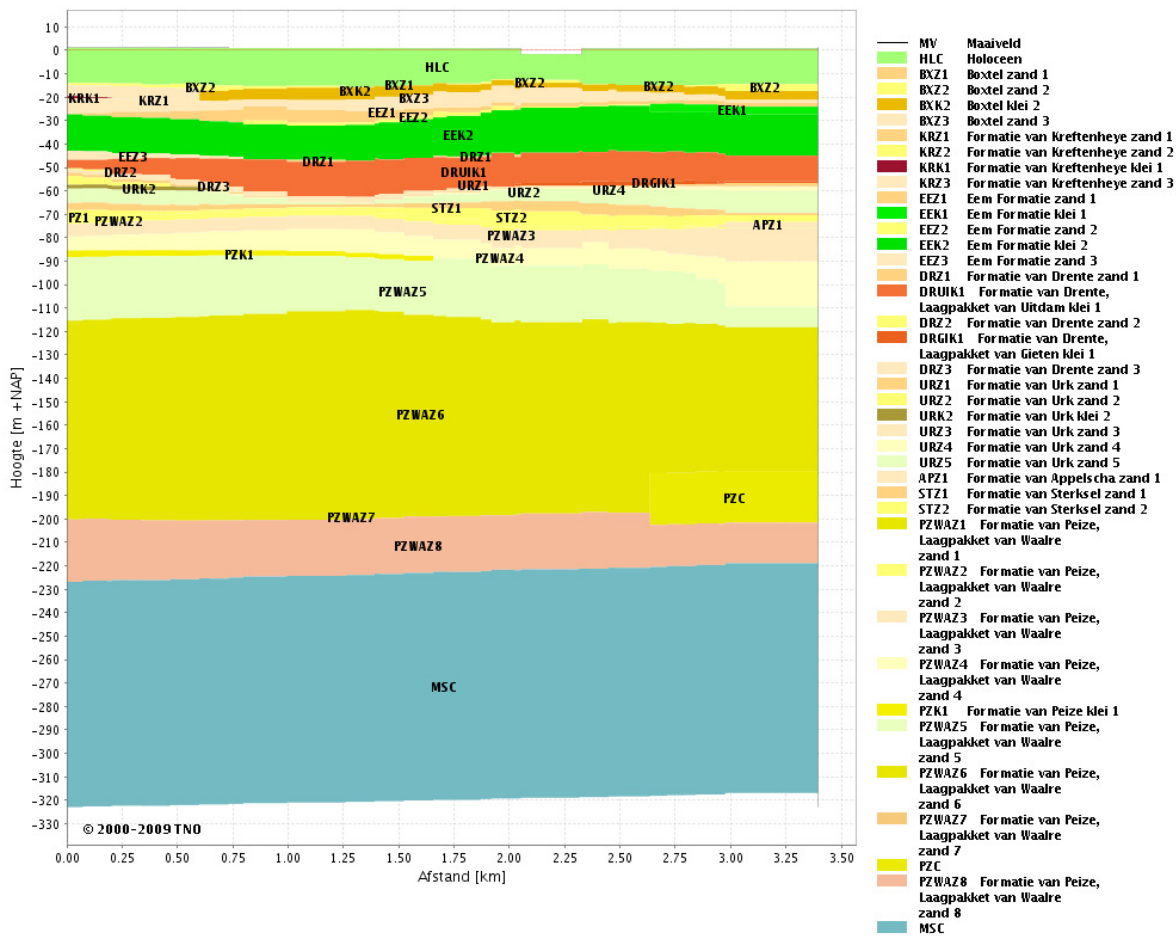- The hydraulic gradient is 0.025% in south-southwest direction.

Figure 29: Graph taken from REGIS, showing the subsurface below the centre of Amsterdam, from north-west on the left to south-east on the right (TNO, 2009).

6.1.1 Horizontal hydraulic conductivity

The hydraulic conductivity values have been estimated using the drilling descriptions of the Stopera wells as well. For this estimation several methods may be used, of which the methods of Shepperd, Hazen, Alyamani & Sen and Cozeny-Carmen are the most well known. The choice of the method depends on the available data. For some methods only an effective particle diameter is needed, while for other methods also other characteristics of the sieving curve are required. The available data from the Stopera wells consist of the median sand particle diameter plus text descriptions of the amount of silt and gravel. For these specific data, and for the Dutch subsurface, a method was developed by Van Rees Vellinga (Pomper, 1996). The descriptions of the soil are translated to a U-number and correction factors, after which the hydraulic conductivity can be calculated. This method is further described in Appendix 4.

The hydraulic conductivity of the two drillings for the energy storage system of the Stopera can be estimated by this method, as can be seen in Figure 30. The estimated values are very rough however, as is the case with any method to estimate hydraulic conductivity from drilling descriptions. Therefore, the average hydraulic conductivity was taken from the capacity tests, as shown above. For the distribution along the screen of an ATES system, the drilling descriptions can be used. The estimated hydraulic

conductivity generally varies between 10 and 35 m/d, where the estimated median conductivity is 27 m/d. There are some gravel layers however, where the estimated hydraulic conductivity is much larger. What can be seen is, that not all high conductive layers are found in both drillings. Especially the high conductivity at the bottom of drilling B25E0918 is not seen in drilling B25G0974. This could be caused by the fact that drilling B25G0974 is only 175 deep and the high conductivity layer is beneath this depth at drilling B25G0974.

In both drillings, the high conductivity zone between NAP -126 and -138 m is present. Therefore, this is a good case to use for the model, to test the influence of a gravel layer in the subsoil. The layer with the higher hydraulic conductivity is also shown in Figure 30, under model 2.

The hydraulic conductivity of clay layers is set to 0.005 m/d.
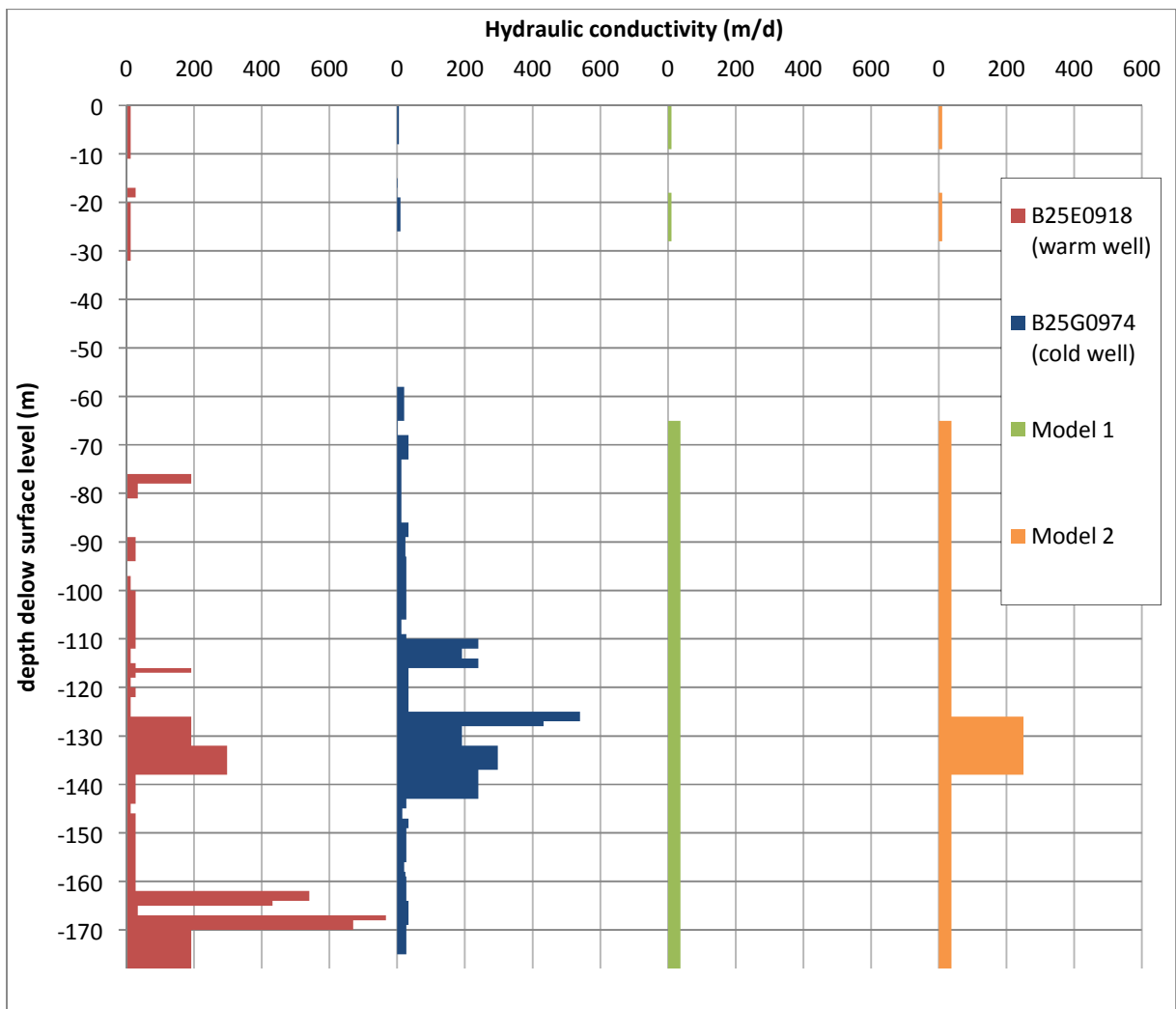

Figure 30: The hydraulic conductivity of the sand layer of the two drillings of the Stopera, together with the homogeneous model schematization and the schematization of the model with a gravel layer.

6.1.2 Vertical hydraulic conductivity

The vertical hydraulic conductivity is estimated to be 1/5th of the horizontal hydraulic conductivity. This is a conservative value, as normally this value is closer to 1/10th. The losses due to flow towards the layers below and above the screen will be larger when a value of 1/5th is used.

6.2 Thermal conductivity

The bulk thermal conductivity of the soil is calculated from the conductivity of the soil and the conductivity of the water according to the following formula:

$$k_{Tbulk} = \theta \, k_{Tfluid} + (1-\theta) k_{Tsolid}$$
[43]

Where: k_{Tbulk} is the total thermal conductivity [W/(m^{o}C)]; k_{Tfluid} is the thermal conductivity of water [W/(m^{o}C)]; and k_{Tsolid} is the thermal conductivity of the soil particles [W/(m^{o}C)].

The Peize Formation consist of about 90 % quartz and 10 % other sediments ('veldspaat'). The Waalre Formation consists of about 80 % quartz and 20 % other sediments (Berendsen, Fysisch-geografisch onderzoek, chapter 9: Grind analyse, 2005). Quartz has a high thermal conductivity. The values from the N.V.O.E. for the thermal conductivity of sand were taken, as these are assumed to be representative for the Dutch case. The bulk thermal conductivity for sand then is 1.76 W/(m^{o}C), and the thermal conduction term, see section 4.4, is 0.104 m^2/d.

Table 6:   Values for the thermal conductivity.

Substance	k_T (W/(m^{o}C))	reference
Fresh water	0.58	Engineering Tool Box (2007)
Granite	1.73-3.98	Marble Institute of America (2007)
Quartzite	5.38	Marble Institute of America (2007)
Marble	2.07-2.94	Marble Institute of America (2007)
Sandstone	1.83-2.90	Marble Institute of America (2007)
Limestone	1.26-2.15	Marble Institute of America (2007)
Dolostone	3.8	Cote and Konrad (2005)
Clay	1	Ingebritsen and Sanford (1998)
Quartz	3	Engineering Tool Box (2007)
Calcite	3.59	Horai (1971)
Sand	2.4	(N.V.O.E., 2006)
Clayey sand	2.3	(N.V.O.E., 2006)
Sandy clay	1.8	(N.V.O.E., 2006)
Clay	1.7	(N.V.O.E., 2006)
Clay with peat layers	1.4	(N.V.O.E., 2006)
Peat	0.4	(N.V.O.E., 2006)

6.3 Heat capacity

To determine the retardation factor with regard to heat transport through the aquifer, information about the heat capacity of the water and the soil is also needed. Table 7 lists the heat capacity of different substances. One can see that the heat capacity of water decreases with increasing temperature

and increasing salt concentration. These differences are so little however, that a constant value is assumed, of 4.190 kJ/(kg^{o}C). As stated above, the greatest part of the sand is quartz, which has a low heat capacity. The values from the N.V.O.E. were taken for the heat capacity, as these are assumed to be representative for the Dutch case. The thermal distribution factor, see section 4.4, for sand then is 2.12 *10^{-4} m^3/kg, and the retardation factor will be 2.03.

Table 7:   Values for the specific heat capacity

Substance	c_p (kJ/(kg^{o}C))	reference
fresh water (5°C)	4.204	
fresh water (10°C)	4.193	
fresh water (15°C)	4.186	
Seawater (2°C)	3.93	
Granite	0.79	(Cote and Konrad, 2005)
Marble	0.88	(Cote and Konrad, 2005)
Sandstone	0.92	(Cote and Konrad, 2005)
Limestone	0.84	(Cote and Konrad, 2005)
Dolomite rock	0.92	(Cote and Konrad, 2005)
Clay	0.92	(Engineering Tool Box, 2007)
Quartz	0.71	(Cote and Konrad, 2005)
Calcite	0.84	(Cote and Konrad, 2005)
Sand	0.89	(N.V.O.E., 2006)
Claiy sand	0.92	(N.V.O.E., 2006)
Sandy clay	1.00	(N.V.O.E., 2006)
Clay	1.09	(N.V.O.E., 2006)
Clay with peatlayers	1.20	(N.V.O.E., 2006)
Peat	2.18	(N.V.O.E., 2006)
Water	4.19	(N.V.O.E., 2006)

7. Calibration

The model was calibrated on the measured extracted temperatures. One thing that was noticed right away, is that it is very easy to get some nice results. The first time the SEAWAT model was run for the Stopera case, the modeled temperatures were already close to the measured temperatures. This is caused by the way the model depends on the injected temperature. When a well is injecting, the water at the well is equal to the temperature of the injected water. Only the pattern in which the water temperature goes back to the ambient groundwater temperature during pumping is determined by the parameters of the model. This temperature change depends on the dispersion and conduction parameters.

Figure 31 shows the modeled and measured temperatures of the Stopera. Only the measured monthly temperatures, when a well is not infiltrating, are shown. The measured temperature data from the first two years have been estimated from the charged and supplied energy, as no temperature measurements were available. The measured and simulated temperatures are quite close. Only at the end of summer are the measured temperatures a bit higher than the simulated ones for the cold well.

The temperature of the cold well rises to about 12.5 ^{o}C at the end of each summer. The temperature in the cold well of a normal ATES system would not raise this high, but this is not a normal ATES system. This system is used as a cold storage only, where far more water is pumped from the cold well to the warm well in summer to supply cold, than the other way around in winter to charge cold. In this way, all the cold is retrieved from the subsurface, but the temperature in the cold well will increase more as water that was not stored the season before is attracted.
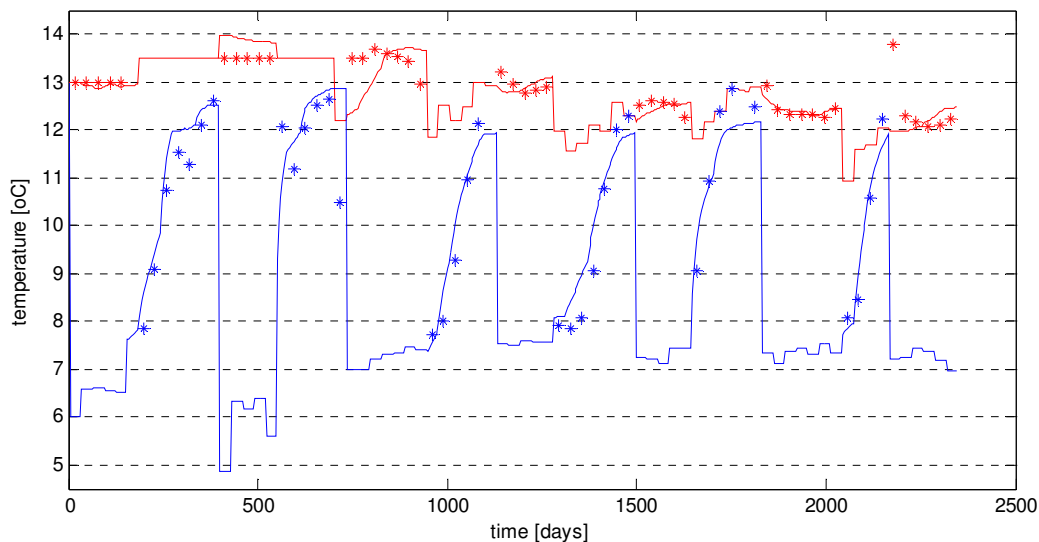

Figure 31: Simulated (-) and measured (*) temperatures in the warm (red) and cold (blue) well of the Stopera.

As mentioned before, the temperature profile in Figure 31 is quite independent on model parameters. It would be better to calibrate the model on some observation wells close to the cold and warm well. Measured temperatures from other wells would have more meaning, but these are not available.

8. Model results

8.1 Influence of variable density and viscosity

Variations in density and viscosity were thought to have a large influence on model results. This does not seem to be very evident in the model results. The warm bubble becomes a little cone shaped with the wide part upwards, due to some density flow, see Figure 32. The cold bubble shows the same shape, but then with the wide part downwards. For energy storage with higher temperatures the density effects would become more evident.
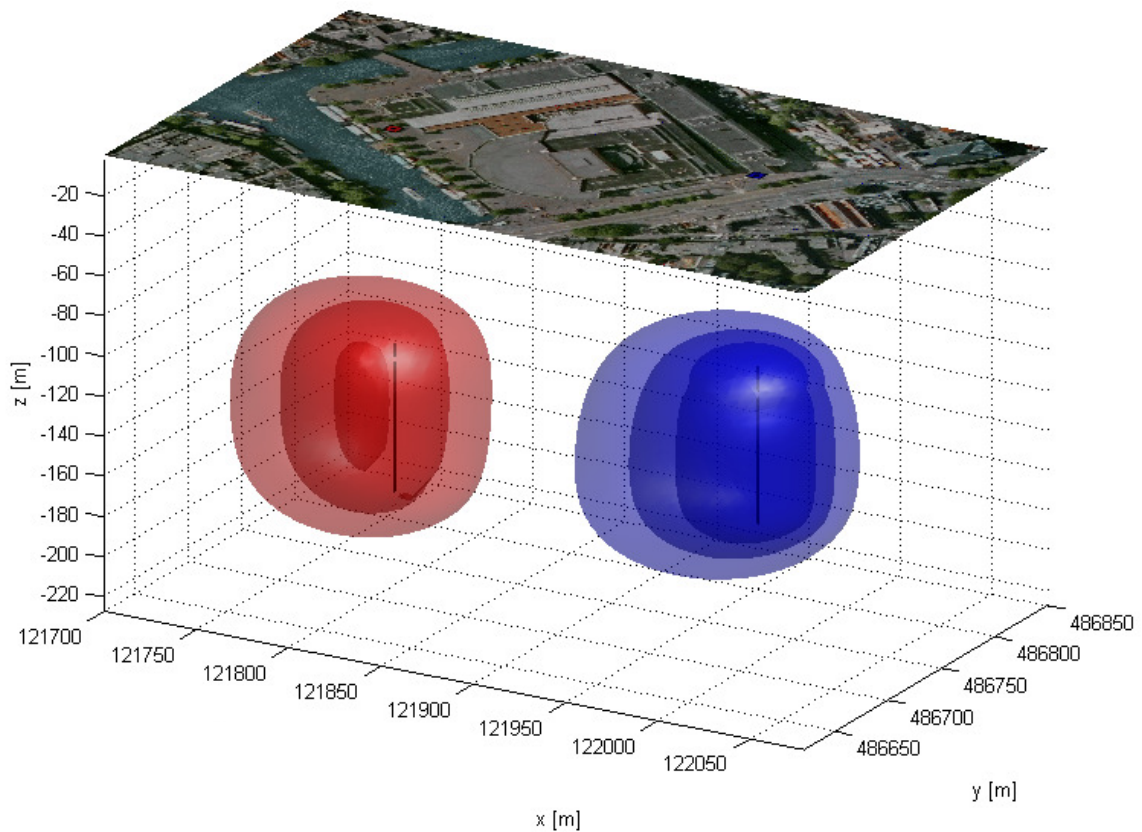

Figure 32: The results for the Stopera for a homogeneous subsurface, after 7 years in the middle of winter.

8.2 Heterogeneity

Heterogeneity was taken into account in two different ways: in the form of a layer with a higher hydraulic conductivity and in the form of simulation of conductivity fields in the horizontal surface. In the next sections are the results for both cases.

8.2.1 Results with gravel layer

The results with a gravel layer are shown in Appendix 8 and Appendix 10. Because the gravel layer has a higher conductivity while the hydraulic gradient stays the same, the ambient groundwater flow through this layer is larger. Therefore the energy flows away more quickly and the cold bubble flows into the warm bubble, see Figure 33. This makes the efficiency much lower when a gravel layer is modeled, as can be seen in Figure 35. Especially the warm bubble is affected, as it is located downstream of the cold bubble. The efficiency of the warm well with a gravel layer of 250 m/d is almost 10 % lower than that of an ATES in a homogeneous aquifer.
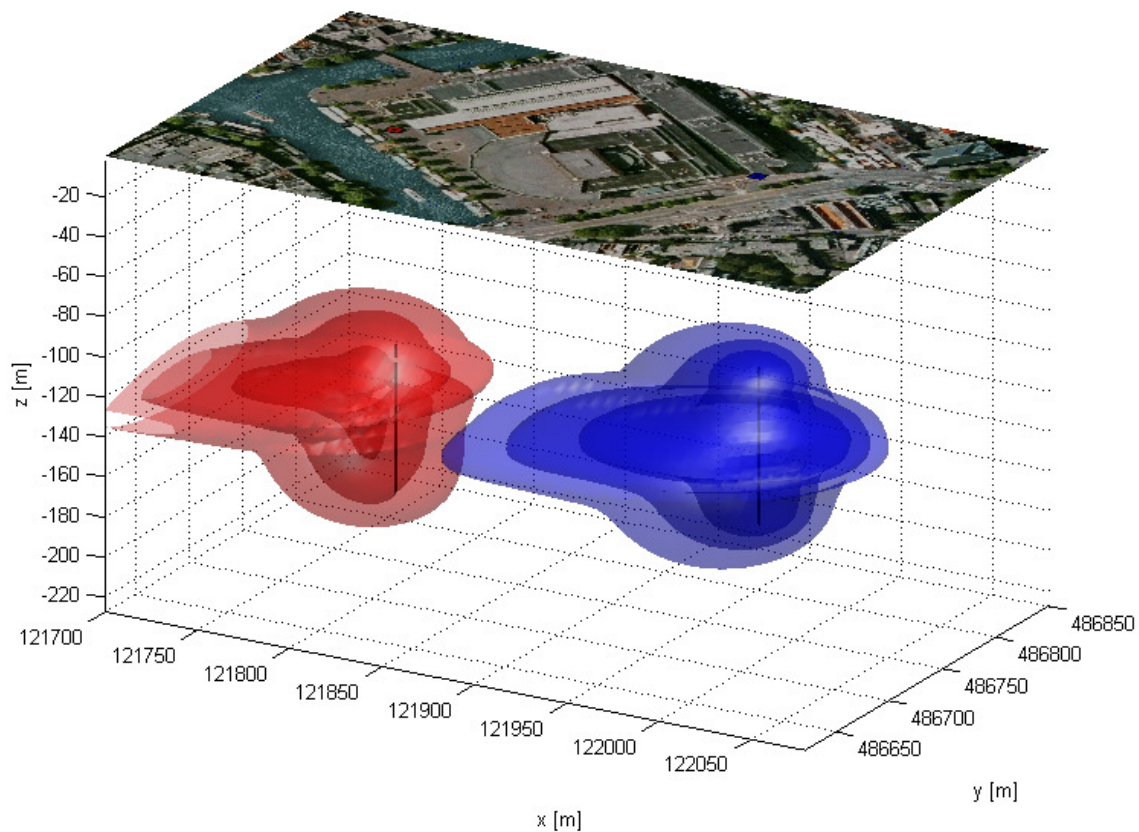
Figure 33: A 3d graph of the Stopera for a gravel layer with a hydraulic conductivity of 250 m/d.

When a blind pipe is installed at the elevation of this gravel layer, no water or energy flows directly from the screen to this gravel layer. Still, some of the energy that has been injected in the layers above and below the blind pipe, flows through the gravel layer away from the well, see Appendix 9 and Appendix 11. A difference compared to the case without the blind pipe is that the energy does not spread upstream through the gravel layer, something that was seen in Figure 33. The efficiency is still less than in the homogeneous case. After five years, the efficiency of the warm well, for example, is still about 5 % lower than that of an ATES in a homogeneous aquifer.
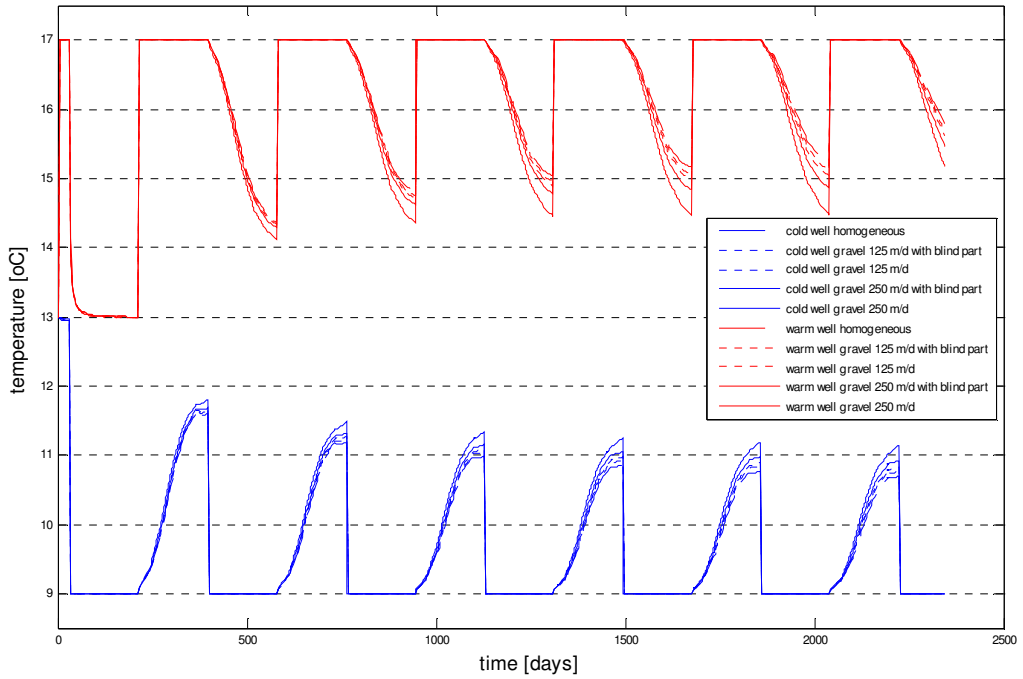
Figure 34:   The temperatures at the cold and warm well with a gravel layer of different hydraulic conductivity.
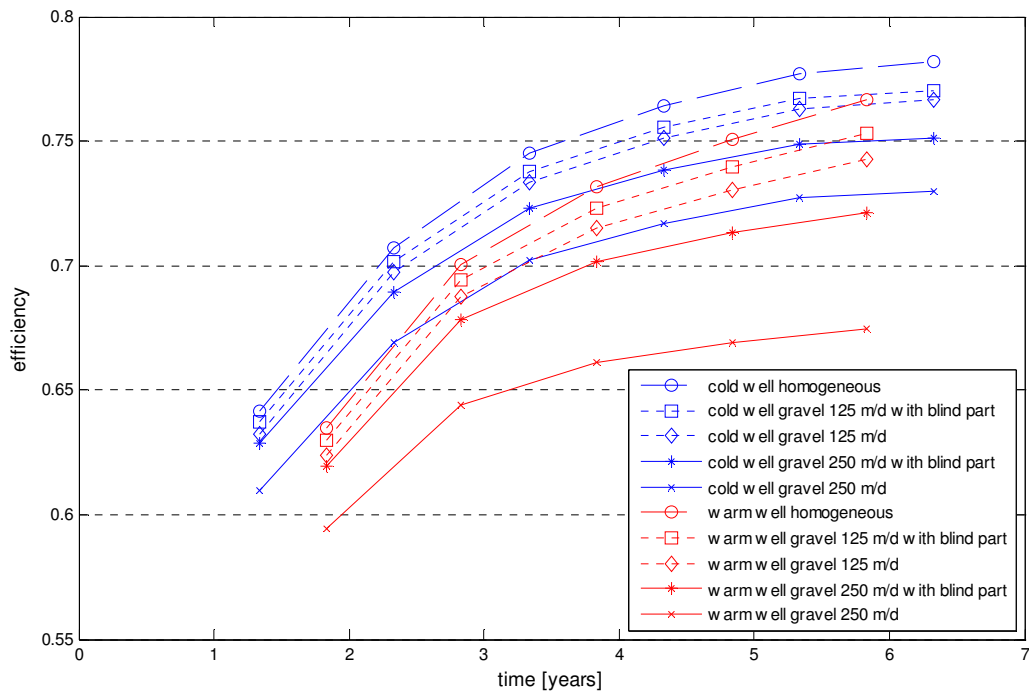

Figure 35:   The energy efficiency of the cold and warm well with a gravel layer of different hydraulic conductivity, with and without a blind pipe at this gravel layer.

8.2.2   Effect of aerial heterogeneity

The results for the Stopera wells with varying heterogeneity, as described in section 3.1.2, are shown in Appendix 12, Appendix 13 and Appendix 14. The heterogeneities have a significant effect on the shape of the cold and warm bubbles, compared to the homogeneous case in Figure 32. This effect is more evident for larger length scales of the heterogeneities in the aquifer. When the temperature is plotted however, in Figure 37 and Figure 38, there is only a small difference in retrieved temperatures. Therefore the difference in efficiency of the system is small, see Figure 39. Only the temperature and efficiency of the warm well for the case with heterogeneities of a length scale of 200 m is noticeably less than the homogeneous case. This is caused by the fact that the bottom of the warm screen is located in a region of larger hydraulic conductivity, with an effect similar to the gravel layer described before. In fact, such situations may be expected when larger structures as channels are screened. This can be seen in Figure 36, where the warm bubble has spread more around the lower part of the screen.
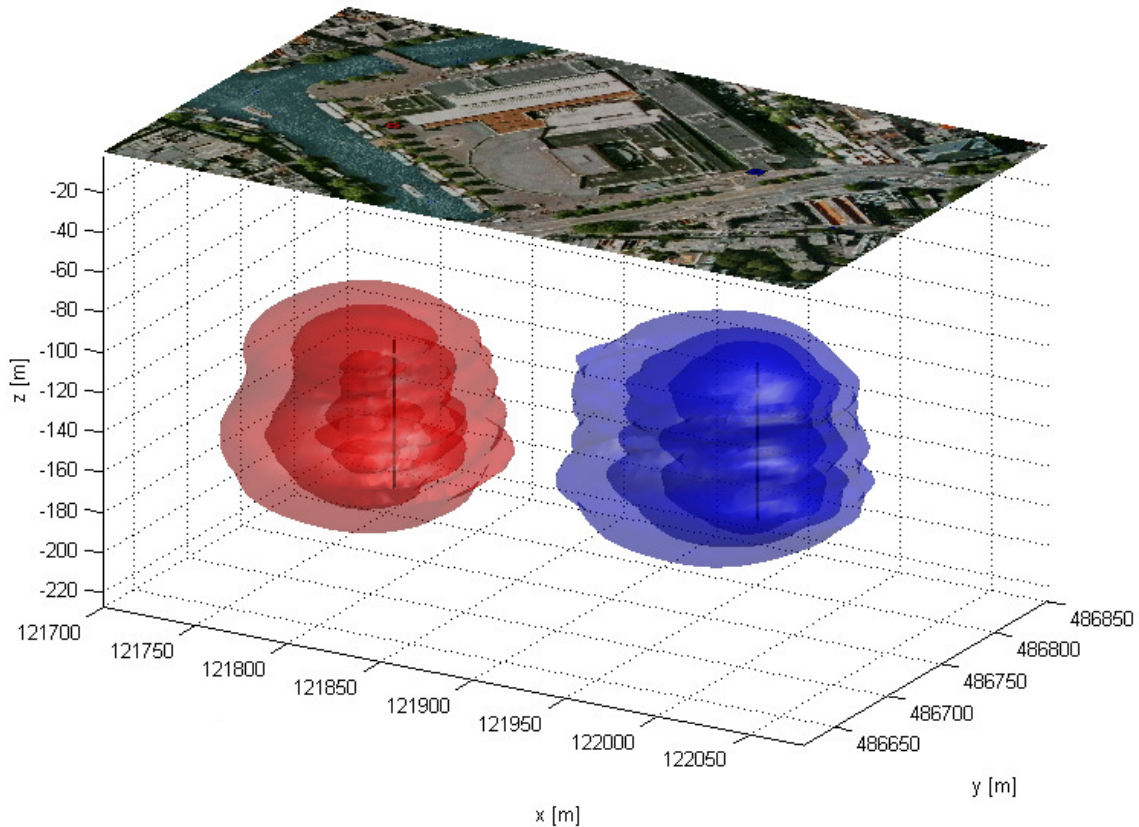

Figure 36:   A 3d view of the cold and warm bubble of the ATES system of the Stopera in February 2009 for the case with heterogeneity with length scale of 200 m and a standard deviation of 37 m/d.
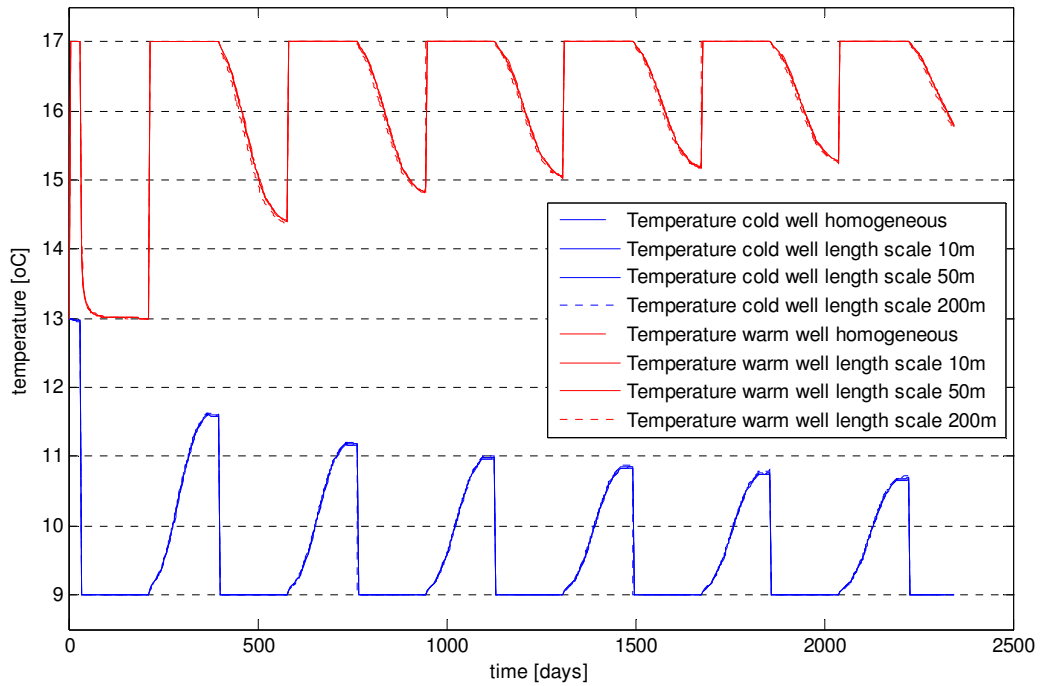
Figure 37: The temperature at the cold and warm well for the different length scales of the heterogeneities. The first 6.5 years are plotted.
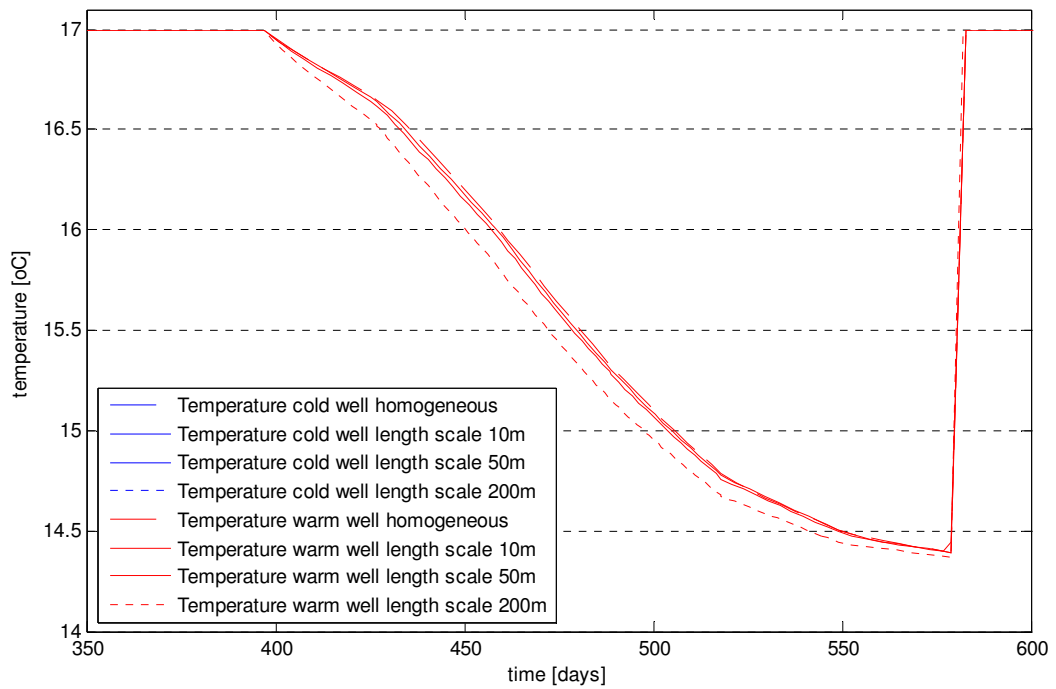

Figure 38: The temperature in the warm well for the different length scales of the heterogeneities in the first winter the system is fully functional.
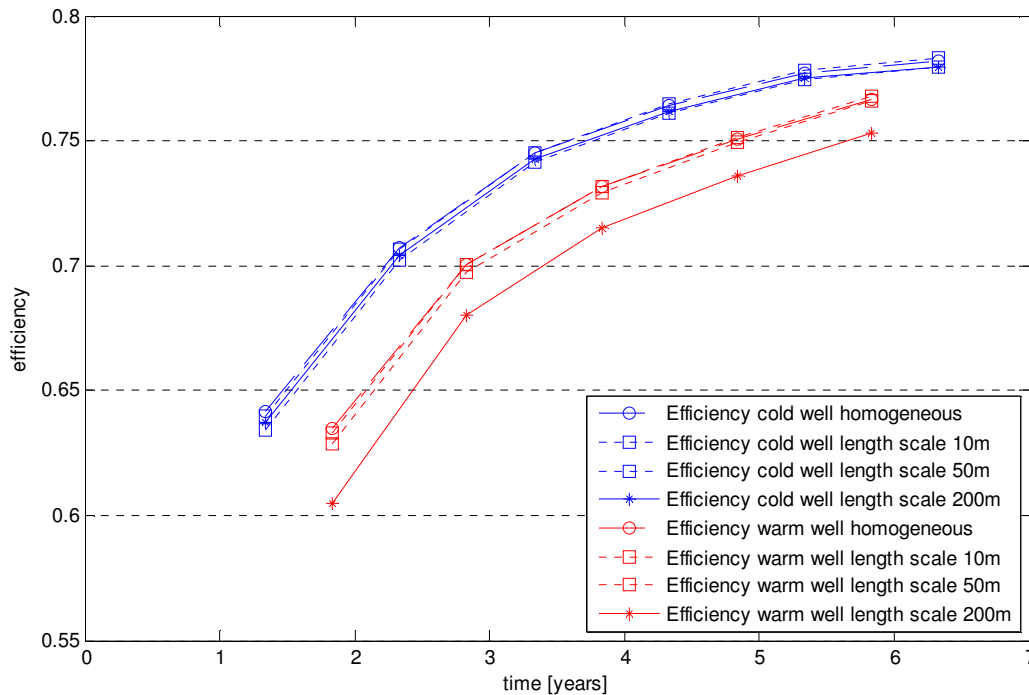
Figure 39: The energy efficiency at the cold and warm well for different length scales of the heterogeneities.

8.3   Vertical mixing of the salinity

As shown, the salinity below Amsterdam has a distinctive vertical gradient. This gradient is destroyed locally by the ATES system. The change in vertical and horizontal density distribution may cause density flows that affect the efficiency of ATES systems. These effects can be simulated with the SEAWAT model.

The original Stopera discharges were modeled, to not only show the results of a normal ATES system, but also show the result if there is an imbalance in volumes of water. As was mentioned earlier, the Stopera pumps more water from its cold well to the warm well, than the other way around, in order to retrieve all the energy that resides around the cold well.

Figure 40 and Figure 41 show the resulting salt concentrations, along with the temperature profile, at the end of simulation in the end of February 2009. The salinity effects around the cold well are minimal and only show when there is pumping from the warm well to the cold well. The salinity effects at the warm well are larger and these build up in time, as more water is pumped from the cold well. Density flow however, restores the original salinity gradient, and the impact on the salinity will remain within 100 m from the well.

The shown increase of the salinity in the cold well, which was shown in Figure 23 in section 5.1, could not be explained by the results.
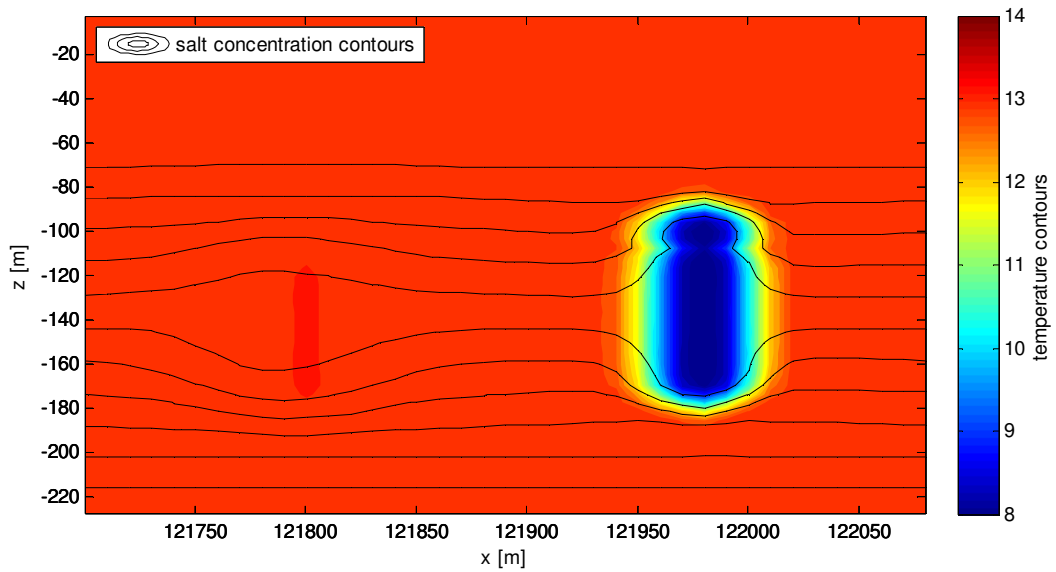
Figure 40: Vertical cross-section through the cold well from east to west, showing the salt concentration contours, with a resolution of 1kg/m^3, in the middle of winter, after 7 years.
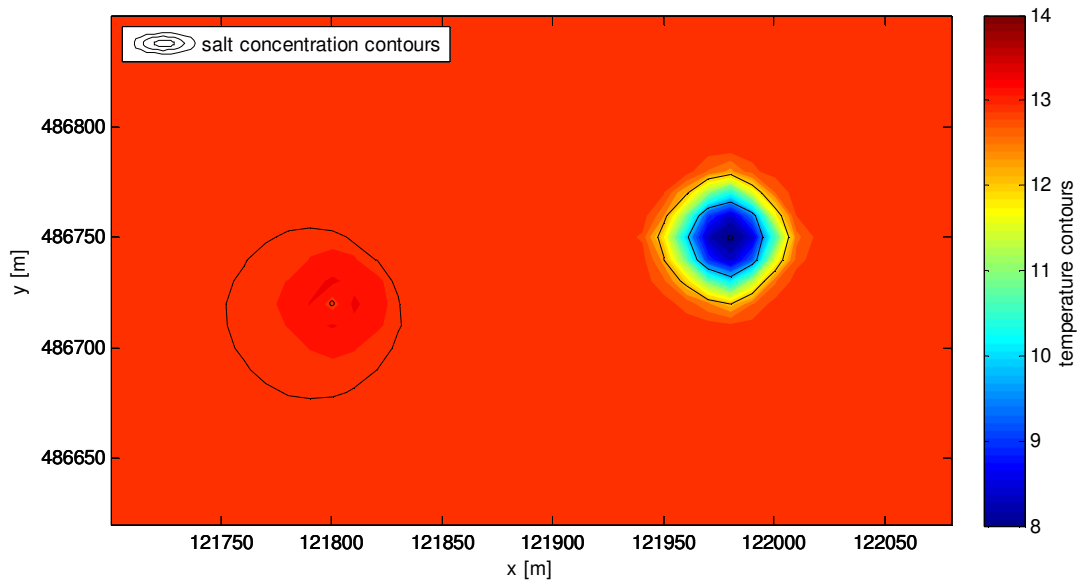

Figure 41: Horizontal cross-section at NAP -103 m, showing the salt concentration contours, with a resolution of 1kg/m^3, in the middle of winter, after 7 years.

8.4 Results for the Dam Square

The specific results for each of the three Dam Square cases are shown in Appendix 15, Appendix 16 and Appendix 17. Figure 42 shows the energy efficiency of all the wells for the three cases. As one can see, the energy efficiency is greater for the grouped case than for the mixed case. The difference is about 7 % for the cold wells and 5 % for the warm wells. The efficiency of the grouped case is larger, because the distance between cold and warm wells is made as large as possible for the total system, and the total

thickness of the aquifer is used, compared to the mixed case, where the distance between wells is not optimized for the entire system and some wells only use the upper part of the aquifer.
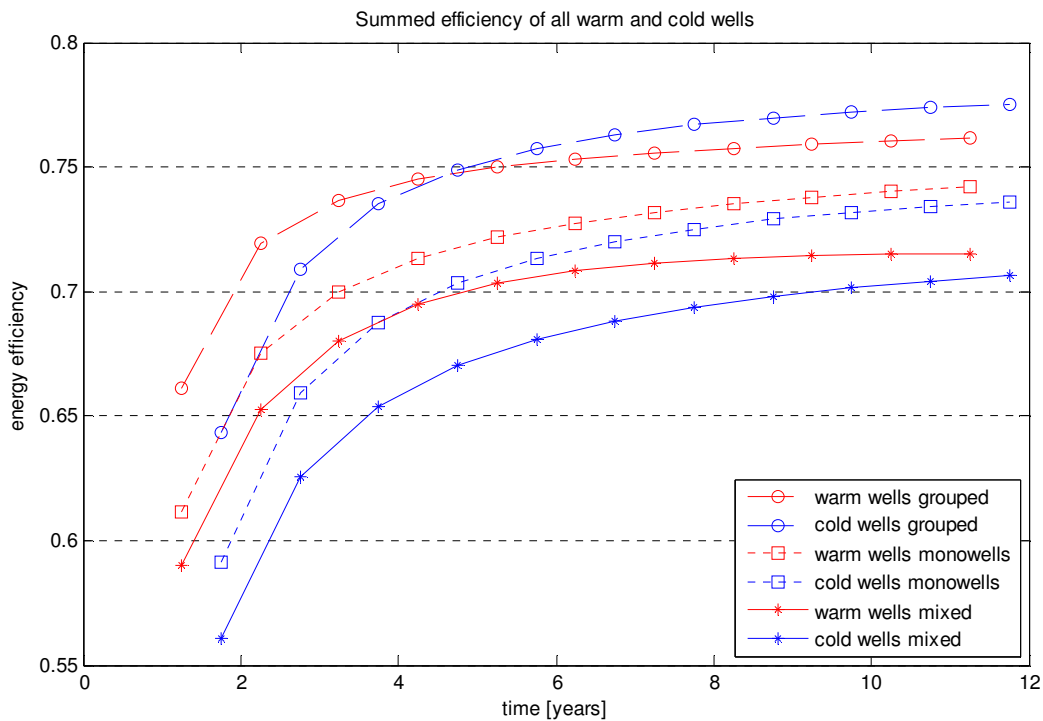

Figure 42: The energy efficiency of the three cases for the Dam Square.
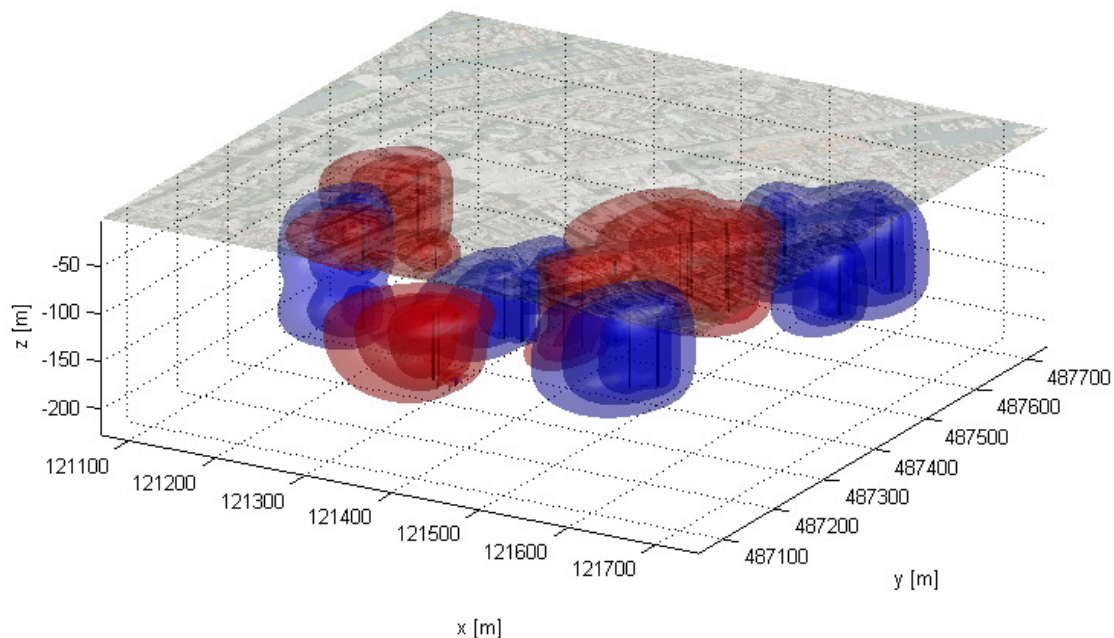

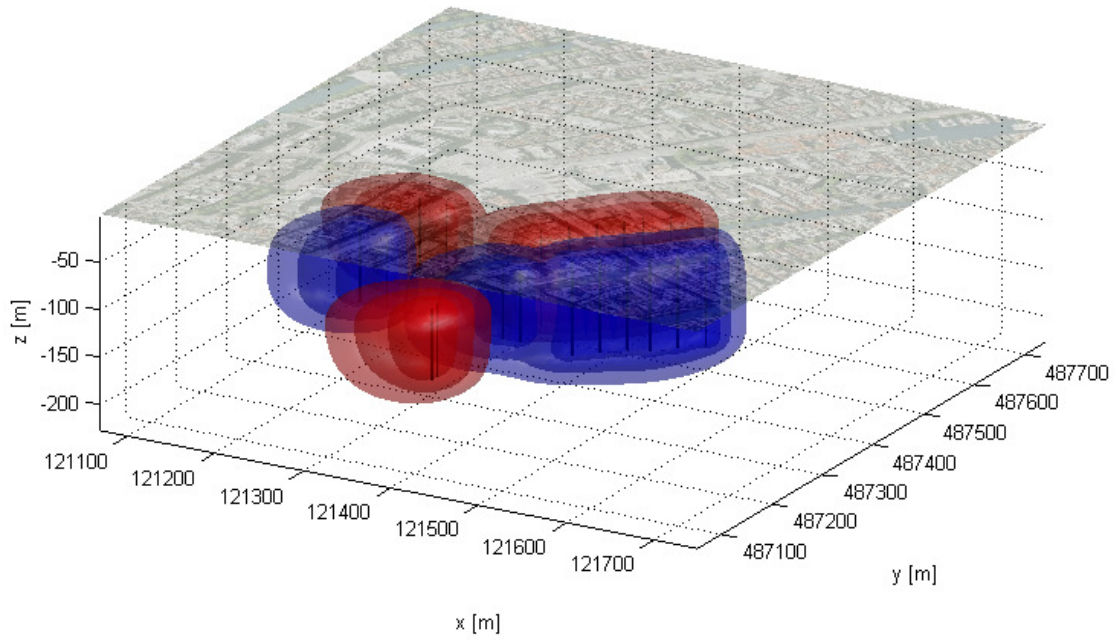**Figure 43: Temperature profile for the mixed case at the end of simulation, in the middle of winter.**

For the grouped case, the warm wells first have a higher efficiency than the cold wells, while after four years the cold wells have the higher efficiency. This is probably due to the fact that the warm wells of group 1 are located downstream of the cold wells, and after four years the cold bubble influences the warm bubble.
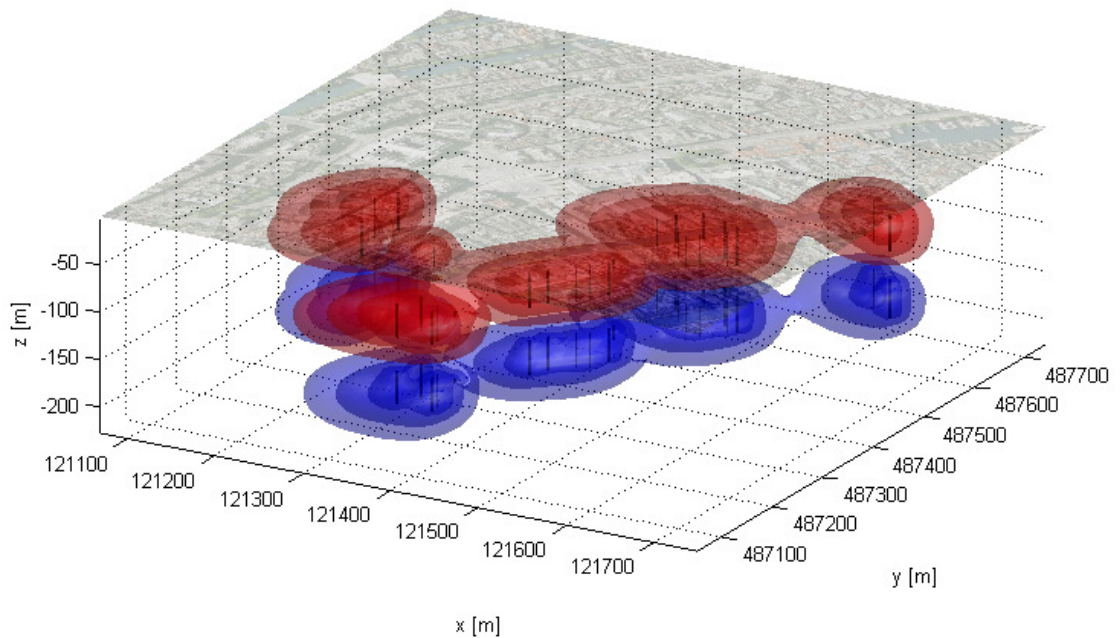
The efficiency of monowells is lower than that of the grouped ones, which uses doublets. This difference is 4-5 % for the cold wells and 2-4 % for the warm wells.

The screens of the warm part of the monowells are distributed in the top of the aquifer, and the cold screens in the bottom. In summer the head in the top of the aquifer will increase and the head in the bottom will decrease, caused by pumping from the cold screens to the warm screens. This causes extra flow in the top of the cold screens to the lower part of the warm screens. This can be seen in the flows, calculated by the MNW package. In the top of the cold screens and the bottom of the warm screens the flow is noticeably larger, while the temperature in these areas is affected the most. Therefore, the wells attract water closer to the ambient groundwater temperature, and the energy efficiency of the wells is lower than in the grouped case.

This effect increases as the difference in head between the upper and lower part of the aquifer increases. These heads are dependent on the distance from the head boundaries, however, and it may be that the used distance of 1000 m from the wells, is not far enough. So in reality the head difference between the upper and lower part of the aquifer may be larger, which causes larger hydrological effects on the temperature profile as well.

8.4.1 Simulation of the grouped case with heating by Euronext in the 1990's

The abandoned ATES system of Euronext was used to test the influence of old energy storage systems, which did not meet an energy balance. The simulation period is more than 30 years: from 1988 to 1999, when the storage was in use, from 1999 until 2010, where no pumping of ATES systems takes place, and finally from 2010 to 2020 for a hypothetical new energy storage system below the Dam. The grouped case was used for this system, as this configuration produced the most optimal efficiency and is the most likely configuration to be installed.

A comparison could be made between the modeled temperatures and the measured temperatures, while the ATES system of Euronext was still in use. The modeled temperature of the water at the extraction wells does not rise as fast as was measured, just like was shown in a modeling exercise in 1995 (IF Technology, 1995). In this modeling it was assumed that thermal short-circuiting took place through the borehole of the wells, causing the water to flow upwards through the wells shaft. This caused the temperature to reach the location of the extraction wells above sooner. This thermal shortcutting through the well shaft is not modeled for this report.

From the abandonment of the system in 1999 until 2010, three processes occur. The bubble of warm water flows downstream by the ambient groundwater flow, it moves upward by density flow caused by the higher temperature of the bubble, and the edge of the bubble becomes less sharp due to conduction and dispersion, see Figure 46 and Figure 47.

As the new system of the Dam Square starts pumping in 2010, the screens of most wells of group 1 are located in the warm water bubble. Therefore warm water is pumped from the aquifer, while still water of 17 $^{\circ}$C is put into the subsurface. This causes a very high overall efficiency for the warm wells, but a lower efficiency for the cold wells, which in the first year is more than 15 % lower than the case without the heating by Euronext, see Figure 48.
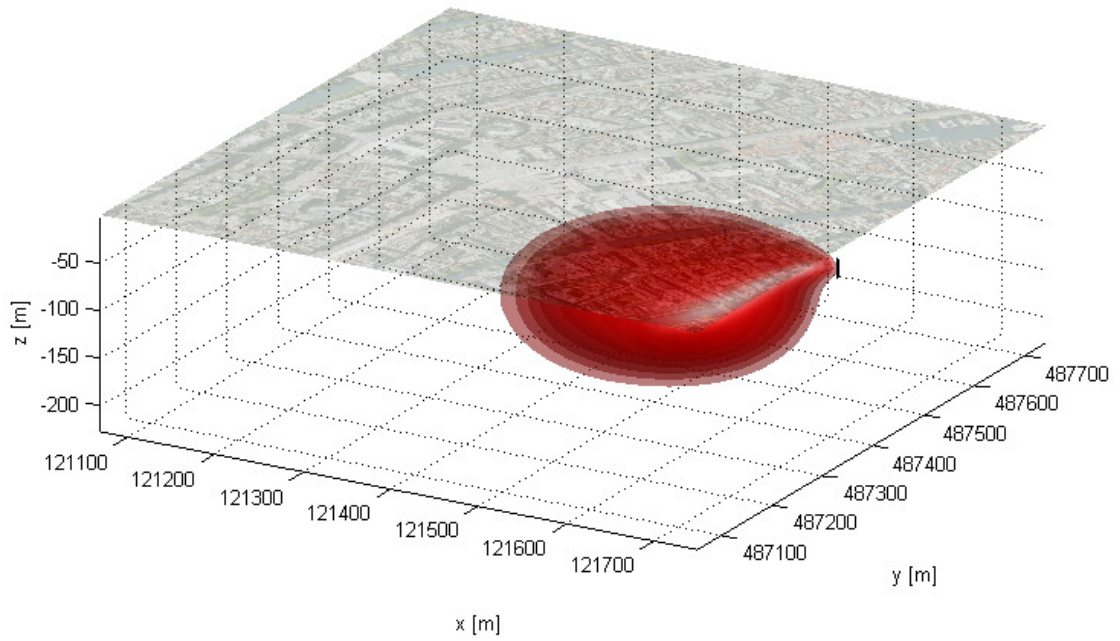
Figure 46: A 3d view of the subsurface below Euronext showing the temperature profile surrounding the abandoned Euronext wells in 1999.
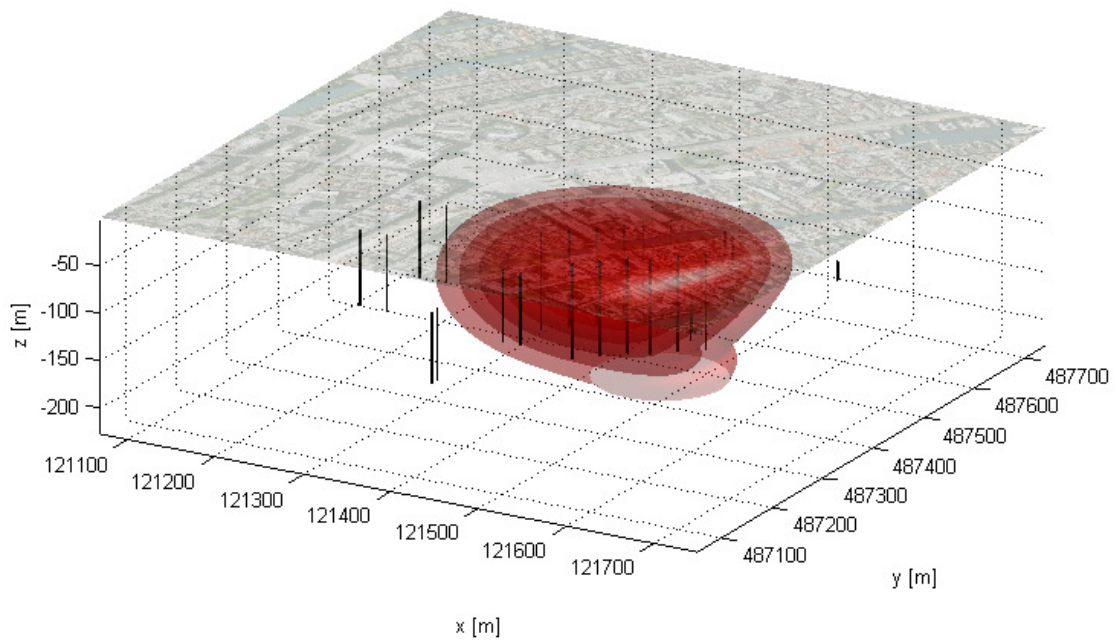

Figure 47: A 3d view of the subsurface below Euronext, after 10 years of no nearby pumping, in 2010, just before the coupled Dam Square system starts pumping.
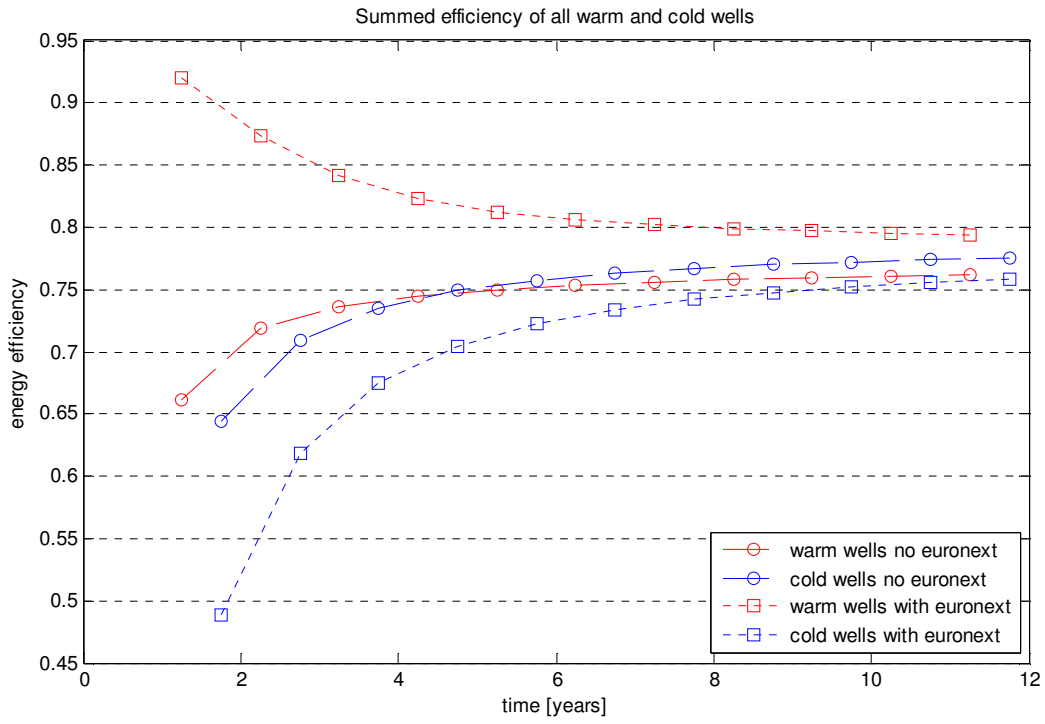
Figure 48: The energy efficiency of the wells of the coupled Dam Square case, with and without heating of the subsurface by the Euronext system.

8.5   Long term development of ATES systems in a city

The simulation of cold and warm wells in a city was done using a MATLAB model, build to show the difference between a situation where buildings are allowed to place their wells wherever they want and a situation where an authority restricts the area where the wells can be placed in cold and warm lanes.

Figure 49 shows the simulation results with and without lane enforcement, for the same buildings. One can see that even without lanes, wells automatically tend to group with their own kind (warm or cold), as a result of the applied rules.
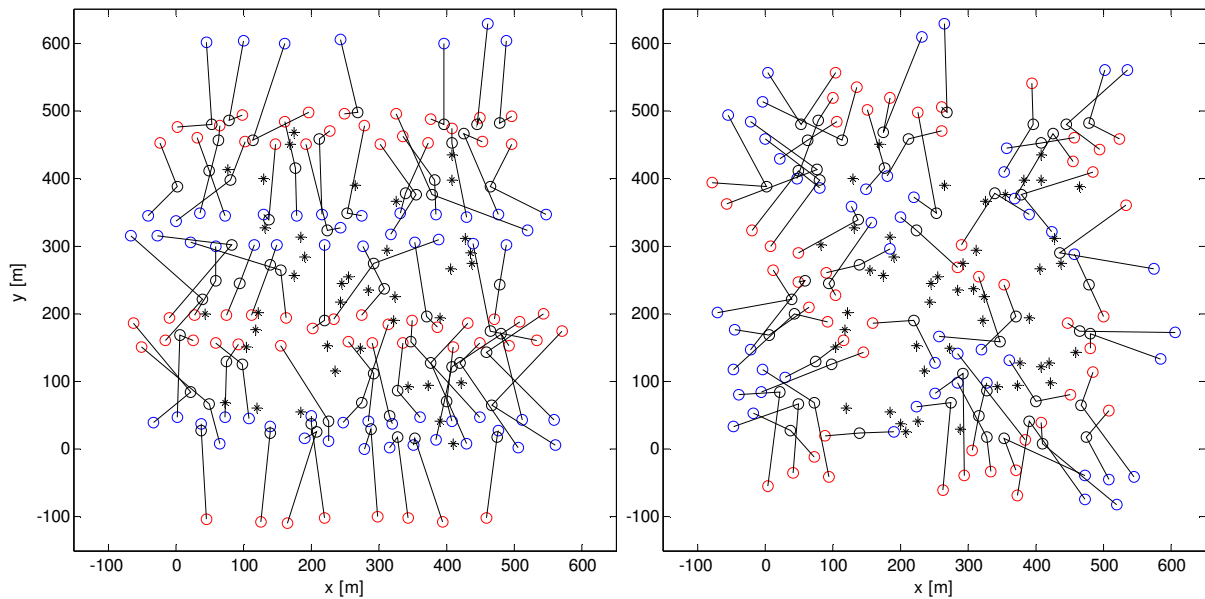

Figure 49:   **Simulation of buildings with their cold (blue o) and warm (red o) wells. Buildings that were able to place their wells (black o), along with the connectors to their wells, and that were unable to place their wells (black *) are also shown. This left graph is for the case with lanes, while the right one is for the case without lanes.**

The number of buildings for this small area can be coupled to real locations in Amsterdam, in order to make the results more meaningful. Two areas are considered. The first is the city center area, as this is the area under consideration in the other sections in this report. The second area is the Zuidas, a newly developed office and housing area, which is still expanding, and can be seen as an upper limit with a maximum building density.

A simple parameter to distinguish between these two areas is the Floor Space Index (FSI), the ratio of the total floor area of all buildings on a certain location to the land area of that location. The centre of Amsterdam has an FSI of 0.8 on average (Uytenhaak, 2008), while the Dam Square area has an FSI of 1.3 (Dienst Ruimtelijke Ordening). The centre of the Zuidas is an area of approximately 500 by 500 m, see Figure 50, that will have an FSI of 4 to 6 (Gemeente Amsterdam, Dienst Ruimtelijke Ordening, 2009), which will be the highest FSI in the Netherlands when the district is finished.
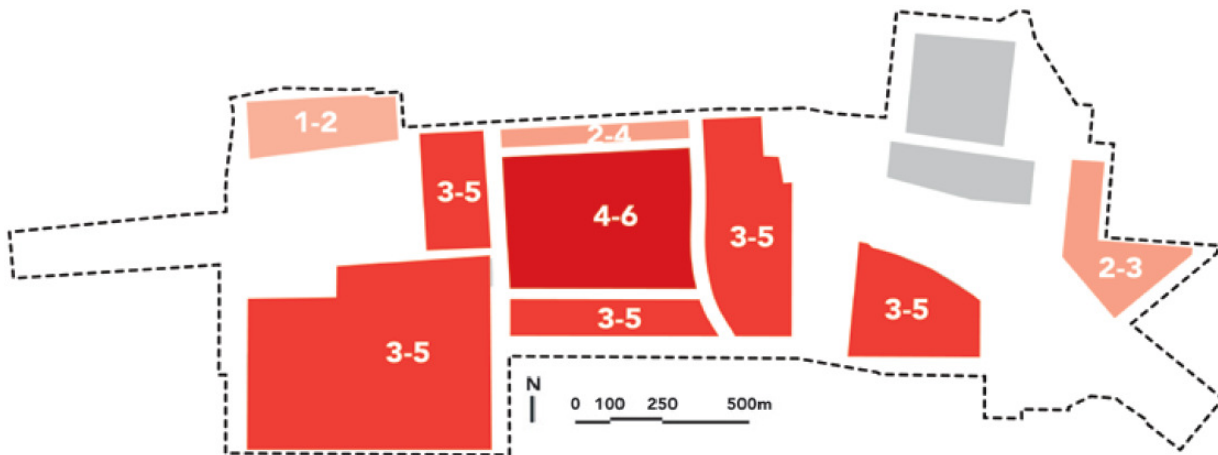
From these FSI values, the thermal energy demand for an area of 500 by 500 m can be established, using rule of thumbs for the required thermal energy per square meter floor. For cooling as well as for heating this is assumed to be 50 kWh/(m^{2}a). In reality this depends strongly on the type of building and insulation, but for simplicity this value is held constant for the two areas. For an FSI of 1, the required cooling and heating energy are each 500*500*50 = 12500000 kWh/a = 12500 MWh/a.

To couple this to a certain number of wells, the amount of energy one doublet can deliver needs to be determined. If we assume that one doublet in a densely built area pumps a bit more water than an average doublet in Amsterdam (see section 1.4), so 200000m^3/well, the supplied amount of energy, with a temperature difference ΔT of 6 ^{o}C is 200000 x 6 x 1.16 = 1392000 kWh/season = 1392 MWh. The number of doublets for the Zuidas will then be (12500 x 5)/1392 = 45 doublets. For the city centre this will be (12500 x 0.8)/1392 = 8 doublets, and for the Dam (12500 x 1.3)/1392 = 12 doublets would be used.

The simulation, discussed at the beginning of this section, is repeated 50 times, after which some conclusions may be drawn. Figure 51 shows the number of buildings that are able to place their wells. In the beginning all buildings are able to place their wells, but, as more buildings have done this, the subsurface gets more crowded. After about 30 buildings, some cannot find a good location for their wells anymore, and so are unable to use ATES. The number of buildings that can use ATES in the case of lanes is larger than the case without lanes, after this 30 buildings.
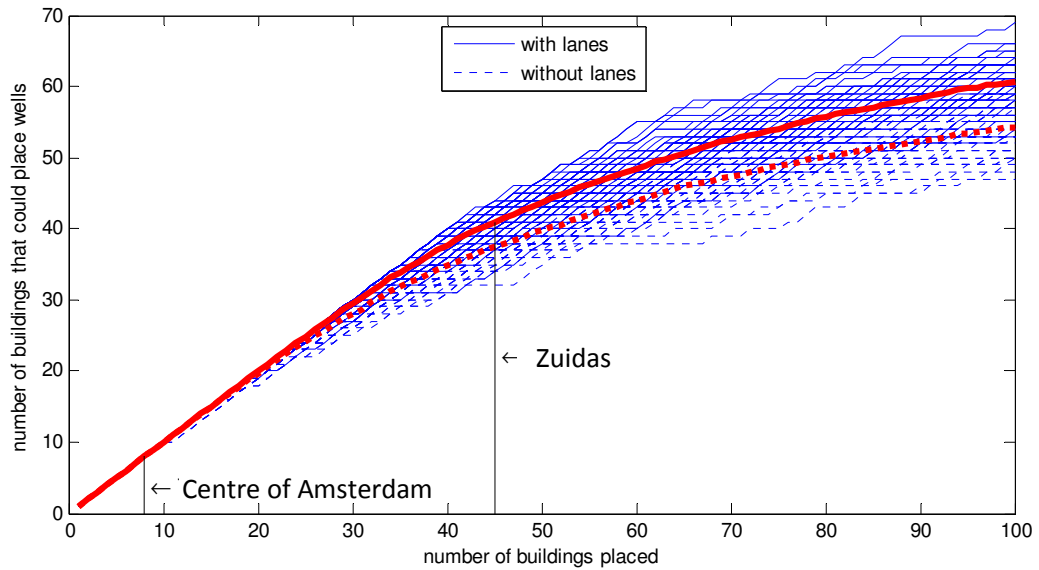
Figure 51: Number of buildings with ATES for 50 simulations, with the average plotted in red.

As more buildings are placed, it gets harder to find a suitable location for the wells. The average distance between a building and its wells gets larger, see Figure 52. For the case with lanes, the average distance between a building and its well is large already at the start of simulation, caused by the forced placing of the wells in lanes. This distance slowly rises as more and more buildings make use of energy storage, while for the case with no lane enforcement the distance rises more quickly. After about 45 buildings, the average distance between a building and its wells will be larger for the laissez-faire simulation.
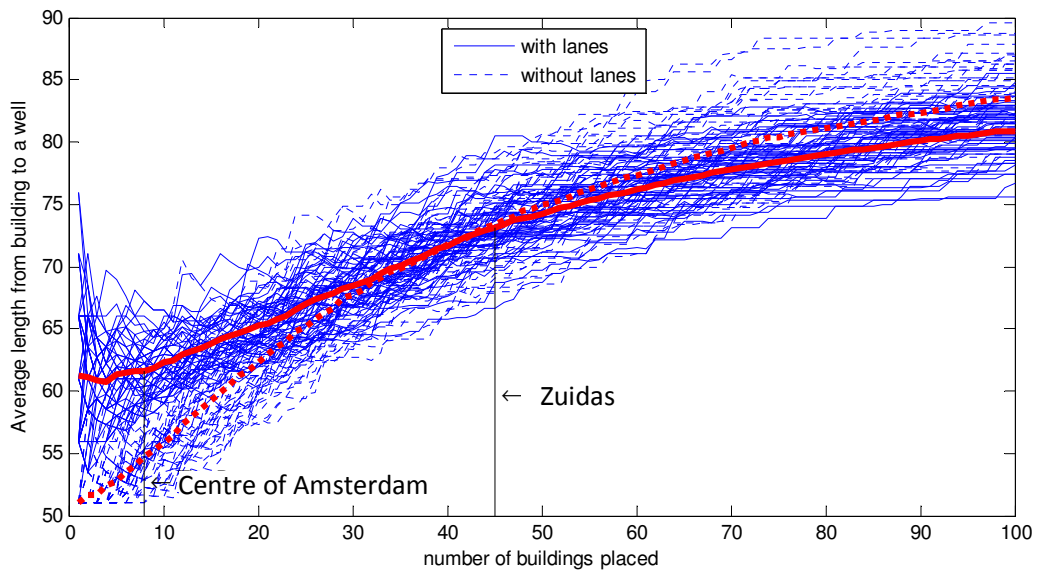

Figure 52: The average distance of wells to their building for 50 simulations, with the average plotted in red.

The simulations can also be tested with the use of the model, using a simplified model setup, with only one model layer for the storage aquifer, to explore the differences in efficiency of both ways of arranging. Figure 55 shows the model results for one of the simulations after 10 years, where the ambient groundwater flow is in west direction, for the situation with as well as without lanes. For the case with lanes the ambient groundwater flow positively influences the other wells of the same kind (warm or cold). In the case without lanes this is not the case, and there is more negative influence between cold and warm wells. Therefore the efficiency will be lower as well, which can be seen in Figure 54. 10 simulations have been performed for four different number of ATES systems: 8, 12, 26 and 45. For all three number of ATES systems, the situation with lanes performs better than the situation without lanes, by 2-3 %. With 8 systems, the simulation results between different simulations differ quite much, while all the simulations with 45 buildings follow the same pattern more closely. This is probably caused by the fact that the spread of wells throughout the model area can be quite different for different simulations of 8 buildings, while for the case with 45 systems the area is full of wells, and the spread between different simulations is equal.

In the first few years the efficiency is higher for a larger density of buildings, which is caused by positive influence of closely spaced wells of the same kind. After 6 years however, for the high density of 45 buidings, the efficiency will become lower than the simulation with 26 buildings, as the previously formed borders of buildings start influencing the borders of bubbles of the other kind.
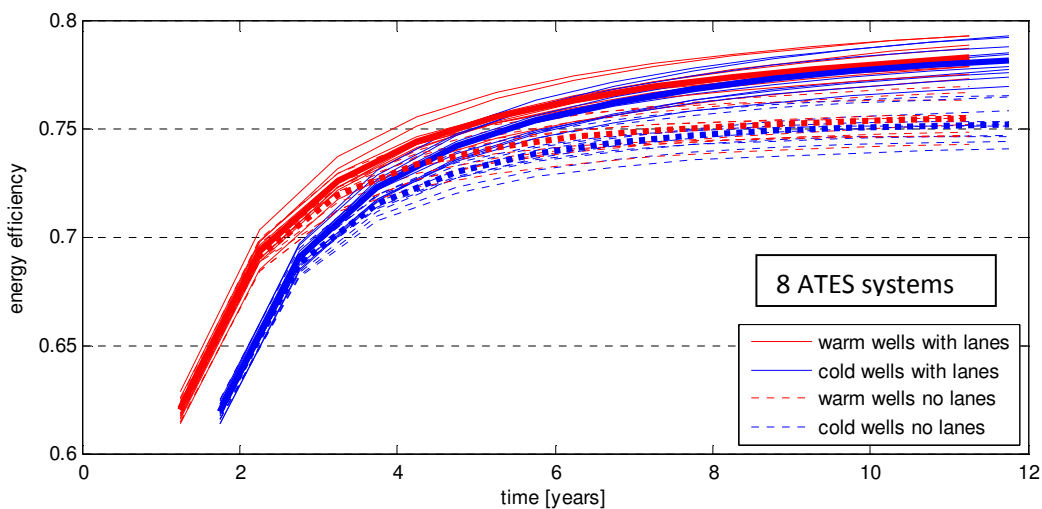

Figure 53: **Energy efficiency for the warm and cold wells for 10 city simulations, each with and without lanes, for 8 buildings, The average over these 10 simulations is plotted thicker.**

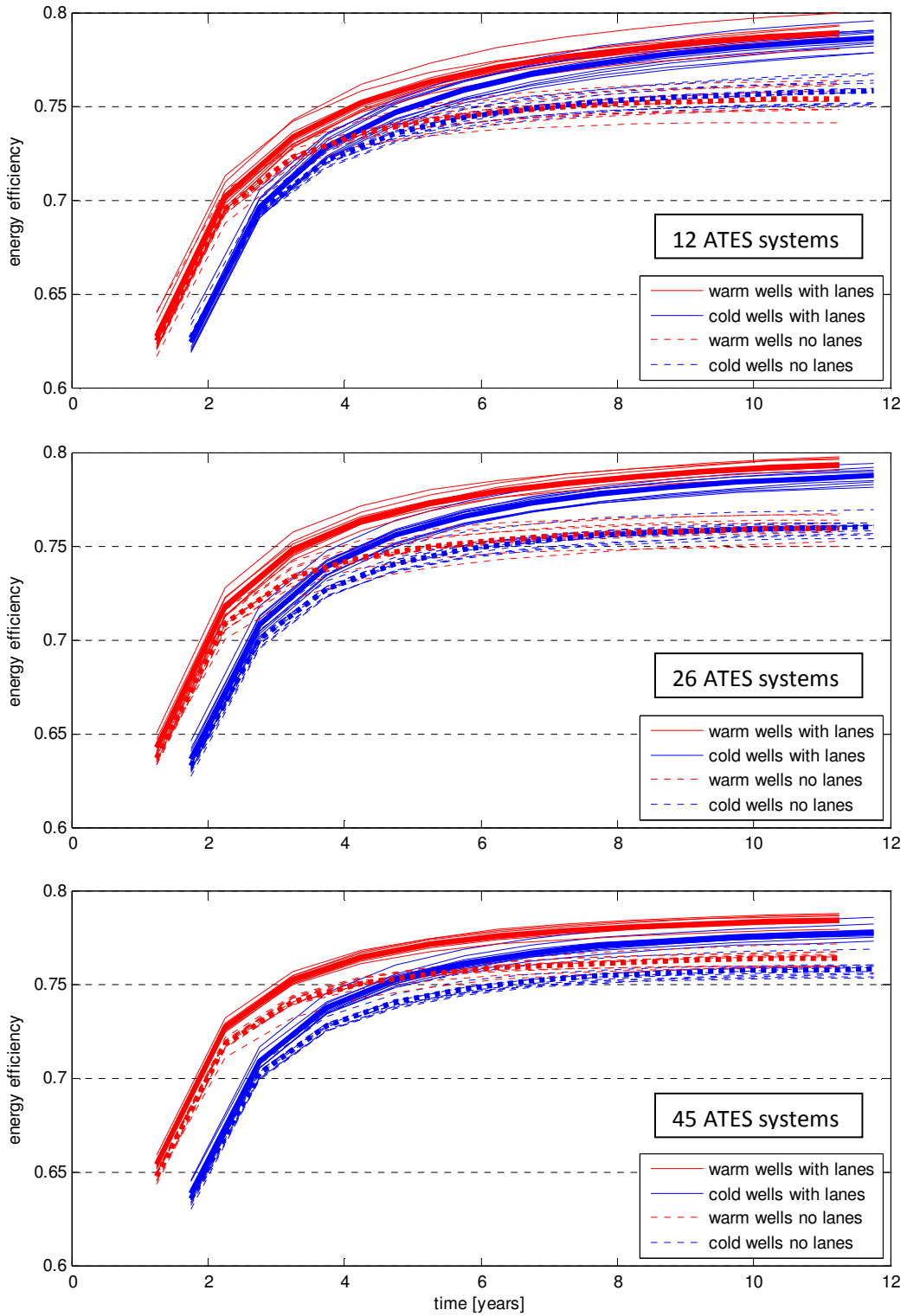**Figure 54:** Energy efficiency for the warm and cold wells for 10 city simulations, each with and without lanes, for 12, 26 and 45 buildings, The average over these 10 simulations is plotted thicker.
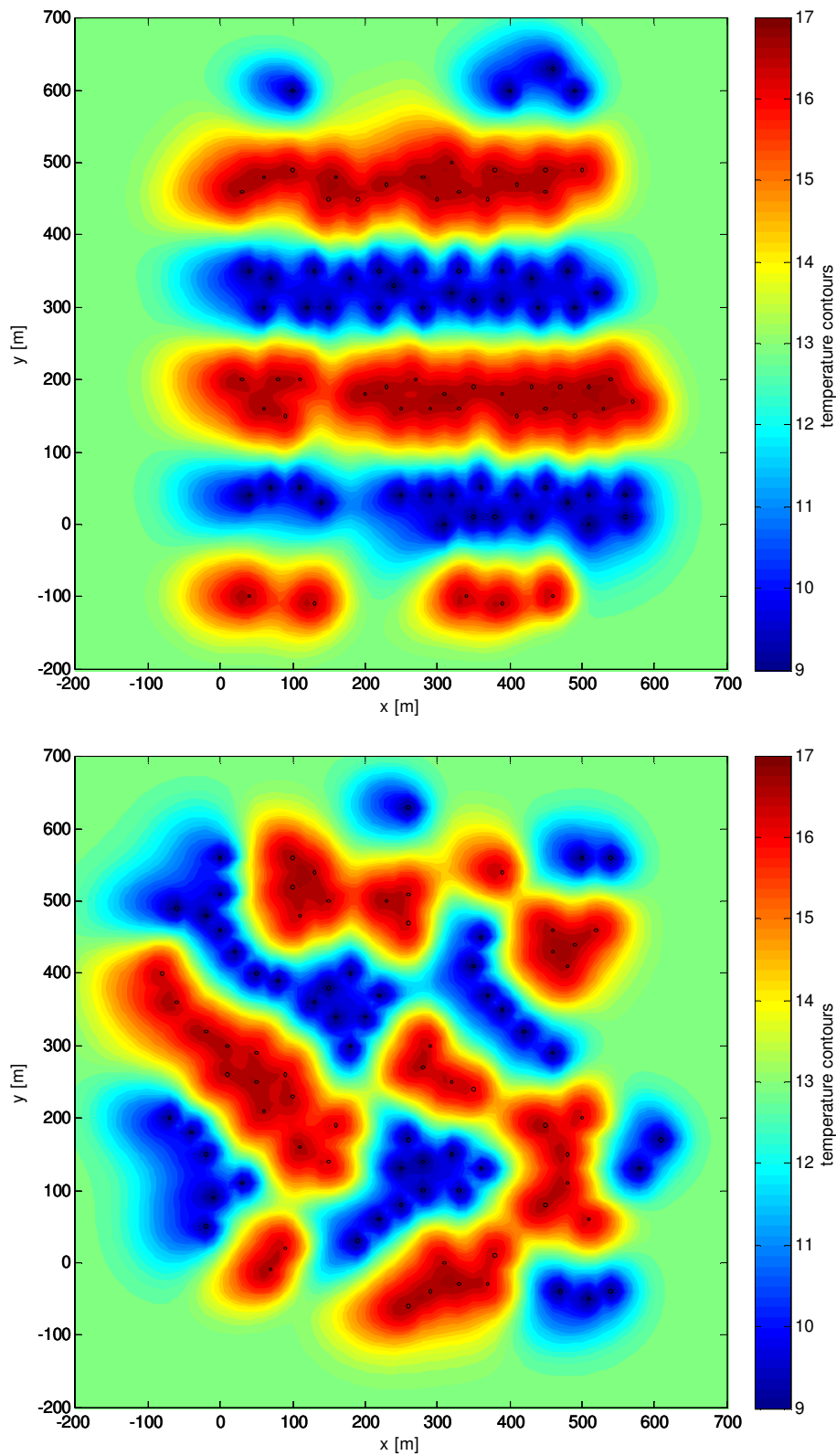
Figure 55: Resulting temperature profile in a horizontal cross-section through the storage aquifer for one simulation of 45 buildings with and without lanes, after 10 years, in the middle of winter.

9. Discussion

Some side-remarks, that were not dealt within the presentation of the results, but that are worth remembering, are discussed in this section.

The model was run with parameters that were taken from related research, reports and articles. It was impossible to calibrate the model or to verify these parameters in a distinctive way. Therefore, the model results could be a bit different in reality. The values for the parameters have been chosen with care however, so that the results can be assumed to represent reality.

The results for the presence of a gravel layer are influenced by the flow through this layer. The layer is assumed to be present in the entire model domain, causing a large flow through this layer, transporting the thermal energy away from the wells. If the gravel layer is not present throughout the model domain and it is only available locally, the gravel layer will not have such a strong influence. So the calculations in this report represent a worst-case scenario for this aspect.

The simulations done for this research have been done with the characteristics of the subsurface of Amsterdam. This means there is low groundwater flow, below 10 m/a, and the corresponding losses are not dominant. In systems where there is far more groundwater flow, like in the east and south of the Netherlands, these losses will be larger, and the results of this thesis may not be valid. Also, Amsterdam has a very thick aquifer with a large capacity to store thermal energy. In other parts of the Netherlands this can be different. In the area around Rotterdam for example, the total screen length of ATES systems is about 40 m, totaled over several aquifers, which are divided by clay layers. The storage capacity per well is then less. For these reasons, it can be concluded that the subsurface of Amsterdam is ideal to store thermal energy.

When simulating the wells for the Dam Square, the injected and extracted amounts of thermal energy were kept equal: the systems were subject to an energy balance. If more heating than cooling is needed, the capacity of an ATES is determined by the needed cooling, and the surplus of heating energy is assumed to be produced by conventional heating systems. So only the base load is delivered by an ATES, and extra capacity is gained from a large connection with the energy company for peak demand, which may not be desirable. Therefore, it might be better to design the ATES on the maximum heating or cooling capacity, whichever is the largest, and regenerate the aquifer with warm or cold water, to achieve an energy balance.

The results show that the grouped case performs better when the energy efficiency is regarded. One could argue that this is because in the mixed case the wells have been placed quite close to each other, causing a decline in efficiency. But when these wells were placed, the cold and warm wells were placed furthest from other wells as possible, while still remaining close to its own building. This would be a real-life situation. In reality, maybe some of the wells would not get a permit, because they would be too close to other wells. The total amount of energy that could be stored would then drop, making the grouped case more optimal from that point of view.

Besides the higher energy efficiency described in the previous paragraph, some other advantages of collective ATES systems are present, which do not follow directly from the model results:

- Buildings can be of a very different nature, from the energy consumption perspective. This is caused by different types of building use as well as by different building properties, such as insulation and the type of heating and cooling system. The installed thermal energy system is often dictated by the age of buildings and limit the most optimal use of subsurface energy storage, for instance due to the temperature requirements of their heating system. Different requirements between buildings favor collective systems, as that facilitates meeting an overall energy balance. A single building will be less able to reach an energy balance, and will either store less energy and use more conventional heating and cooling for peak demand, or use extra energy to regenerate the subsurface temperature. Collective systems cancel out some energy imbalances between buildings, while only having to regenerate the subsurface for the remainder. Fewer regeneration installations are then installed on roofs. This may a large selling point for historic city centers, like in central Amsterdam.
- Not only do systems influence each other by means of their distance and screen elevations. They also influence each other by desynchronized pumping resulting from demand differences over time, which causes ATES systems to push around each other's cold and warm bubbles. When buildings are coupled, thermal energy can be exchanged between buildings, without intervention of the subsurface. Especially during spring and autumn the different thermal demand characteristics between buildings cause one building to cool, while another heats. Smaller ATES systems suffice, and negative efficiency effects due to desynchronized pumping are diminished.
- Fewer wells also result from the entire aquifer thickness being used for storage. When individual buildings install an ATES system, the smaller ones only require a small system, which, because of costs, will likely be limited to the upper part of the aquifer. The lower part of the aquifer will then consequently not be used for storage.

Heating of the subsurface by discharge of waste heat from the cooling system of the Euronext building from 1989 to 1999 shows that an old thermal pollution may limit the cooling performance of future ATES systems, at least initially. It's expected that for future systems cooling is most important. Such old thermal pollutions have to be taken carefully into account in the design of new systems. As the subsurface insolates, bubbles of water at a temperature different from the ambient groundwater will remain in the subsurface for decades. Enforcement of an energy balance is thus essential. Also, old wells have to be sealed properly, to prevent vertical short-circuiting near future systems.

10. Conclusions

Amsterdam has ideal subsurface conditions for energy storage. A thick aquifer is available with hardly any clay from NAP -70 to -180 m, with a small ambient groundwater flow of 10 m^3/a. This aquifer is covered by thick clay layers protecting the phreatic surface against negative effects of pumping. Therefore it's essential that this capacity is put to its maximum beneficial use. Throughout this thesis, knowledge was gained about the influence of heterogeneities, the mixing of the salt gradient, methods to cooperate, and arranging patterns of ATES systems. From this knowledge, the following conclusions are drawn.

The variable density and viscosity flow and transport model SEAWAT was used to answer the research questions. At first, variable density and viscosity were thought to have a large influence on the cold and warm bubbles of ATES systems. This did not show in the model results, however, for the encountered salt concentrations, 1 to 10 kg/m^3, and temperature range, 9 to 17 ^{o}C. Therefore, for designing ATES systems within these margins, a simpler model could be used, without temperature dependency of density and viscosity. This will reduce calculation time, which otherwise can take up to a few days.

An important aspect with regard to ATES systems is the heterogeneity of the aquifer. Heterogeneity can have a significant effect on the shape of the cold and warm water bubble. This thesis approached this problem in two manners: by simulation of a gravel layer, as was found in drillings, and by generating heterogeneities in the horizontal plane for each model layer of 5 m thickness. When a gravel layer is present, more thermal energy is lost by advection due to ambient groundwater flow and conduction and dispersion through the top and bottom of the gravel layer. The retrieved energy will be up to 10 % lower, compared to a homogeneous subsurface. This efficiency loss can be reduced by installing a blind piece of casing opposite this layer, reducing the maximum efficiency loss to 5 %. With heterogeneities in the horizontal plane, the retrieved temperatures, and therefore the retrieved amount of energy, seem to be virtually independent of these heterogeneities. The range of heterogeneities was tested, which showed that only for large ranges, in the order of the distance between the warm and cold well, there is a decline of 3 % in efficiency. Little information about the heterogeneity of the subsurface is available. However, the model showed that it does not seem necessary to map this extensively before designing an ATES system. The location of gravel layers should be examined however. In the subsurface below Amsterdam there is plenty of space in the sand layers below NAP -70 m, so probably there is no need to place a screen in the gravel layers. In other places, where the available depth for screens is smaller, the total length of screen would be reduced significantly when no screens are placed at gravel layers.

ATES systems will not only pump water, but also salt, back and forth from along the screens of its wells. This will inevitably mix the salt and change the original vertical salt gradient into a horizontal one. It was shown this effect remains within 100 m from the wells.

The simulations in this report show that the overall energy efficiency of a collective system is higher than that of individual systems. On top of that, the thermal energy can be stored with less pumping, as an energy balance then pertains to the entire group instead to individual buildings. Therefore, less regeneration of subsurface temperatures has to take place to reach this energy balance. This saves water displacement, energy and money. Also, the number of wells will decrease, as smaller systems, with

multiple wells can be combined in systems of a few wells with longer screens. The subsurface is used more efficiently, as maximum beneficial use requires the system size to be such that the entire aquifer thickness is utilized. Finally, thermal energy can be exchanged between buildings in a collective system. For these reasons, it is necessary that building owners cooperate in designing and operating of ATES systems, in order to achieve maximum beneficial use of the subsurface, and realize the ambitious energy goals of the municipality of Amsterdam.

Monowells are an interesting alternative for collective systems in a thick aquifer, with little space to install the wells. All warm and all cold wells join into two large warm and cold bubbles at different elevations, which, due to its size, is hardly influenced by ambient groundwater flow. Because there is no horizontal influence, the wells can be placed wherever one wants. Amsterdam has a thick aquifer, causing the capacity of long doublets to not be limited by the injection speed on the borehole wall, but by the capacity of the pumps, which is 200 m^3/h at maximum for standard systems. Therefore, it is possible to use monowells with a large capacity, even though screens cannot be placed in the vertical part of the aquifer between the warm and cold screen. A disadvantage of monowells is the larger flow between the upper part of the cold screens and the lower part of the warm screens, causing larger thermal energy losses than the doublets of a collective system. Another disadvantage can be hydrologic effects. In Amsterdam, the screens of a monowell are placed in one aquifer, and there is little vertical resistance. When this is larger, and collective systems start pumping all at the same time, large hydrologic effects can take place, which may be unacceptable, especially at the top of the aquifer.

The impact of old thermal pollutions can be quite large. It was shown that the warm bubble of the abandoned Euronext system has a negative influence of up to 15 % on the energy efficiency of the cold wells in the first years of use of a hypothetical collective ATES system near the Dam. One of the problems found in this system, is vertical short-circuiting through the boreholes of the wells of the Euronext system. To protect future use of the subsurface, it is vital abandoned wells are sealed correctly.

Warm and cold wells can be arranged in several ways. This thesis examined the difference between arranging the wells in lanes or just randomly. This was done with a MATLAB model simulating a random city pattern of 500 by 500 m. When the wells are arranged randomly, a pattern of clustered warm and cold wells still occurs, as wells of the same sort group together, due to the required distance between warm and cold wells. The simulations are judged on three criteria: (1) the number of buildings that can use ATES, (2) the average distance from the building to its wells, and (3) the average energy efficiency of the wells. Lane enforcement works like a planning ahead for the future, which yields a more optimal situation in the long run, while in the beginning with only few systems such enforcement will increase cost relative to the unrestricted situation. If the most densely built area of Amsterdam, the Zuidas, uses ATES for its entire thermal energy consumption, lane enforcement has its benefits: more buildings can use ATES and the wells will have a higher efficiency, while the distance between buildings and their wells is equal for both situations. For all less densely built areas, the laissez-faire situation and lane enforcement both have their advantages. In both situations all buildings can install an ATES system. The laissez-faire situation will reduce pipe length, and, therefore, cost of installation, while the performance of the situation with lanes is 2 to 3 % higher.

11. Recommendations

Some recommendations that were encountered throughout this research are discussed is this chapter.

In section 4.4 was shown that SEAWAT can be used to simulate heat flow. However, in SEAWAT the density depends on temperature using a linear relationship, which is not realistic. This must be quite easy to change into a more complex one. This has been done for viscosity, where the user can choose between several formulas to calculate the dependency of the viscosity on temperature. So there is no reason why this cannot be done for density. For this research it was not really important that a linear relationship was used, as the temperature interval was quite small form 9 to 17 ^{o}C, and the temperature dependency could be simplified to a linear relationship. But for other research with a larger difference in temperatures this should be changed.

During the modeling some problems occurred with modeling the wells. First the MNW (Multi Node Well) package for MODFLOW was thought to be useful, as it could represent wells that cross more than one (model-) layer. But it turned out this package is not fully compatible with SEAWAT. Another problem occurred with recirculation wells. These recirculation wells could be used to set the salt concentration of the infiltrating water equal to the salt concentration of the discharged water from the other well of the doublet. However, the recirculation wells in MODFLOW can only couple one cell to another cell, and no multi node wells. Ideally one would like to have multi node wells that work in SEAWAT, and that can be coupled to each other using recirculation wells. For now this is not possible, and it would have taken too much time to implement it for this thesis.

To more approach reality while modeling, it would be better if the well discharge would be dependent on the retrieved temperature. An ATES system needs to produce a specific amount of energy, while the temperature with which the water is injected into the subsurface is constant. When the temperature in the warm well for example drops, more water needs to be pumped to produce the same amount of energy. The model right now determines the needed discharge beforehand, without regard of the extracted temperature. This could be changed by generating a new input file for each model time step, in which the discharges depend on the output of the previous time step. This could have been done, just like was done for the mixing of salt, but would take too much time for calculating all the different cases. One could try to implement this directly in SEAWAT.

Maybe SEAWAT is not the right model to simulate ATES wells. MODFLOW, and therefore SEAWAT, uses a rectangular grid. The wells have circular patterns, where the locations near the wells have to be modeled more precise than the rest of the grid. This is easier with a finite element grid, consisting of triangles for example. In this way, it is possible to refine the model grid around the wells. In MODFLOW 2000 this is also possible, but the grid can only be refined for entire rows or columns. Therefore many cells have a close grid spacing while they do not really need one. In MODFLOW 2005 it is possible to refine the model in certain cells, but this version is not used for SEAWAT. A good alternative therefore could be FEFLOW. This software is especially designed for density dependent flow with a finite element grid. It is not free or open source however, and it has a steeper learning curve than MODFLOW. MODFLOW also has the advantage that it is being used all over the world, has a rectangular grid is easy to understand.

The knowledge about heterogeneity of the subsurface in the Netherlands could be improved. Now there is no data about heterogeneity of layers in REGIS yet, while it could be of some use when designing an ATES, or for other transport research. Currently there is a project going on by Deltares/TNO, for which 300 drillings until NAP -30 m will be made. In the drillings elaborate hydraulic conductivity measurements and drilling descriptions will be examined to map the variation in hydraulic conductivity, firstly in the vertical direction, but later possibly also in the horizontal direction. This process is only in its initial phase however, and it will take several years until these drillings will reach the Peize and Waalre Formations.

Simulation of heterogeneities in the horizontal plane showed that when the range is of the same order as the distance between the ATES wells, the heterogeneity starts influencing the energy efficiency of the wells. Therefore, when more is known about the heterogeneity of the subsurface, the wells should be placed at a distance apart that is smaller than the range of the variogram of these heterogeneities. Also, as the Peize and Waalre Formations were deposited by old braided rivers, heterogeneities could show large anisotropy, where the spatial dependency in west-east direction could be much larger than the spatial dependency in north-south direction. The influence on the placing of the wells and their efficiency could be examined.

As could be seen gravel layers influence the results of energy storage. The energy will flow away from the well more quickly and a lot of energy is lost from the wells. By installing no screen at this gravel layer these losses can be reduced.

The forced placement of wells in lanes might not be the best solution for the subsurface of Amsterdam. Instead, when drawing a master plan, the clusters of warm and cold wells, that naturally occur, should be contained, so that these clusters will not get too large and start influencing other clusters negatively.

For future research a further evaluation of the simulation of a city can be undertaken. For this report buildings were placed randomly in a grid of 500 by 500 m. At any moment a randomly chosen individual actual building tries to install an ATES. This simulation could be improved by coupling this to an actual map with existing buildings, streets and other urban characteristics. Then the size of each ATES could be made proportional in size to the contents of the building. Different kinds of cities could be tested, according to their buildup, with different kinds of buildings, categorized by their use of thermal energy throughout the year. There are quite some interesting opportunities to look into this subject more extensively.

References

Bachmaier, M., & Backes, M. (2008). Variogram or semivariogram? Understanding the variances in a variogram. *Precision Agric* , 173–175.

Berendsen, H. (2004). *De vorming van het land: inleiding in de geologie en de geomorfologie.* Assen: Van Gorcum & Comp. B.V.

Berendsen, H. (2005). *Fysisch-geografisch onderzoek, chapter 9: Grind analyse.* Utrecht: Koninklijke van Gorcum.

Bonte, M., van den Berg, G., & van Wezel, A. (2008). Bodemenergiesystemen in relatie tot grondwaterbescherming. *bodem* , 22-26.

Bridger, D. W. (2006). *Influence of aquifer heterogeneity on the design and modelling of Aquifer Thermal Energy Storage (ATES) systems.* Burnaby, Canada: Simon Fraser University.

De Ruiter Boringen en Bemalingen bv. (n.d.). *Flyer De Ruiter Standaard WKO systemen.* Retrieved oktober 1, 2009, from BAM: http://www.bam.nl/baminternet/baminternet/portalen/De_Ruiter/Brochures/20050117_Flyer_standaard.pdf

Deutsch, C. V. (1997). *GSLIB: Geostatistical Software Library and User's Guide.* New York: Oxford University Press.

Dienst Ruimtelijke Ordening. (n.d.). *FunctieMix en Spacemate van Amsterdam*. Retrieved december 13, 2009, from GISDRO: http://gisdro.nl/FUNCTIEMIX/

Doughty, C., Hellstrom, G., & Fu Tsang, C. (1982). A Dimensionless Parameter Approach to the Thermal Behaviour of an Aquifer Thermal Energy Storage System. *Water Resources Research* , 571-587.

Ecofys. (2009). *Schaalsprong duurzame energieopwekking in Amsterdam.* Amsterdam.

Encyclopædia Britannica Online. (2009). *Ocean*. Retrieved May 19, 2009, from http://www.britannica.com/EBchecked/topic/424285/ocean

Engineering Tool Box. (2007). Retrieved June 2, 2009, from The Engineering Toolbox: Tools and Basic Information for Design, Engineering and Construction of Technical Applications: http://www.EngineeringToolBox.com

Ferguson, G. (2007). Heterogeneity and Thermal Modeling of Ground Water. *GROUND WATER* , 485-490.

Fitts, C. R. (2002). *Groundwater Science.* Scarborough, Maine: Academic Press.

Gelhar, L. W., Welty, C., & Rehfeldt, K. R. (1992). A critical Review of Data on Field-Scale Dispersion in Aquifers. *Water Recour. Res.* , 1955-1974.

Gemeente Amsterdam, Dienst Ruimtelijke Ordening. (2009). *Visie Zuidas.* Amsterdam: gemeenteraad Amsterdam.

Halford, K., & Hanson, R. (2002). *User Guide for the Drawdown-Limited, Multi-Node Well (MNW) Package for the U.S. Geological Survey's Modular Three-Dimensional Finite-Difference Ground-Water Flow Model, Versions MODFLOW-96 and MODFLOW-2000.* Sacramento, California: U.S. Geological Survey.

Harbaugh, A. W., Banta, E. R., Hill, M. C., & McDonald, M. G. (2000). *MODFLOW-2000, The U.S. Geological Survey Modular Ground-Water Model—User Guide to Modularization Concepts and the Ground-Water Flow Process.* Reston, Virginia: U.S. Geological Survey.

Hardin, G. (1968). The Tragedy of the Commons. *Science* , 1243-1248.

IF Technology. (1995). *Effectenbeurs Amsterdam, Analyse Grondwaterkoelsysteem.* Arnhem.

IF Technology. (1999). *Koudeopslag Stadhuis Amsterdam Voorontwerp grondwatersysteem.* Arnhem.

IF Technology. (2001). *Ontwerpnormen voor bronnen voor koude/warmteopslag.* Arnhem: Novem.

IF Technology. (2004). *Temperatuureffecten op grondwaterkwaliteit: Samenvatting bestaande kennis.* Arnhem.

Langevin, C. D., Thorne, D. T., Dausman, A. M., Sukop, M. C., & Guo, W. (2008). *SEAWAT Version 4: A Computer Program for Simulation of Multi-Species Solute and Heat Transport.* Reston, Virginia: U.S. Geological Survey.

Langevin, C., & Zygnerski, M. (2006). *Axisymmetric simulation of aquifer storage and recovery with SEAWAT and the Sea Water Intrusion (SWI) Package for MODFLOW.* Fort Lauderdale, FL, USA: U.S. Geological Survey.

Log-normal distribution. (2009). Retrieved October 12, 2009, from Wikipedia: http://en.wikipedia.org/wiki/Log-normal_distribution

Lusczynski, N. (1961). Head and flow of ground water of variable density. *Journal of Geophysical Research* , 4247–4256.

N.V.O.E. (2006). *Nederlandse Vereniging voor Ondergrondse Energieopslagsystemen - Richtlijnen Ondergrondse Energieopslag.* Woerden: NVOE.

Nielsen, K. (2003). *Thermal Energy Storage A State-of-the-Art.* Trondheim: Department of Geology and Mineral Resources Engineerin NTNU.

Olsthoorn, T. N. (2009). *mflab*. Retrieved from http://code.google.com/p/mflab/

Omer, A. M. (2007). Green energy saving mechanisms. *Renewable & Sustainable Energy Reviews* .

Pomper, A. B. (1996). Schatting van doorlaatfaktoren (k-waarden) aan de hand van in boorarchieven aanwezige boorbeschrijvingen. *Stromingen 2, nr 4* , 37-46.

Post, V., Kooi, H., & Simmons, C. (2007). Using Hydraulic Head Measurements in Variable-Density Ground Water Flow Analyses. *Ground Water* , 664–671.

Reilly, T. E., & Harbaugh, A. W. (1993). Computer note: simulation of cylindrical flow to a well using the U.S. Geological Survey modular finite-difference ground-water flow model. *Ground Water* , 489-494.

Rosen, M. A. (1999). Second law analysis of aquifer thermal energy storage systems. *Energy* , 167-182.

Schäfer, W. (n.d.). *Volresungsskripten.* Retrieved April 21, 2009, from Dr.-Ing. Wolfgang Schäfer Grundwassermodellierung: http://www.schaefer-gwm.de/downloads/transport_modelling.pdf

Shaw-Yang, Y., & Hund-Der, Y. (2008). An analytical solution for modeling thermal energy transfer in a confined aquifer system. *Hydrogeology Journal* , 1507–1515.

Sommer, W. (2007). *Het effect van ruimtelijke dimensionering op het rendement van warmte-koude opslagsystemen.* Almere: Witteveen + Bos.

Speelman, H., & Houtman, H. (1979). *Grondwaterkaart van nederland, Amsterdam.* Delft: Dienst Grondwaterverkenning TNO.

Stuyfzand, P. J., Lebbink, J., & Nienhuis, P. (2008). *Koude-Warmte Opslag (KWO) in grondwaterbeschermingsgebieden: (mogelijke) bezwaren.* Nieuwegein: KWR.

Taskforce WKO. (2009). *Groen licht voor Bodemenergie.* Den Haag: VROM.

The Engineering Toolbox. (2009). *Water - Thermal Properties*. Retrieved May 19, 2009, from http://www.engineeringtoolbox.com/water-thermal-properties-d_162.html

Thorne, D., Langevin, C., & Sukop, M. (2006). Addition of simultaneous heat and solute transport and variable fluid viscosity to SEAWAT. *Computer and Geosciences, v. 32,* , 1758-1768.

TNO. (2009). *REGIS*. Retrieved 10 21, 2009, from Dinoloket: http://www.dinoloket.nl

Uytenhaak, R. (2008). *Steden vol Ruimte: kwaliteiten van dichtheid.* Rotterdam: 010 Publishers.

van Dalfsen, W. (1981). *The shallow subsurface temperature field in the netherlands.* Delft: Groundwater Survey TNO.

van de Weerdhof, B. (2005). *Meervoudige ontwerp- en effectenstudie van koude-warmteopslagsystemen in de binnenstad van Den Haag.* Delft: Technische Universiteit Delft.

Vermaas, D. (2008). *Inventarisatie van mogelijke knelpunten in Koude-/Warmteopslag.* Almere: Witteveen + Bos.

Xu, M., & Eckstein, Y. (1995). Use of Weighted Least Squares Method in Evaluation of the Relationship Between Dispersivity and Field-Scale. *Ground Water* , 905-908.

Zheng, C., & Wang, P. P. (1999). *MT3DMS: A Modular Three-Dimensional Multispecies Transport Model for Simulation of Advection, Dispersion, and Chemical Reactions of Contaminants in Groundwater Systems; Documentation and User's Guide.* Tuscaloosa, Alabama: U.S. Army Corps of Engineers.

Appendix 1. MODFLOW/MT3DMS/SEAWAT Modeling using MATLAB

In this thesis MATLAB is used to steer SEAWAT by writing input-files and reading the output from SEAWAT. Therefore it is possible to use all MATLAB functions, familiar to many people already. Extra functions and resources are available on the internet. The order in which processes are run for one simulation is shown in Figure 56.

For the input of the model, matrixes can be used to determine input for every model cell in the model domain. Other variables, which express calculation or output options can be read from a spreadsheet file. This spreadsheet file consists of several sheets, where MODFLOW , MT3DMS and SEAWAT each have their own sheet. In the first sheet the user can choose which MODFLOW and MT3DMS packages to run and which not to run. Some MODFLOW packages have their own sheet, like the WEL, MNW or CHD package. Also there is a sheet describing the properties of each layer, and a sheet describing the properties of each calculation period. These sheets are read by MATLAB and, together with the earlier defined matrixes, input files are written for MATLAB, MT3DMS and/or SEAWAT, using the scripts of mflab (Olsthoorn, 2009). By selecting what program to run, one can choose what to calculate: flow, flow and transport or density dependent flow and transport.

After the model is run, MATLAB is used to read the output-files and can use any incorporated graphical function to present the results.

Especially for this research code was written to create the calculation grid and determine the input for the wells. This information is read from a spreadsheet called registraties.xls. The calculation grid is generated automatically based on the locations of the wells. The vertical location of the screens of the wells is also read from this file. The total discharge per well is taken from the spreadsheet, after which MATLAB determines the discharge per cell of the well, as each well is located in multiple MODFLOW cells.

Spreadsheet file

3d-matrixes for boundaries and initial conditions

mflab

SEAWAT

mflab-analyze

3d-views

cross-sections

temperature and efficiency graphs
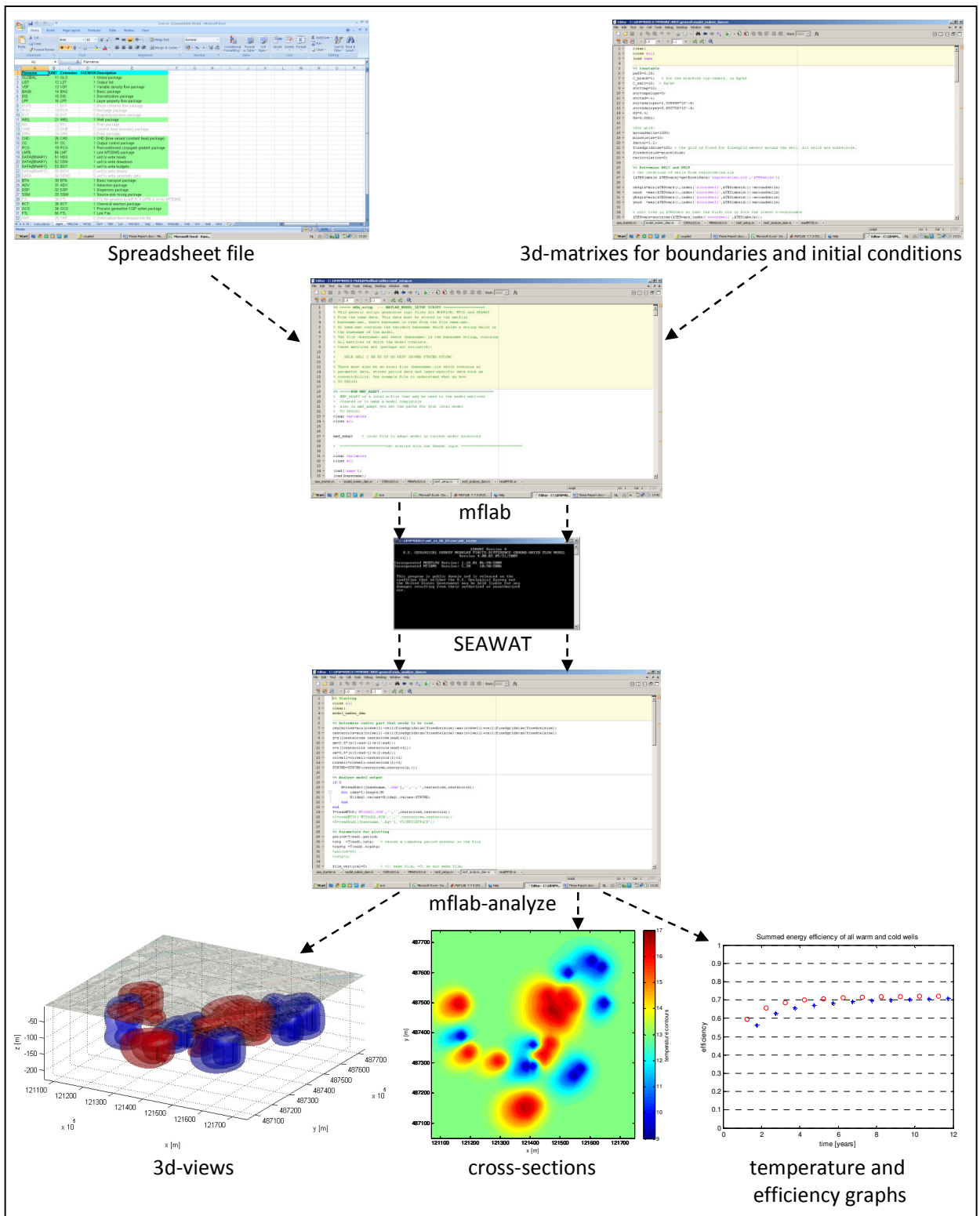
Figure 56: Flow diagram of model steps.

Appendix 2. Validation of MATLAB code with examples from the SEAWAT manual

The MATLAB code is validated with a case from the latest SEAWAT manual (Langevin, Thorne, Dausman, Sukop, & Guo, 2008). In this case the problem consists of a two-dimensional cross section of a confined coastal aquifer initially saturated with relatively cold seawater at a temperature of 5 ^{o}C. Warmer freshwater with a temperature of 25 ^{o}C is injected into the coastal aquifer along the left boundary to represent flow from inland areas. The warmer freshwater flows to the right, where it discharges into a vertical ocean boundary. The ocean boundary is represented with hydrostatic conditions based on a fluid density calculated from seawater salinities at 5 ^{o}C. No-flow conditions are assigned to the top and bottom boundaries. This situation is calculated 7 times, with increased complexity, from only variable density depending on the salt concentration, to variable viscosity and density on the salt concentration, temperature and pressure, and retardation taken into account for temperature.

The objective is to get results that are equal to the results in the SEAWAT manual. All 7 cases have been calculated with Mflab. Below is the graph from case 7 of the example in the SEAWAT-manual. In this case the temperature boundary is different from the salt boundary, in the way that conductive transport is possible from the temperature boundary. Different boundaries for different species are not yet possible in mflab, so the boundary is set as a non-conductive boundary. This is why the results differ slightly at the right boundary of the model area.
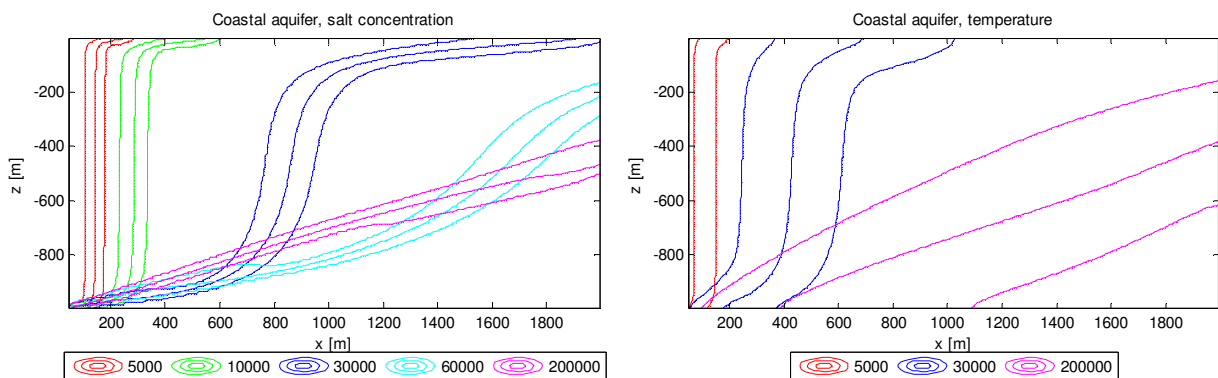
Figure 57: The salinity and temperature transition zones, as calculated by SEAWAT with MATLAB. The lines represent the 1, 50 and 99 percent salinity or temperature values. These change in time, and some time steps are plotted, each in another color as indicated in the legend, which shows the amount of days simulated.

A

time=60,000 days

time=10,000 days

time=5,000 days

time=10,000 days

time=30,000 days

time=30,000 days

time=60,000 days

time=200,000 days

time=200,000 days

time=5,000 days
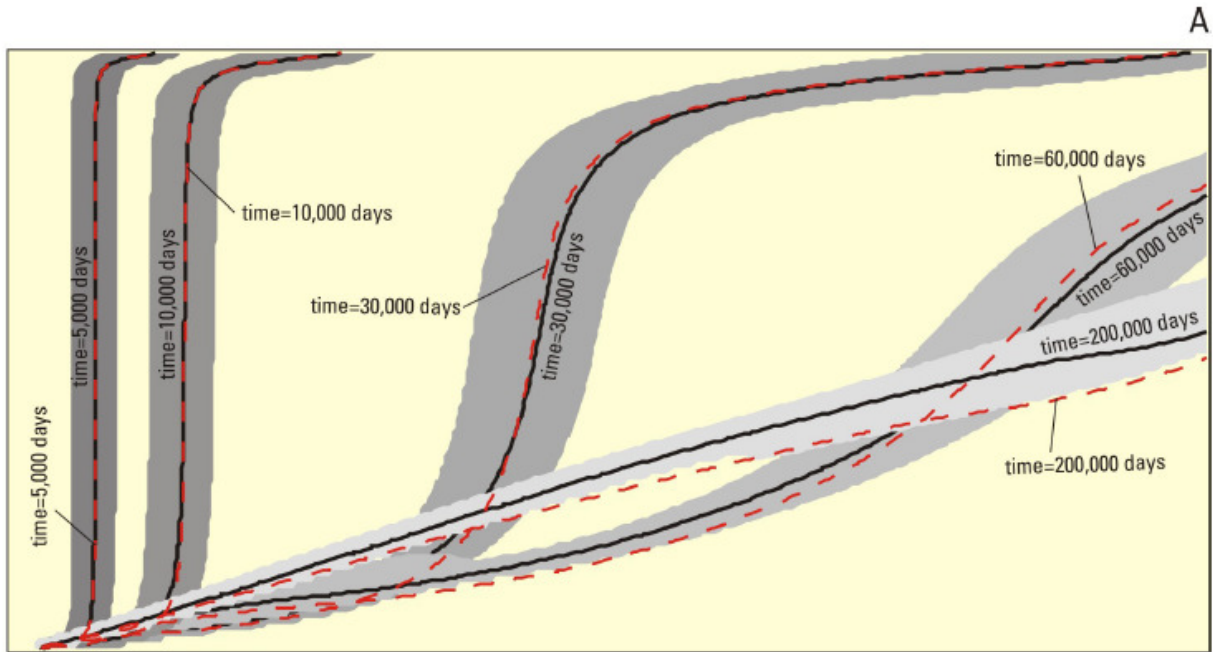
EXPLANATION

— 50 percent seawater line for Case 7

‒ ‒ 50 percent seawater line for Case 6

B

time=5,000 days

time=5,000 days

time=30,000 days

time=30,000 days

time=200,000 days

time=200,000 days
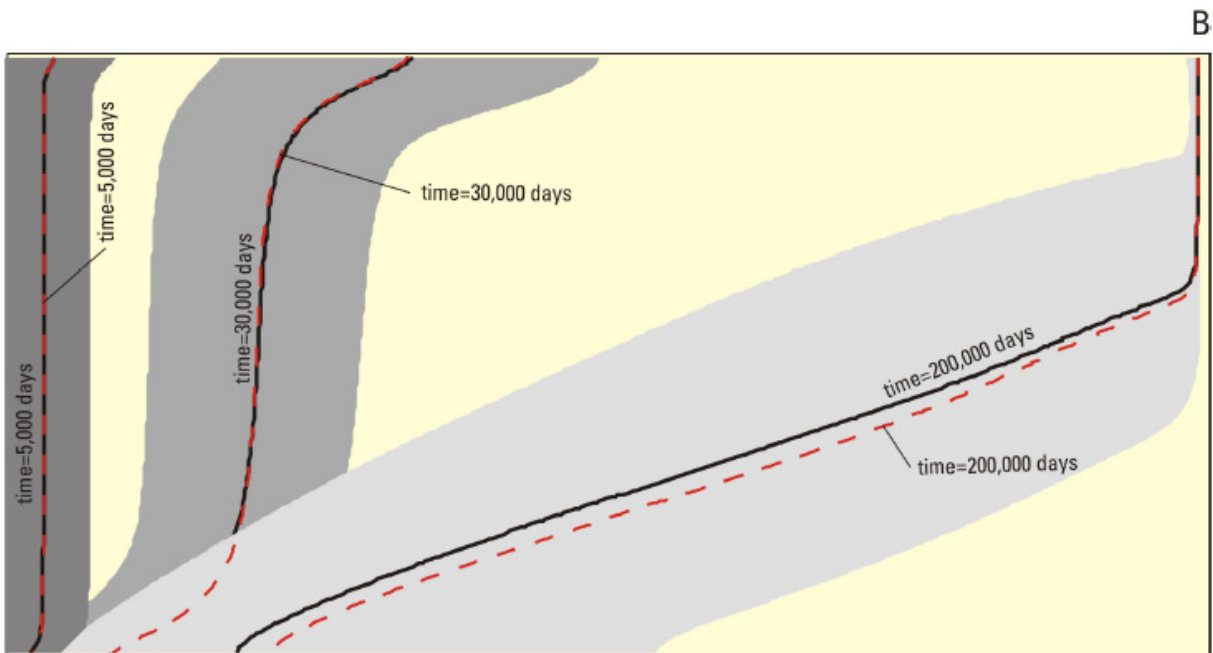
Figure 58: A copy from the SEAWAT-manual, where the results of case 7 of the example are shown. Transient movement of the (A) salinity and (B) temperature transition zones. Gray shading represents the 1 to 99 percent salinity or temperature values. The solid black lines represent the salinity or temperature value equal to 50 percent for Case 7. For comparison, dashed lines represent the 50-percent line for Case 6.

Appendix 3. Radial model

To calculate more efficiently also a radial model is developed. MODFLOW is originally developed to calculate rectangular grids, but there are some way to calculate with radial coordinates. With radial coordinates a cross-section of the model represents the entire circular model around one well (Figure 59). In this way, the problem is calculated in 2 dimensions instead of 3, and the model can be solved much more efficiently.

There are some drawbacks however. The radial coordinate begins at the well at r=0 and ends at the boundary condition, so only one well can be modeled. Another drawback is that for the model all variables are equal at equal distances from the well, at the same r. Therefore no ambient groundwater flow can be modeled. So with the method of radial coordinates it is not possible to get an accurate real-world solution, but it can prove useful to test the sensitivity of certain parameters. For this many runs need to be undertaken, and an efficient model is needed.

One way to use radial coordinates is to give the conductance terms in MODFLOW directly, instead of the hydraulic conductivity (Reilly & Harbaugh, 1993). In this approach, additional packages or modified MODFLOW code have to be used.

But with some modification of parameters it is also possible to use radial coordinates (Langevin & Zygnerski, 2006). The model is 'tricked' into calculating with radial coordinates. The horizontal and vertical hydraulic conductivity, the specific storage and the effective porosity values have to multiplied by 2πr. The way the interblock transmissivity is calculated has to be changed as well. In most cases the harmonic mean method is used, where the hydraulic conductivity is determined by the cell center closest to it. But with radial coordinates the hydraulic conductivity should increase gradually, as we walk along the r-axis. Therefore, the log mean method is chosen. This approach has been tested with an analytical solution and proved to be accurate (Langevin & Zygnerski, 2006).
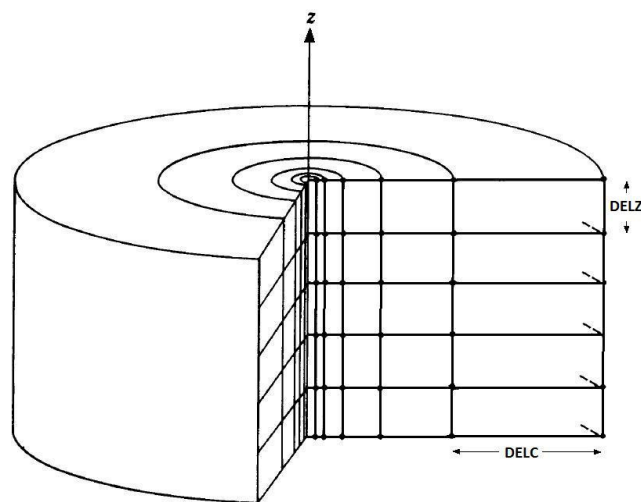
Figure 59: Illustration of an axissymmetrical model in Modflow and how the rows and columns of are used to represent axissymmetrical flow.

In axis-symmetrical flow to a well, the flow occurs through concentric shells that decrease in area in the direction of the well (Reilly & Harbaugh, 1993). The head gradient is increasing in the direction of the well, because the cross-sectional area where the flow passes through is decreasing. To represent this accurately the grid spacing has to be smaller close to the well. Therefore each node is located on a distance from the center of the well that is a multiple of the node interior to it:

$$r_{i+1} = \alpha r_i \qquad \qquad [44]$$

Where: r_i is the distance from node i to the center of the well [m]; and α is a factor larger than 1 [-].

Columns (Δx) now represent the steps in radius r, layers still represent the thickness of layers Δz, and there is only one row with a width of 1 m.

f

Appendix 4. Estimation of hydraulic conductivity using the method from van Rees Vellinga

The available data from the Stopera wells consists of the median sand particle diameter, and text descriptions of the amount of silt and gravel. For this specific data, and for the Dutch case, a method was developed (Pomper, 1996) by Van Rees Vellinga. The descriptions of the soil are translated to an U-number and correction factors, after which the hydraulic conductivity can be calculated using the following formula:

$$k = c_s c_g \frac{C}{U^2}$$ [45]

Where: C is an empirical determined constant of 54000 [m/d]; U is specific surface [-]; c_s is a correction factor for the silt content [-]; and c_g is a correction factor for the gravel content [-].

The U-number can be determined from the median particle diameter or from the text description of the soil, according to Table 8. The correction factors for the silt and gravel contents are in Table 9 and Table 10, respectively. This method only works for sandy soils, for peat and clay other methods have to be used.

Table 8: Text descriptions of the soil, together with the U-number assigned by Van Rees Vellinga.

Description (Dutch)	Description (English)	U-number
Uiterst fijn	Extremely fine	180
Zeer fijn tot uiterst fijn	Very fine to extremely fine	160
Zeer fijn	Very fine	140
Zeer fijn tot middel fijn	Very fine to middle fine	120
Middel fijn	Medium fine	100
Middel fijn tot matig fijn	Medium fine to moderate fine	80
Matig fijn, iets grover	Moderate fine, bit coarser	70
Matig fijn	Moderate fine	60
Matig fijn tot matig grof. iets grover	Moderate fine to moderate coarse, bit coarser	55
Matig fijn tot matig grof	Moderate fine to moderate coarse	50
Matig fijn tot matig grof,iets fijner	Moderate fine to moderate coarse, bit finer	45
Matig grof	Moderate coarse	40
Matig grof tot middel grof. iets grover	Moderate coarse to medium coarse, bit coarser	35
Matig grof tot middel grof	Moderate coarse to medium coarse	30
Middel grof	Medium coarse	25
Middel grof tot zeer grof	Medium coarse to very coarse	20
Zeer grof	Very coarse	15
Uiterst grof	Extremely coarse	10

Table 9:   Text descriptions of the silt content, together with the correction factor.

Description (Dutch)	Description (English)	Silt content (%)	Correction factor
Slibvrij	Silt free	0	1
Slibarm	Almost no silt	0.5	0.9
Zeer zwak siibhoudend	Very weakly silty	1	0.8
Zwak slibhoudend	Weakly silty	1.5	0.7
Slibhoudend	Contains silt	2	0.6
		3	0.45
Fijn slibhoudend zand	Fine silty sand	4	0.35
		8	0

Table 10:   Text descriptions of the gravel content, together with the correction factor.

Description (Dutch)	Description (English)	Gravel content (%)	Correction factor
Zeer weinig grind	Very little gravel	10	1.1
Weinig grind	Little gravel	12	1.25
Grindhoudend	Contains gravel	15-20	1.55
Veel grind	Lot of gravel	25-30	1.775
Zeer veel grind	Very large amount of gr.	45-60	2.425
Uiterst veel grind	Extremely large amount of gr.	80	4

h

Appendix 5. Estimation of the hydraulic conductivity using capacity measurements

The hydraulic conductivity can be estimated in different ways for an energy storage system. One of these ways is to use the capacity tests that were undertaken after the wells were made. In these capacity tests the drawdown is measured at different discharges from the well. In the case of the Stopera the discharge is increased from 100 m^3/h, to 150, 200 and 260m^3/h. Every 30 minutes, the discharge is increased. The pumped water was discharged to the Amstel, so the water was not injected in the other well.

The drawdown in the wells is calculated with the Theis's equation [32]. Because the discharge varies in time, the drawdown has to be super positioned in time, according to:

$$
\begin{aligned}
h_0 - h &= \frac{Q_{100}}{4\pi T} E_1\left(\frac{r^2 S}{4T(t - t_{100})}\right) + \frac{Q_{150} - Q_{100}}{4\pi T} E_1\left(\frac{r^2 S}{4T(t - t_{150})}\right) + \frac{Q_{200} - Q_{150}}{4\pi T} E_1\left(\frac{r^2 S}{4T(t - t_{200})}\right) \\
&\quad + \frac{Q_{260} - Q_{200}}{4\pi T} E_1\left(\frac{r^2 S}{4T(t - t_{260})}\right)
\end{aligned}
\tag{46}
$$

Where: Q_i is the discharge from the well with a discharge of i [m^3/d]; t is the time [d]; t_i is the time that pumping with a discharge of i begins [d]; r is the radius of the well [m]; S is the storativity [-]; T is the transmissivity [m^2/d]; and E_1 is the exponential integral function.

The terms in equation [46] only participate when $t>t_i$. So it really is only valid from $t>1.5$ hours. From $t=1$ to 1.5 hours, only the first three terms are in the formula, from $t=0.5$ to 1 hour only the first two, and from $t=0$ to 0.5 hours only the first term is used.

The following assumptions are made:

- The aquifer is simulated as a confined aquifer with no leakage from other layers.
- For the thickness of the aquifer, the length of the screen is chosen. Vertical flow form the parts of the aquifer above or below the screen is neglected.
- There has been no clogging, and the water finds no resistance from the gravel between the well and the screen.

With equation 46 the drawdown at the borehole wall at r=0.4 m is calculated. This can be compared to the drawdown that was measured after each half hour. Then the hydraulic conductivity value can be calibrated, so that the measured and calculated drawdown is made equal. The drawdown in time for the calibrated warm and cold well is shown in Figure 60 and Figure 61. The drawdown is plotted for both wells against the discharge in Figure 62.

The lengths of the screens are almost equal for both wells, 73 m for the warm well and 72 m for the cold well. The drawdown in the cold well is larger. During calibration this forms a lower hydraulic conductivity. The resulting value for the warm well is 32 m/d, and for the cold well the calibrated value is 42 m/d.
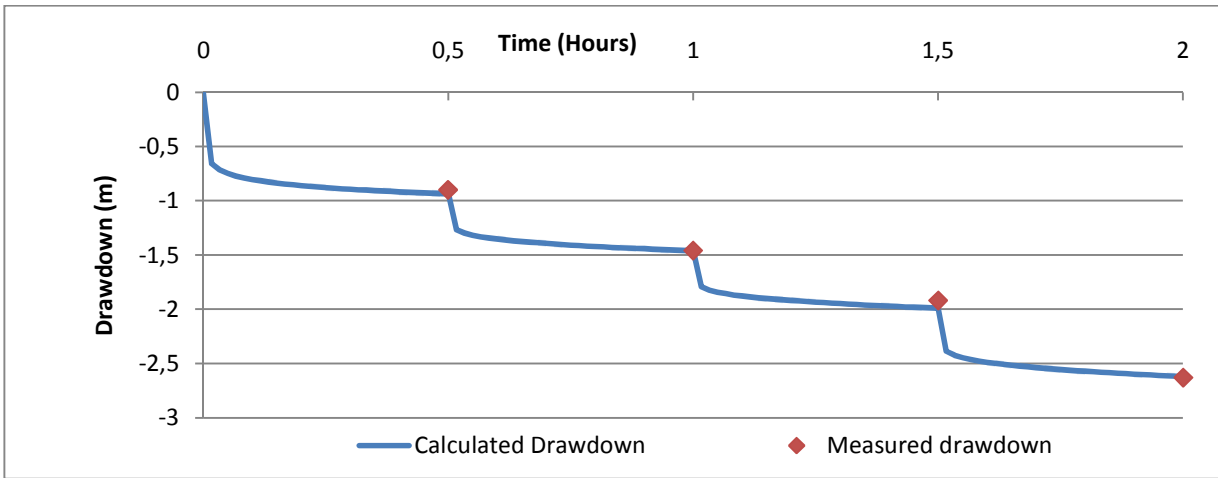
Figure 60: A graph of the calculated and measured drawdown at the warm well during the capacity test.
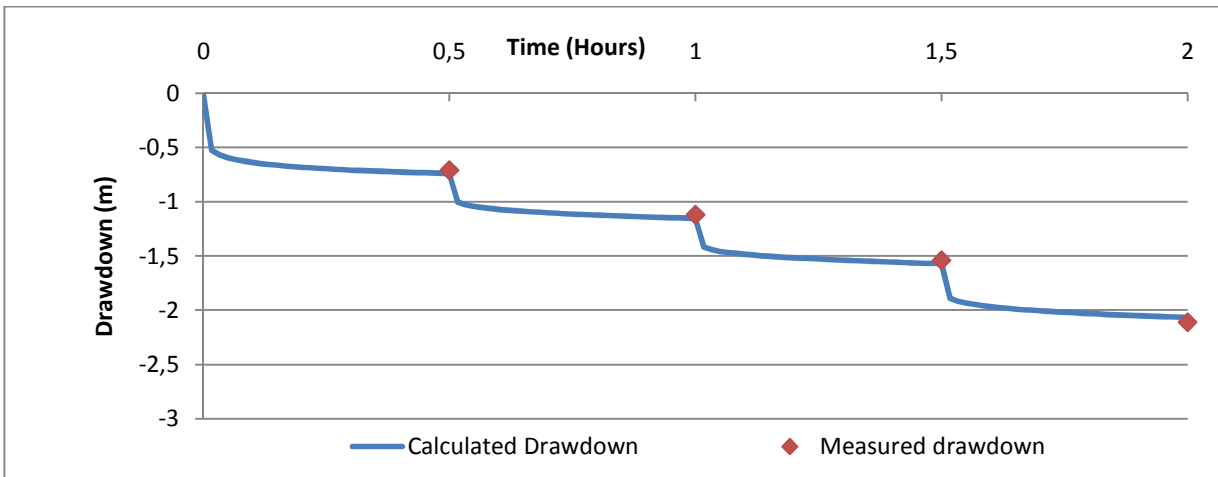
Figure 61: A graph of the calculated and measured drawdown at the cold well during the capacity test.
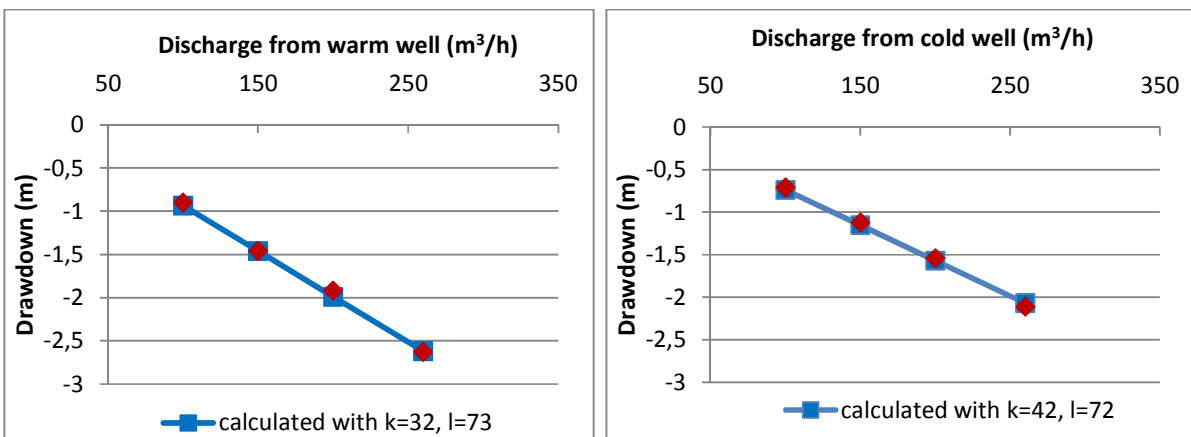
Figure 62: Measured and calculated drawdown in the warm and cold well during the capacity test after calibration.

Appendix 6.   Locations of wells for the cases of the Dam Square

Figure 63: The locations of the wells for the mixed case (above) and for the grouped case (below). Warm wells are plotted with a red circle and cold wells with a blue circle. Monowells are plotted with a green Y.

Figure 64: The locations of the wells for the case with only monowells. These are plotted with a green Y.

Appendix 7. Results for the homogeneous case
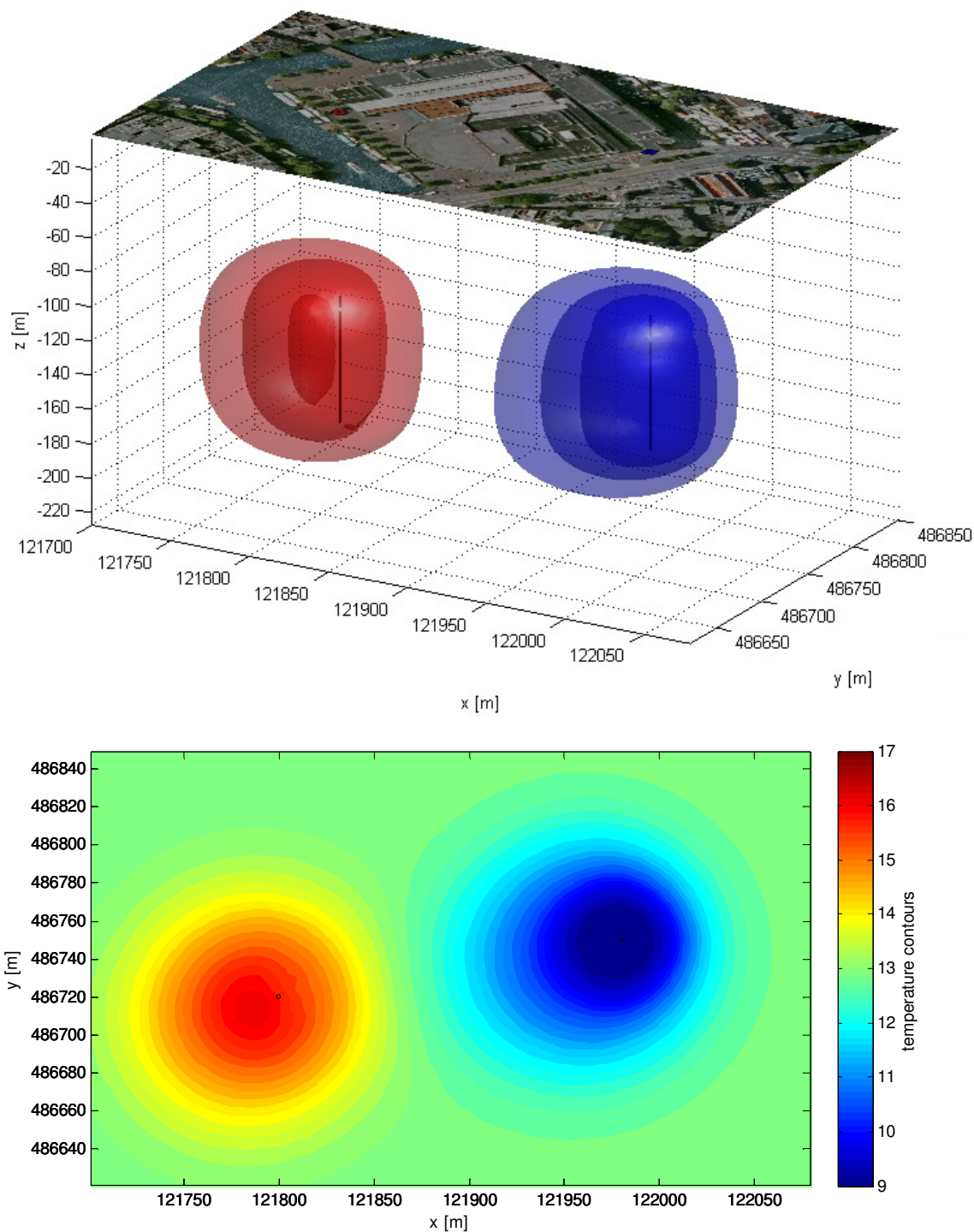
Figure 65: A 3d view of the resulting temperatures and a horizontal cross-section at NAP -140 m for a homogeneous aquifer at the end of simulation in the middle of winter.

Appendix 8. Results with a gravel layer of 125 m/d with screen
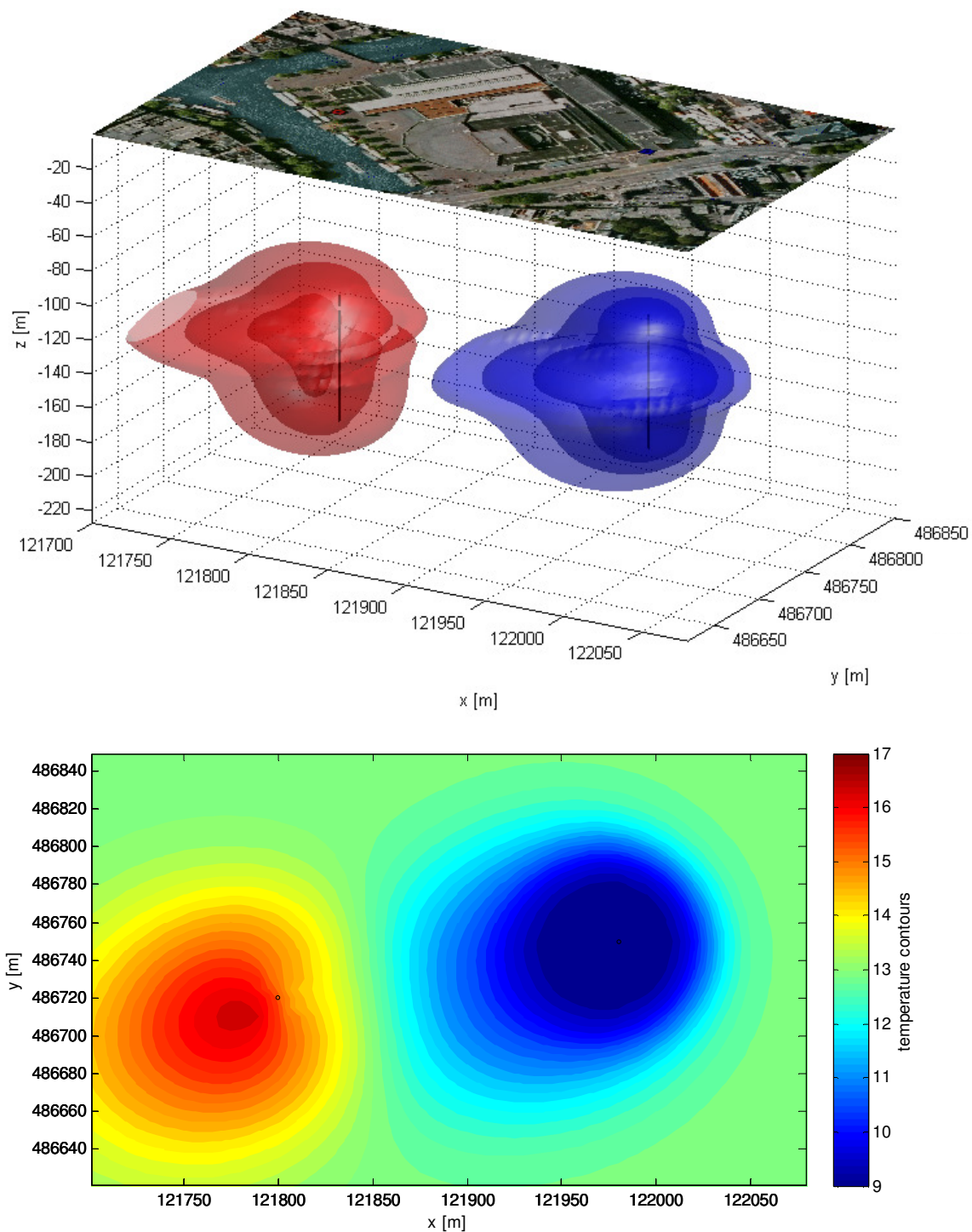
Figure 66: A 3d view of the results with a gravel layer with K_h = 125 m/d and a horizontal cross-section through the middle of the gravel layer at a depth of NAP -132 m.

Appendix 9. Results with a gravel layer of 125 m/d without screen
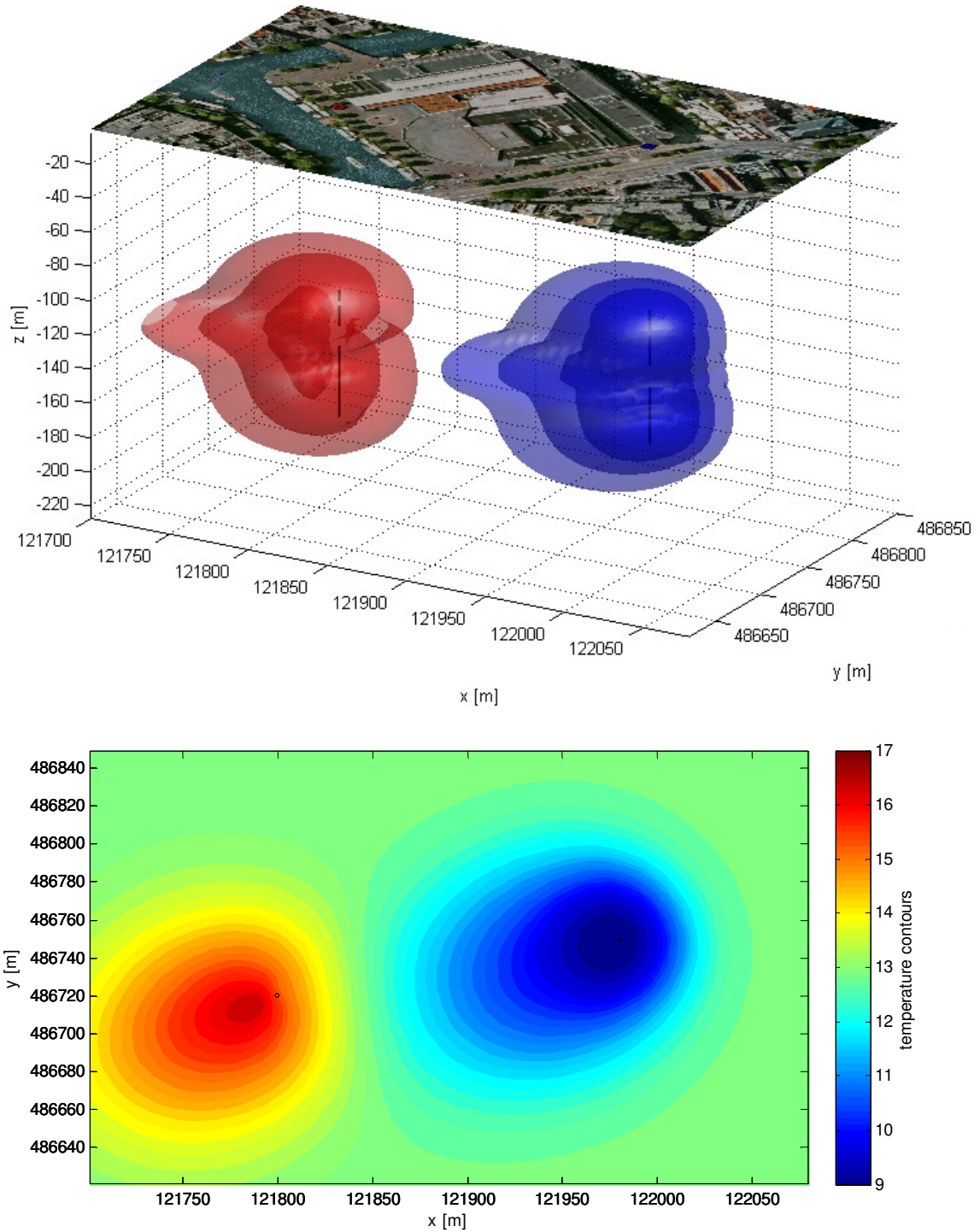
Figure 67: A 3d view of the results with a blind pipe at the gravel layer with K_h = 125 m/d and a horizontal cross-section through the middle of the gravel layer at a depth of NAP -132 m.

Appendix 10. Results with a gravel layer of 250 m/d with screen
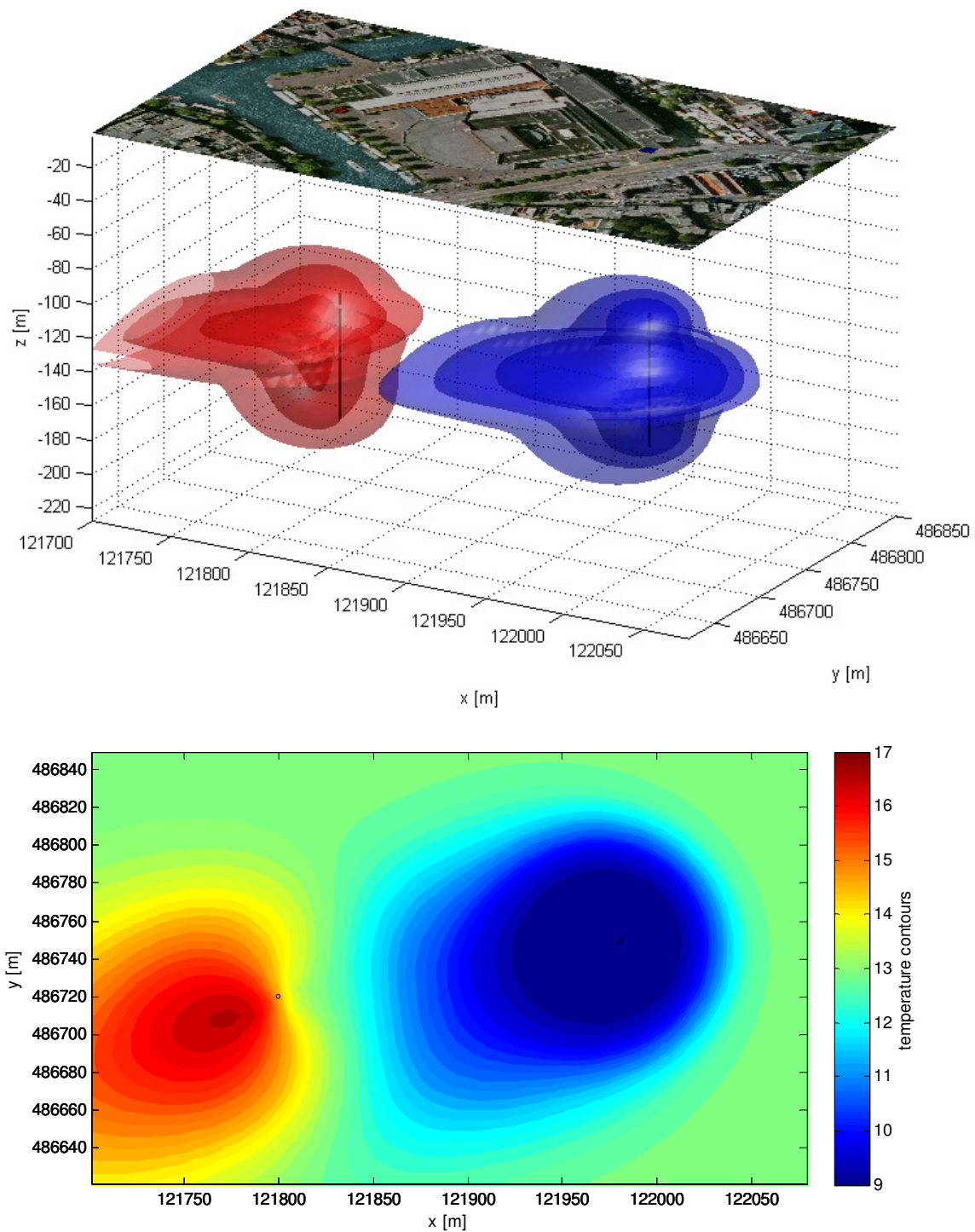
Figure 68: A 3d view of the results with a gravel layer with K_h = 250 m/d and a horizontal cross-section through the middle of the gravel layer at a depth of NAP -132 m.

Appendix 11. Results with a gravel layer of 250 m/d without screen
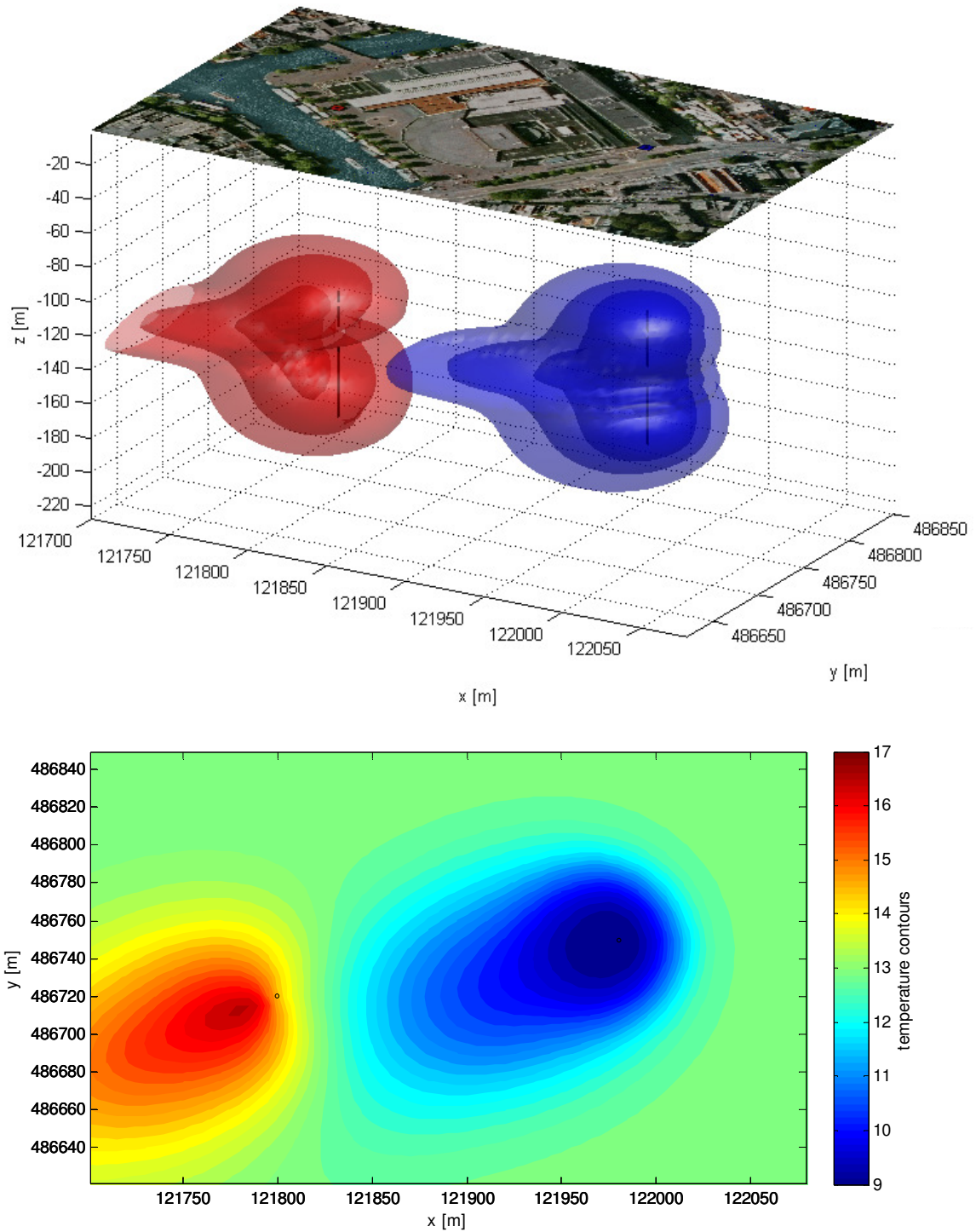
Figure 69: A 3d view of the results with a blind pipe at the gravel layer with K_h = 250 m/d and a horizontal cross-section through the middle of the gravel layer at a depth of NAP -132 m.

Appendix 12. Results for heterogeneity, range of 10 m
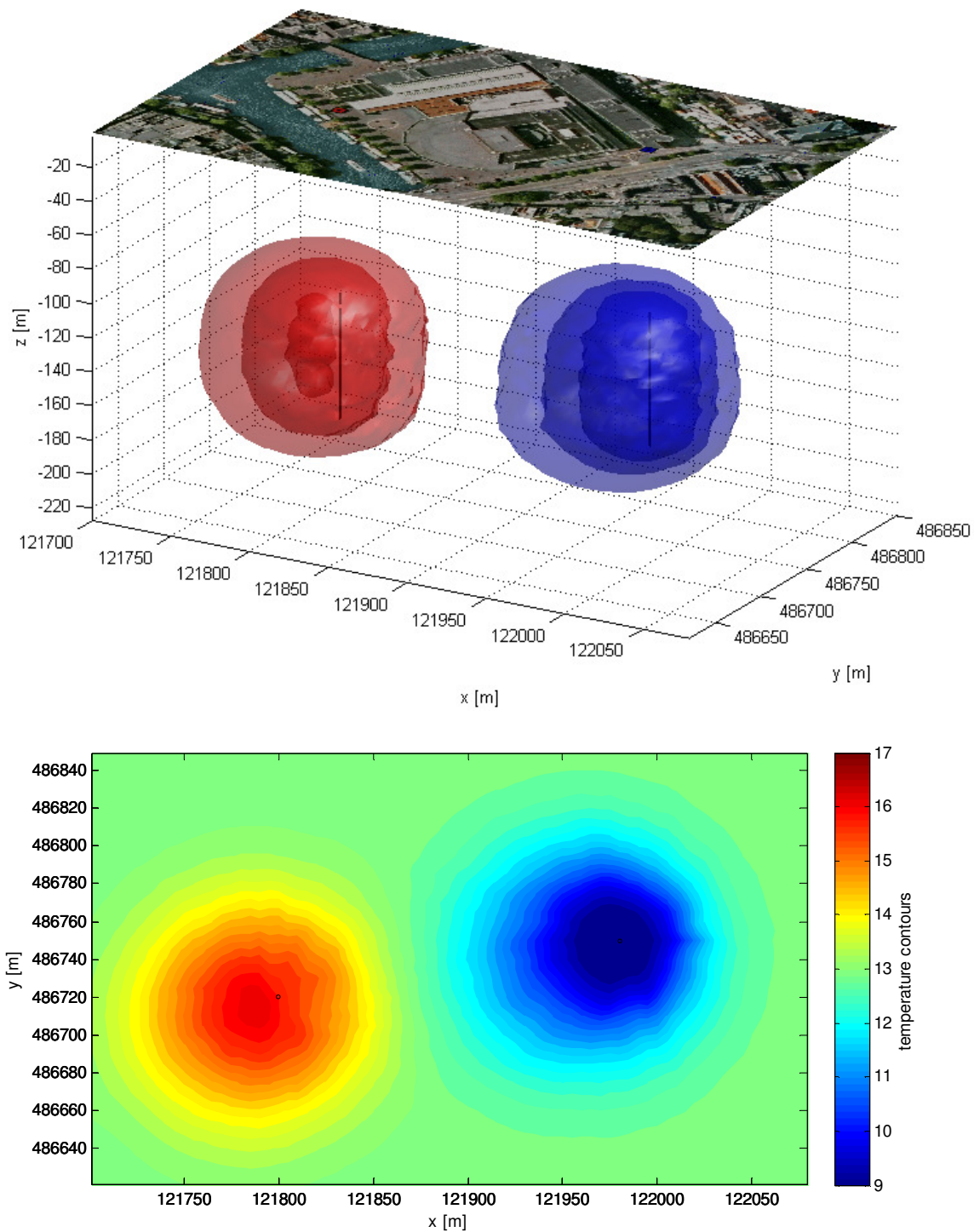
Figure 70: A 3d view of the resulting temperatures and a horizontal cross-section at NAP -140 m for simulated heterogeneities with a range of 10 m at the end of simulation in the middle of winter.

r

Appendix 13. Results for heterogeneity, range of 50 m
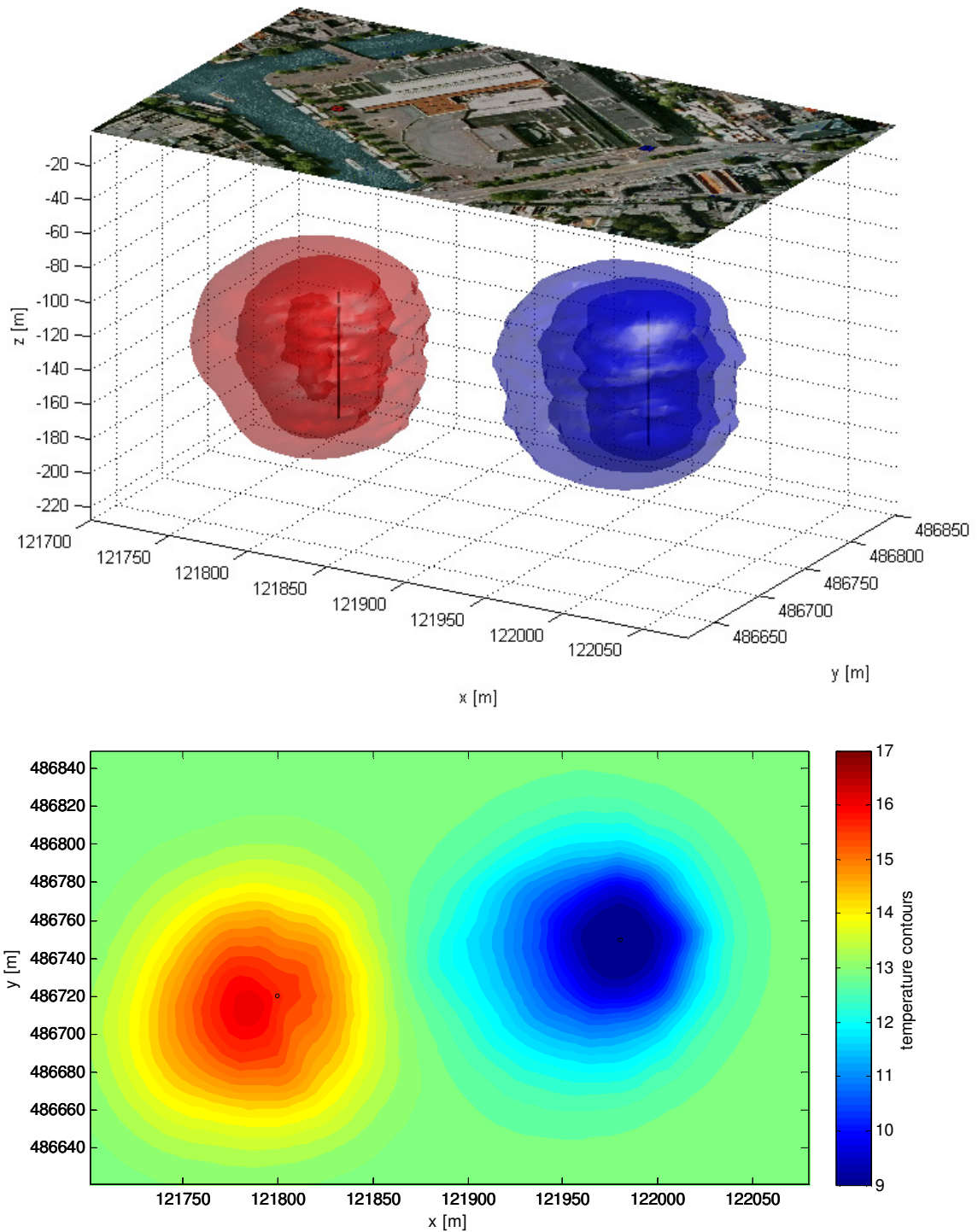
Figure 71: A 3d view of the resulting temperatures and a horizontal cross-section at NAP -140 m for simulated heterogeneities with a range of 50 m at the end of simulation in the middle of winter.

Appendix 14. Results for heterogeneity, range of 200 m
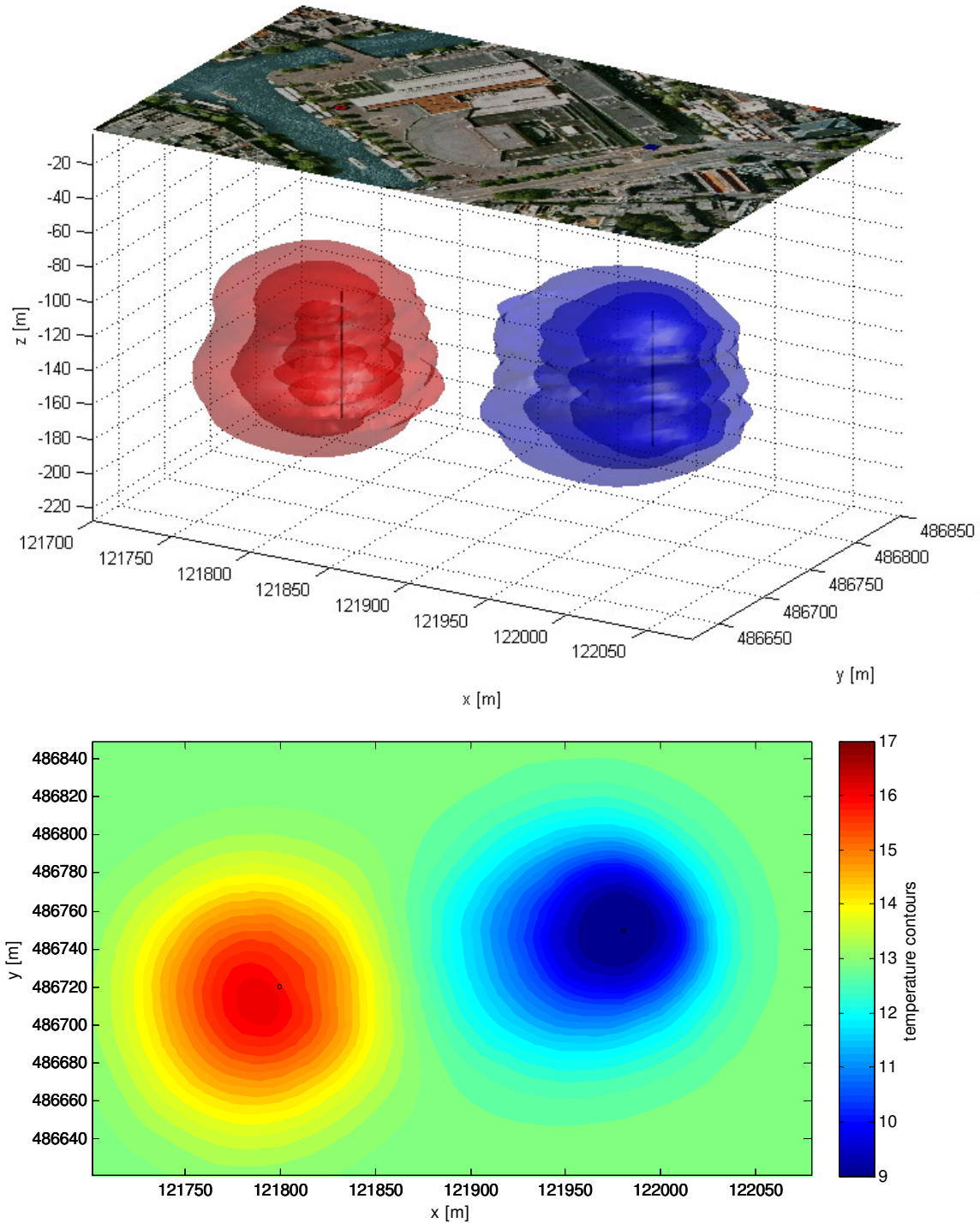
Figure 72: A 3d view of the resulting temperatures and a horizontal cross-section at NAP -140 m for simulated heterogeneities with a range of 200 m at the end of simulation in the middle of winter.

t

Appendix 15. Results for a mix of monowells and doublets

Figure 75: Graphs of cross-sections at 72.5 m and 142.5 m, the top of the warm and cold screens of the monowells, after 10 years of use, in the middle of winter.
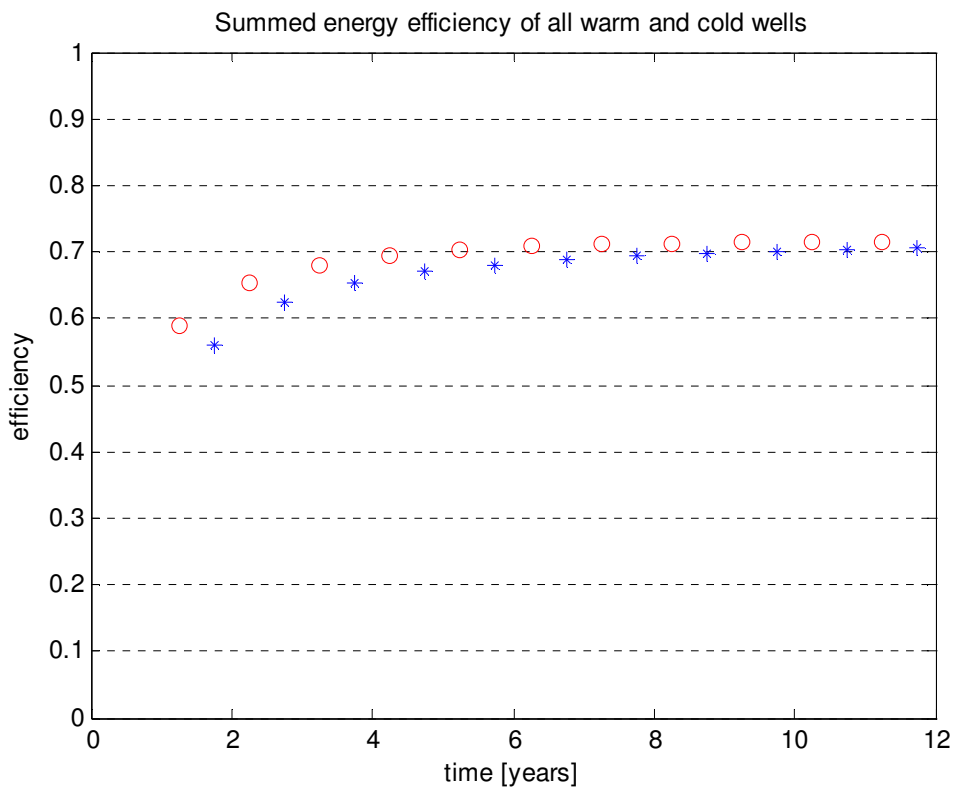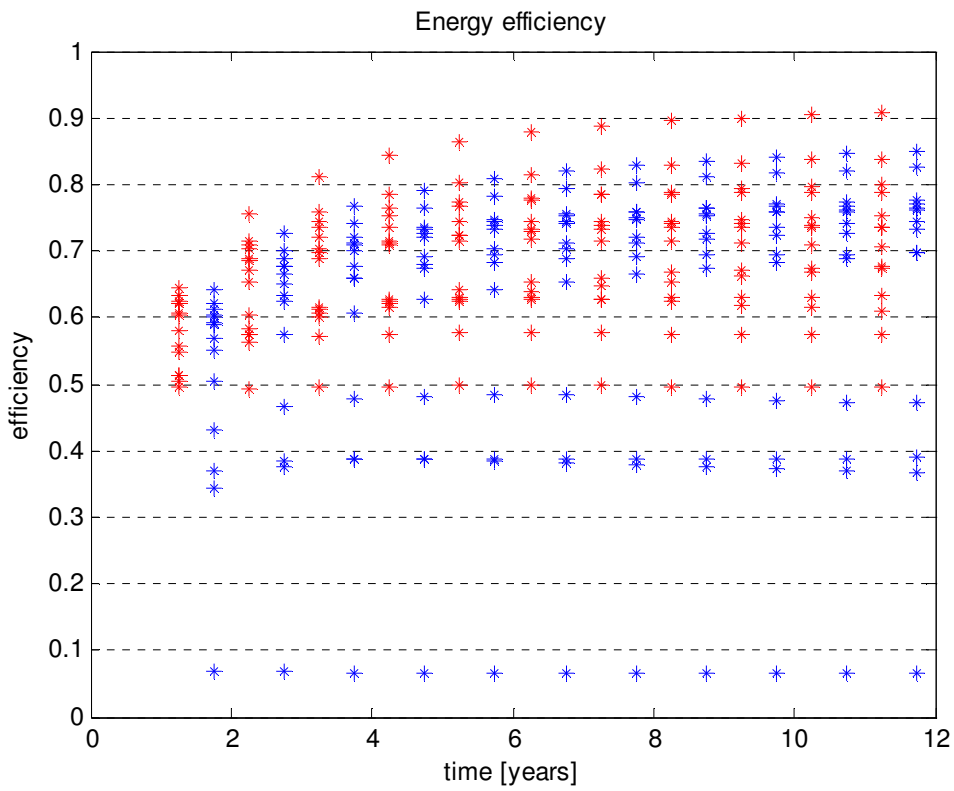
Figure 76: **Energy efficiency for each well and for all wells together for the mixed case.**
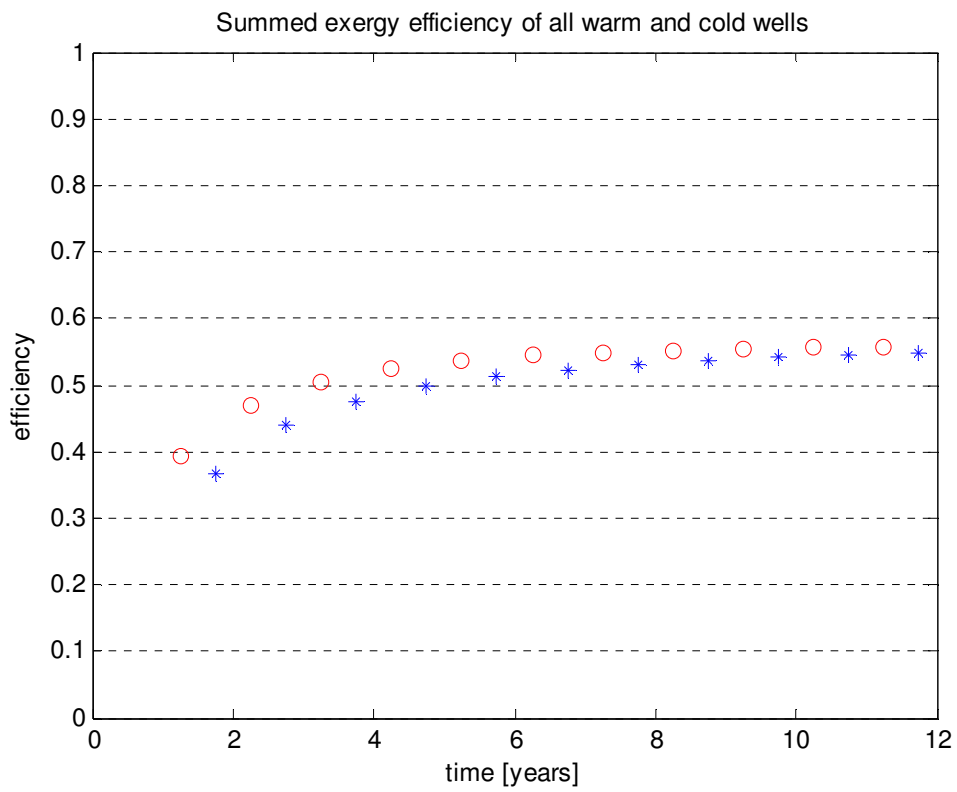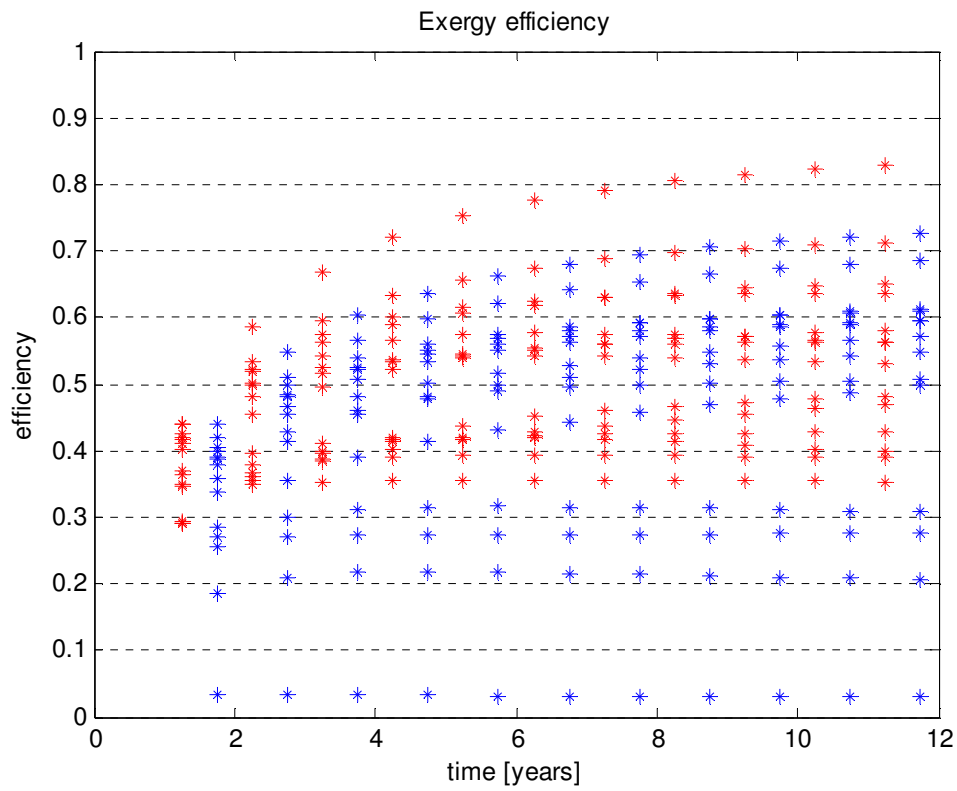
Figure 77: Exergy efficiency for each well and for all wells together for the mixed case.

x

Appendix 16. Results for the grouped system

Figure 80: Graphs of cross-sections at NAP -72.5 m and -142.5 m after 10 years of use, in the middle of winter, for the grouped case.
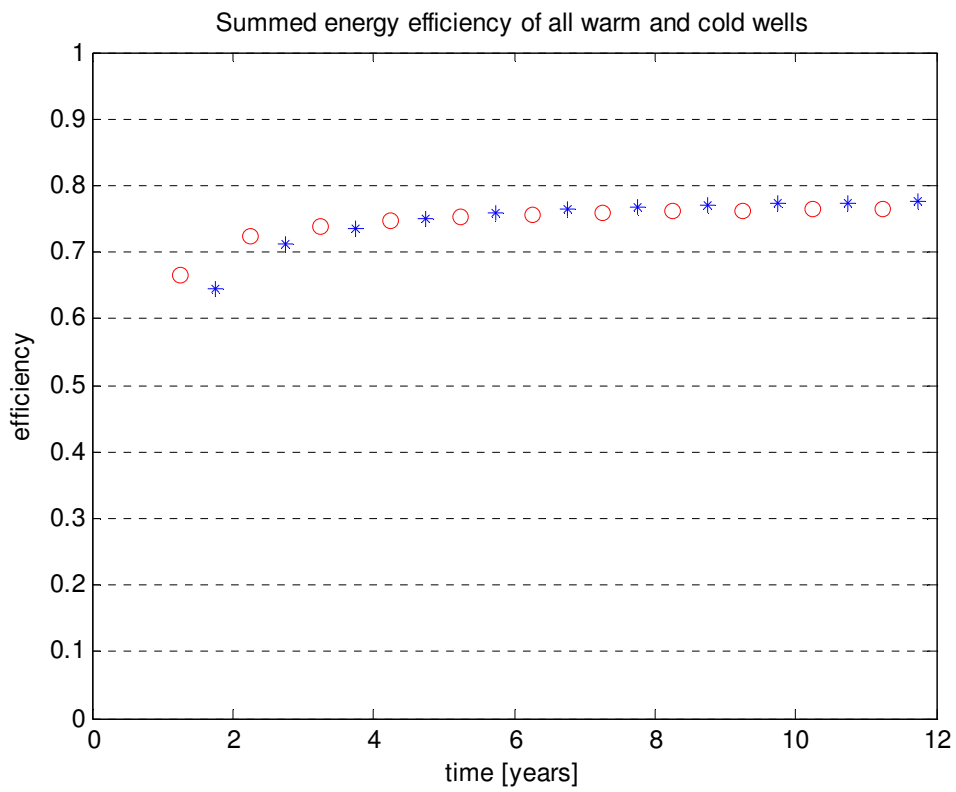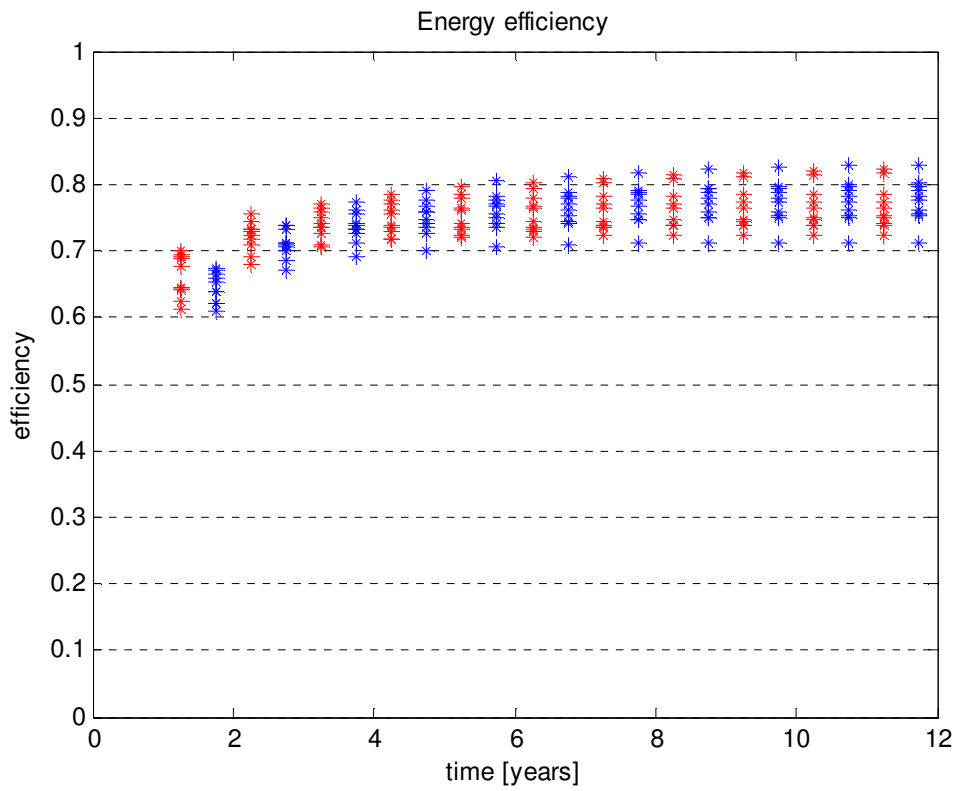
Figure 81: Energy efficiency for each well and for all wells together for the grouped case.
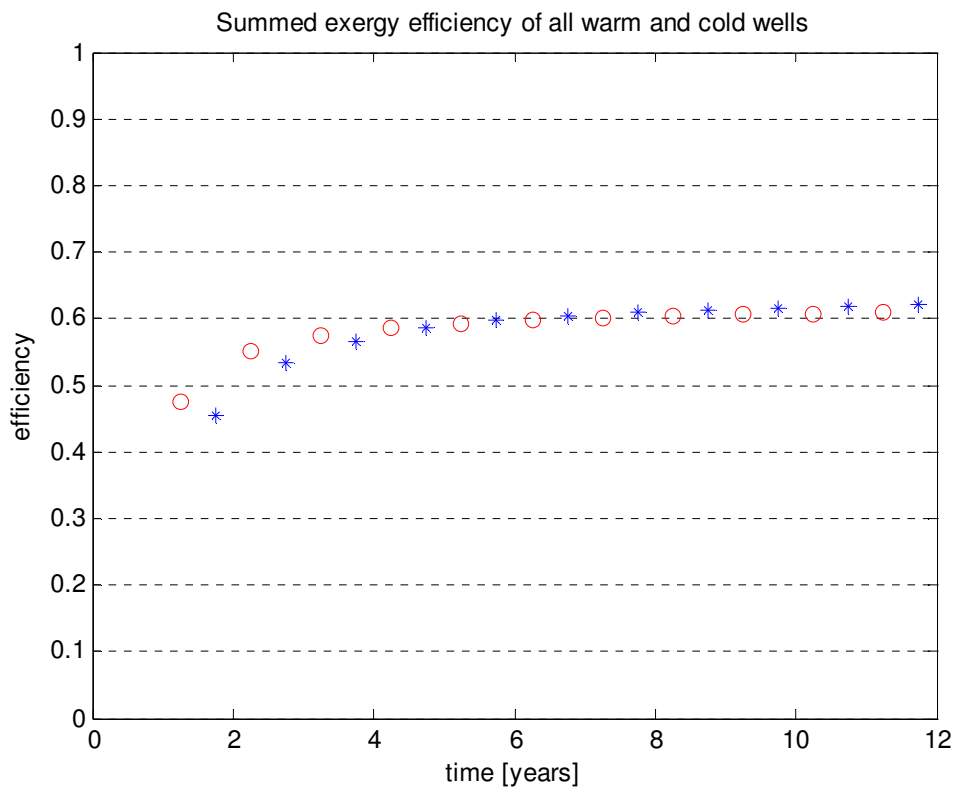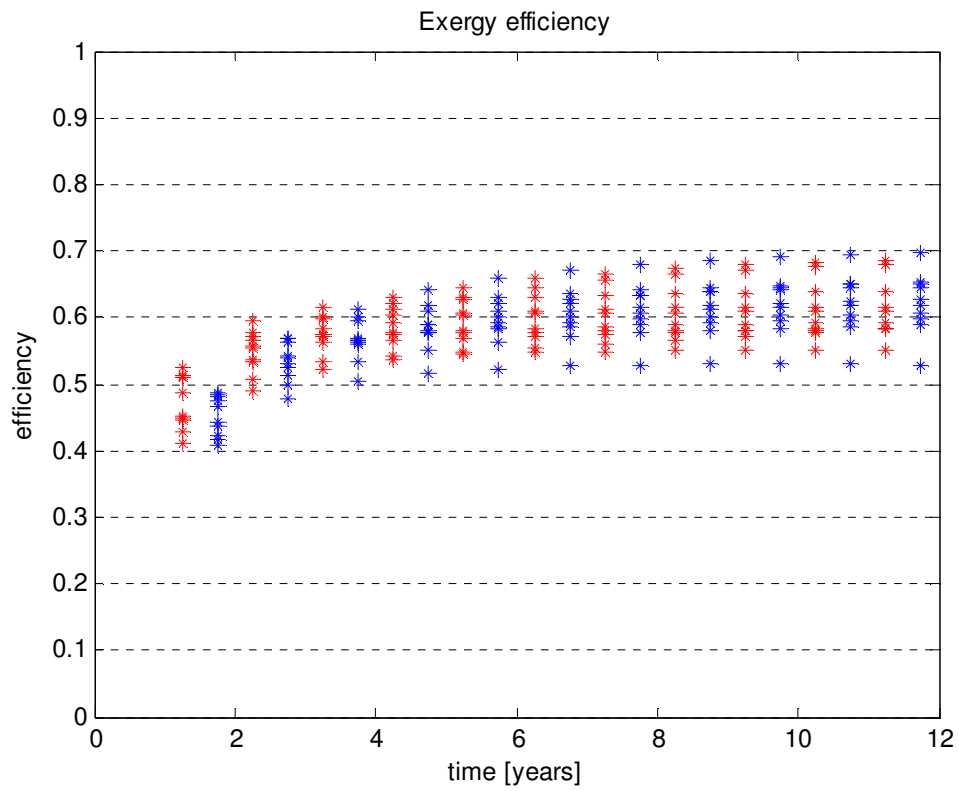
Figure 82: Exergy efficiency for each well and for all wells together for the grouped case.

Appendix 17. Results for monowells
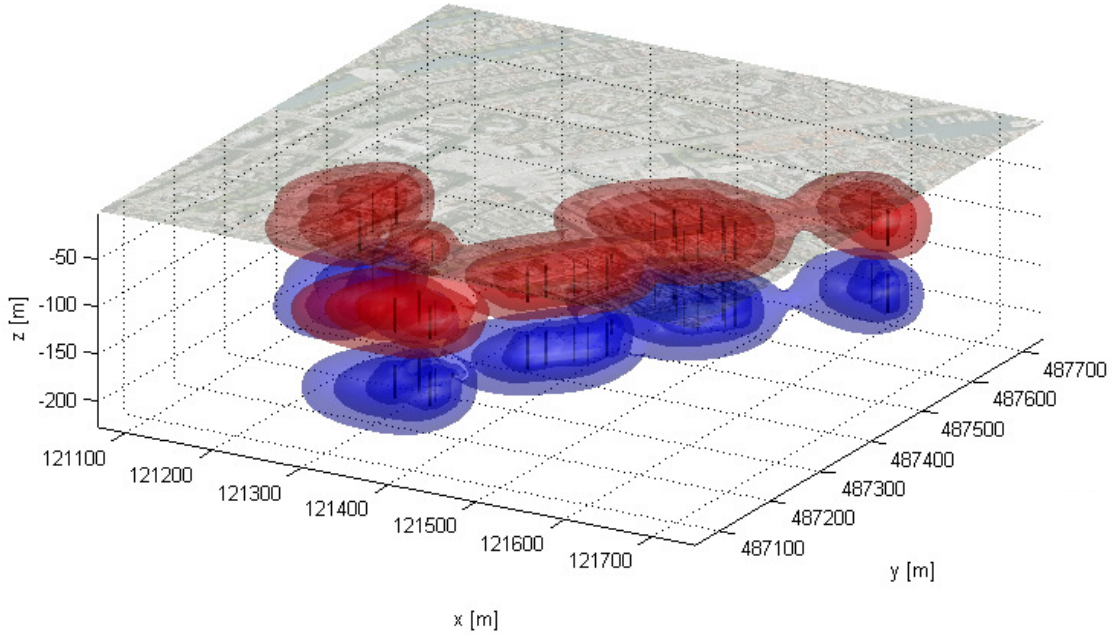
Figure 83: A 3d graph after 10 years of use, in the middle of winter for the case with only monowells.
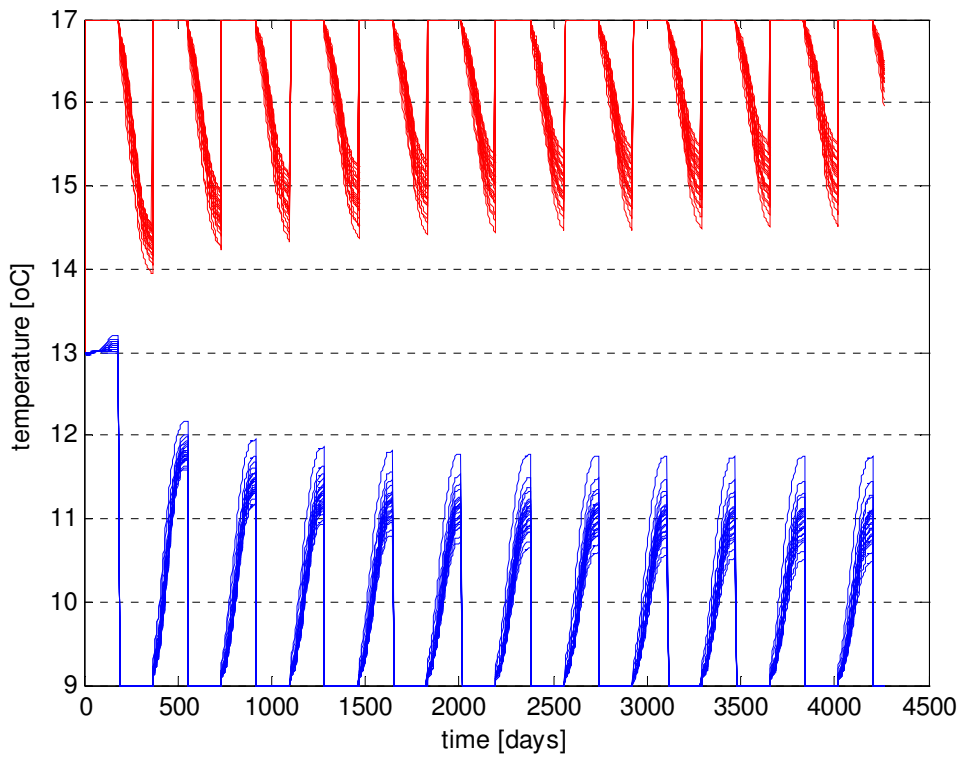
Figure 84: The temperatures at the wells for the case with only monowells.
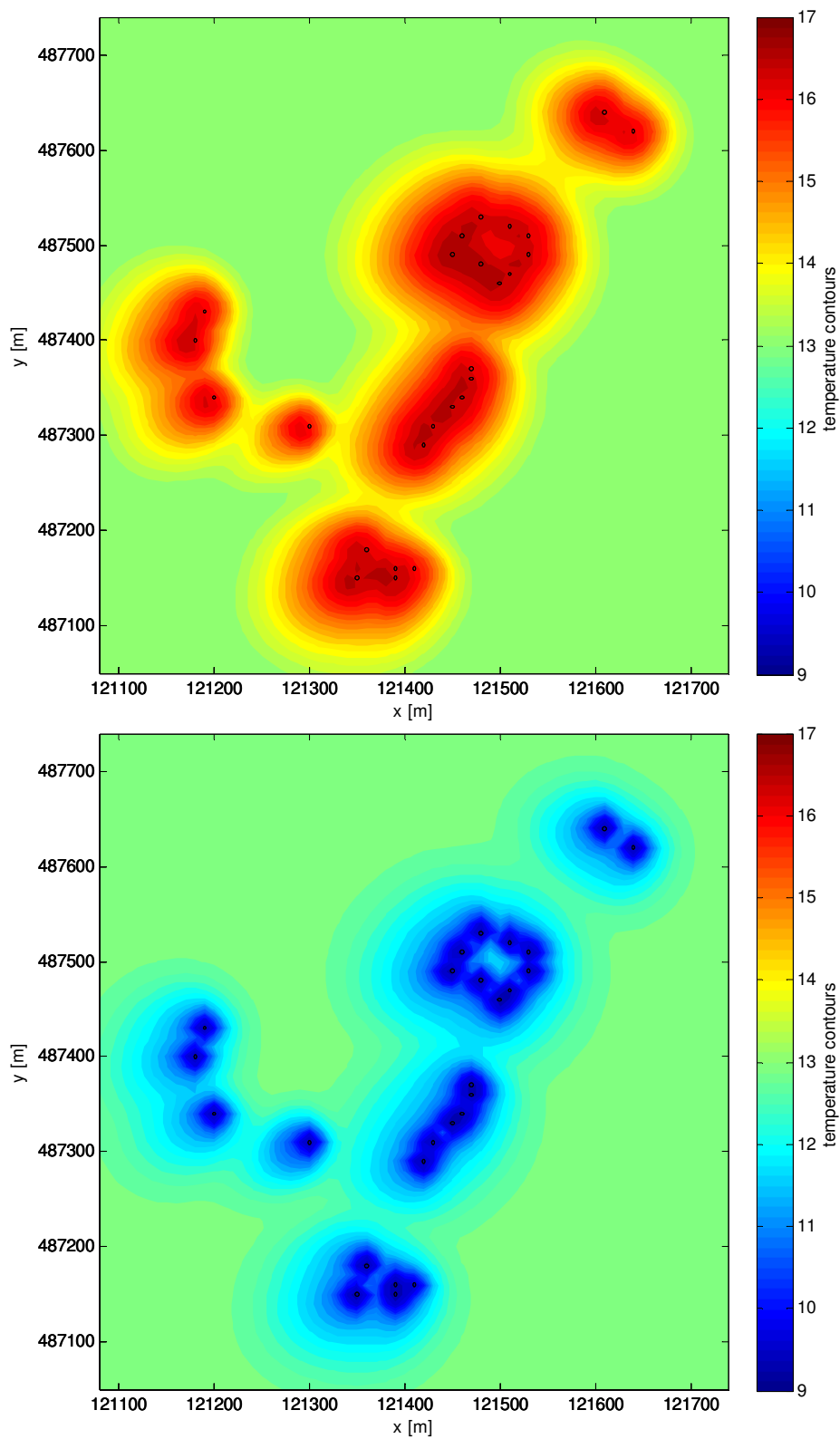
Figure 85: Graphs of cross-sections at 72.5 m and 142.5 m, the top of the warm and cold screens of the monowells, after 10 years of use, in the middle of winter, for the case with only monowells.
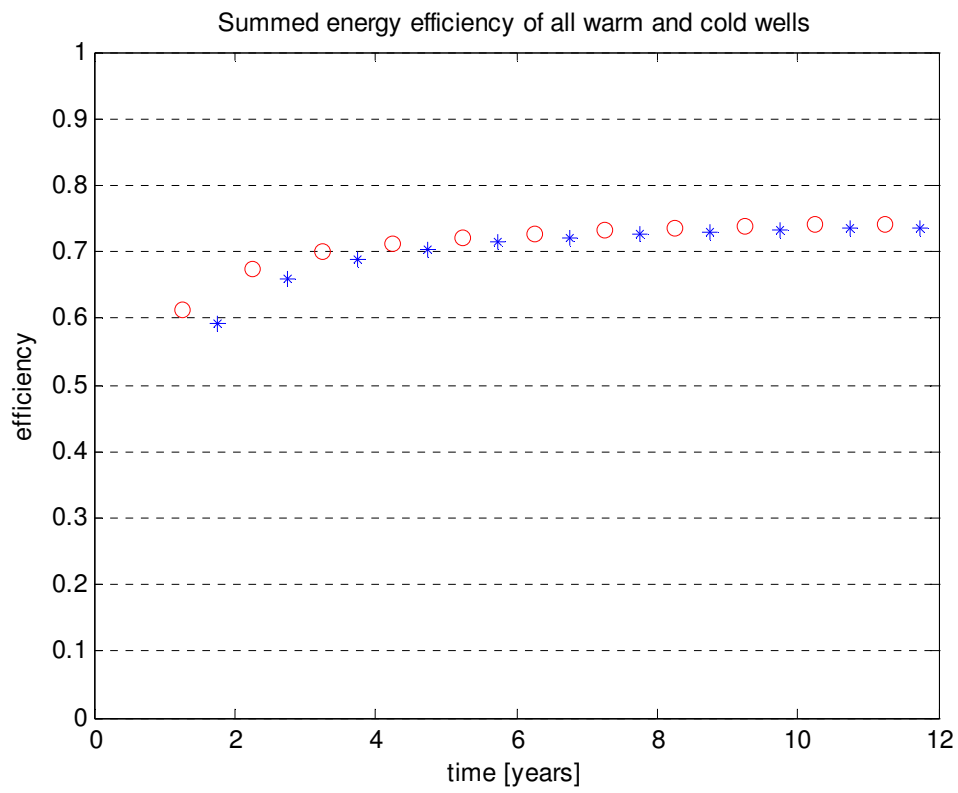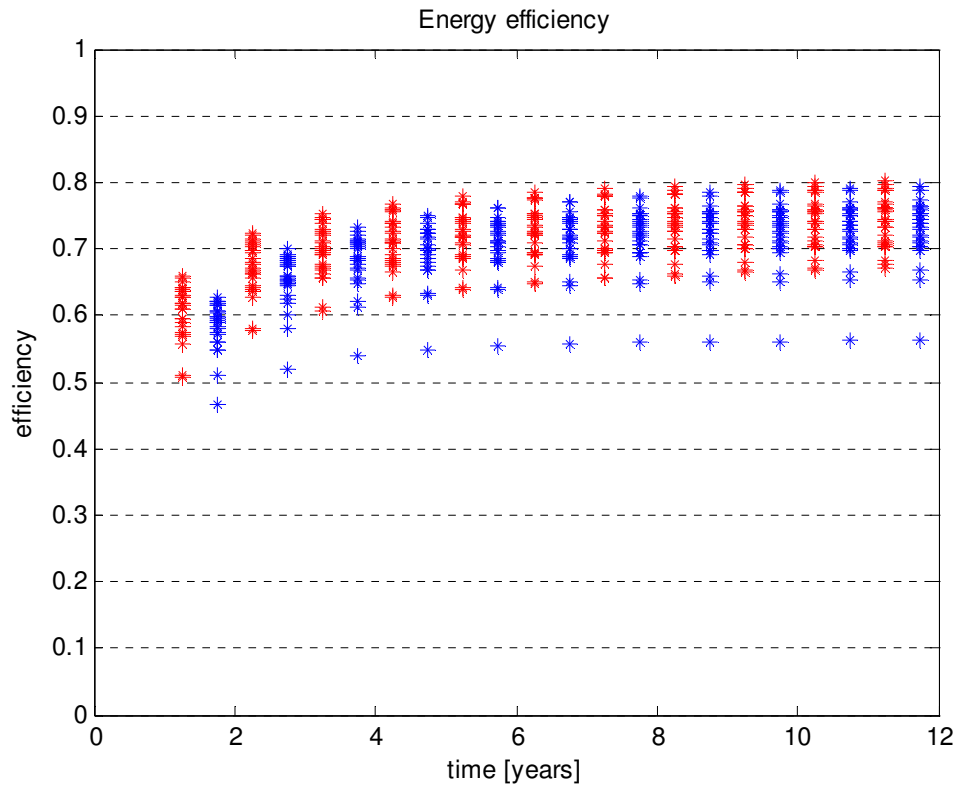
Figure 86: **Energy efficiency for each well and for all wells together for the case with only monowells.**
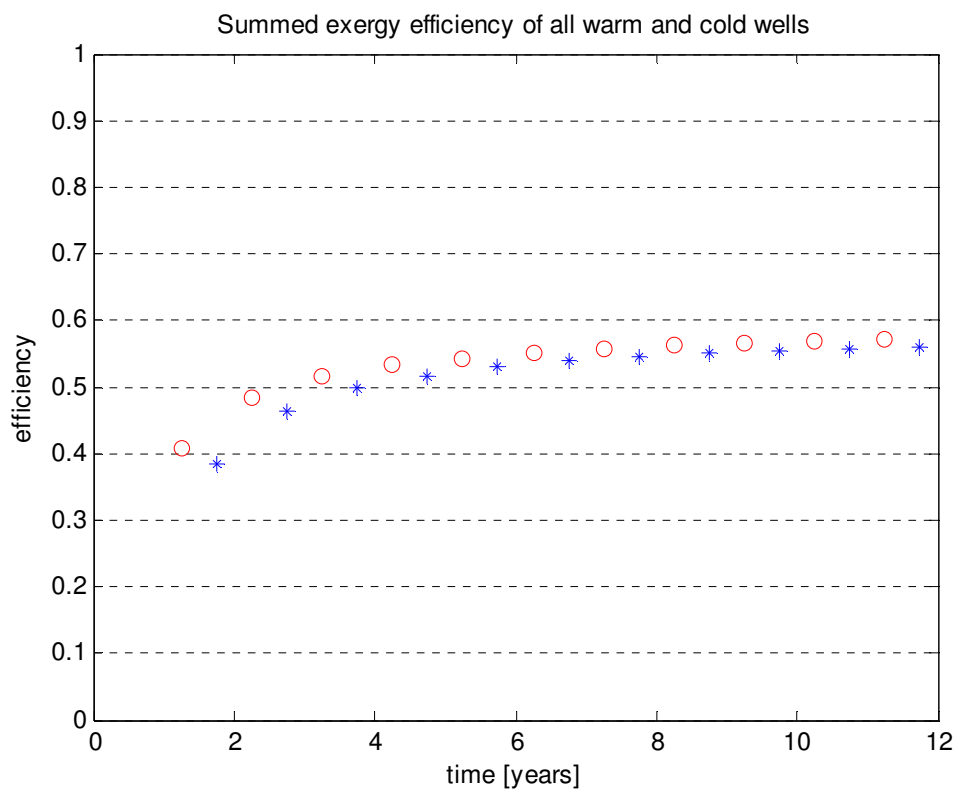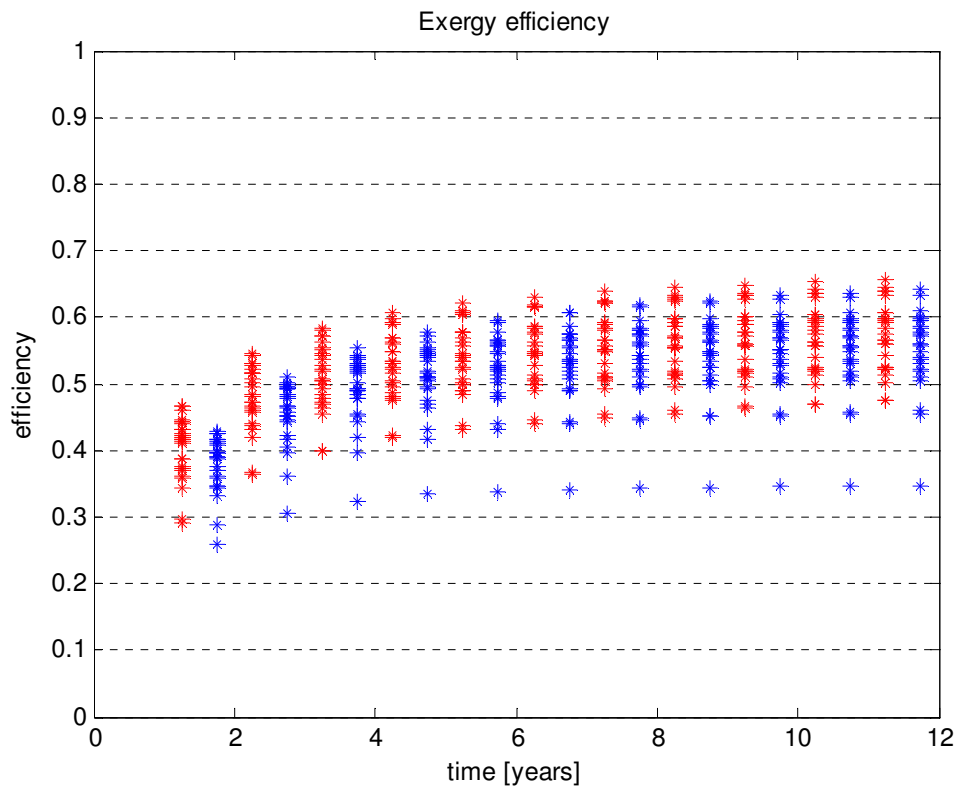
Figure 87: Exergy efficiency for each well and for all wells together for the case with only monowells.